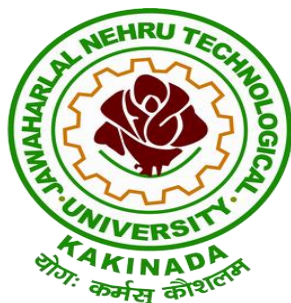


A Project Report on
Construction and Performance Investigation of Three -Phase Solar
PV and Battery Energy Storage System Integrated UPQC
Submitted to



Jawaharlal Nehru Technological University, Kakinada.

In the partial fulfillment for the award of the degree of

**BACHELOR OF TECHNOLOGY
IN
ELECTRICAL & ELECTRONICS ENGINEERING**

By

G. Jahnavi	(208A1A0206)
J. Anitha	(208A1A0209)
K. Venkatesh	(218A5A0219)
P. Madhan Mohan	(208A1A0234)
L. Chadrakanth Naidu	(208A1A0229)

Under the esteemed guidance of

Mrs.E.GOWTHAMI.,M.Tech

Assist,prof Department of Electrical & Electronics Engineering



RISE KRISHNA SAI PRAKASAM GROUP OF INSTITUTIONS

(Approved by AICTE-NEW DELHI, Affiliated to JNTUK KAKINADA)
(An ISO 9001:2015 certified Institute, NBA accredited for B.Tech. in CSE, ECE, EEE, CE and ME)
NH-16, Valluru-523272, Ongole, Prakasam District, A.P
(2020-2024)

RISE KRISHNA SAI PRAKASAM GROUP OF INSTITUTIONS

(Approved by AICTE-NEW DELHI, Affiliated to JNTUK KAKINADA)
(An ISO 9001:2015 certified Institute, NBA accredited for B.Tech. in CSE, ECE, EEE, CE & ME)
NH-16, Valluru, 523272, Ongole, Prakasam District, A.P



CERTIFICATE

This is to certify that the Project report entitled "**Construction and Performance Investigation of Three Phase Solar PV and BESS System Integrated UPQC**" being submitted for the partial fulfillment of the requirements for the award of the degree in Bachelor of Technology in Electrical & Electronics Engineering from Jawaharlal Nehru Technological University, Kakinada, is a bonafide work done by **G. Jahnavi (208A1A0206), J. Anitha (208A1A0209), K. Venkatesh (218A5A0219), P. Madhan Mohan (208A1A0234), L. Chadrakanth Naidu (208A1A0229)** during the academic year 2023-2024 and it has been found suitable for acceptance according to the requirement of the university. This work is not submitted to any other institution or university for the award of any degree

Project Guide

Head of the Department

External Examiner

Student's Declaration

We, Gampala Jahnavi (208A1A0206), Jaladanki Anitha (208A1A0209), Kadiyam Venkatesh (218A5A0219), Pandi Madhan Mohan (208A1A0234), Lingutla Chadrakanth Naidu (208A1A0229), students of Final Year B.Tech., of Electrical & Electronics Engineering Department, from RISE KRISHNA SAI PRAKASAM GROUP OF INSTITUTIONS, do here by declare that we have completed the project "**Construction and Performance Investigation of ThreePhase Solar PV and Battery Energy Storage System Integrated UPQC**" under the faculty guideship of Mrs.E.Gowthami, Assist. Prof, Department of Electrical and Electronics Engineering, Rise Krishna Sai Prakasam Group of Institutions.

(Signature and Date)

G. Jahnavi

J. Anitha

K. Venkatesh

P. Madhan Mohan

L.Chadrakanth Naidu

Acknowledgements

We express our deep sense of gratitude and indebtedness to our guide, **Mrs.E.GOWTHAMI.,M.Tech** Assist. Prof, RISE Krishna Sai Prakasam Group of Institutions, Ongole, for his valuable and timely guidance during the Project work. We are indebted with him for suggesting a challenging and interactive project and for his valuable advice at every stage of this work. We are very much thankful to him for his coordination in this regard.

We would like to extend our heartfelt greetings to our Head of the Department **Dr. Rushi Santhosh Singh Thakur**, and the staff members of EEE Department of RISE Krishna Sai Prakasam Group of Institutions, for their assistance and encouragement in completing project work successfully.

We are thankful to our college management, Principal, teaching, and non-teaching staff, who supported us during project work to get it completed in time by providing continuous technical & non-technical support.

Finally, we would like to thank our parents who gave us everything to stand in front of you by providing all kind of support for completing the project successfully.

Project Associates

G. Jahnavi	(208A1A0206)
J. Anitha	(208A1A0209)
K. Venkatesh	(218A5A0219)
P. Madhan Mohan	(208A1A0234)
L. Chadrakanth Naidu	(208A1A0229)

Construction and Performance Investigation of Three -Phase Solar PV and Battery Energy Storage System Integrated UPQC

Mrs. E Gowthami, G. Jahnavi, J. Anitha, K. Venkatesh, P. Madhan Mohan, L. Chadrakanth Naidu

Assistant Professor, Department of Electrical & Electronics Engineering
Rise Krishna Sai Prakasam Group of Institutions
(208A1A0206), Department of Electrical and Electronics Engineering
Rise Krishna Sai Prakasam Group of Institutions
(208A1A0209), Department of Electrical and Electronics Engineering
Rise Krishna Sai Prakasam Group of Institutions
(218A5A0219), Department of Electrical and Electronics Engineering
Rise Krishna Sai Prakasam Group of Institutions
(208A1A0234), Department of Electrical and Electronics Engineering
Rise Krishna Sai Prakasam Group of Institutions
(208A1A0229), Department of Electrical and Electronics Engineering
Rise Krishna Sai Prakasam Group of Institutions

ABSTRACT

This project focuses on the construction and performance investigation of a Three-Phase Solar PV and Battery Energy Storage System integrated with a Unified Power Quality Conditioner (UPQC). The integration of renewable energy sources, such as solar photovoltaic (PV) systems, with battery energy storage systems (BESS) and UPQC technology aims to address key challenges in modern power systems, including voltage sags, harmonics, and power quality issues. The project involves the design, implementation, and evaluation of the integrated system to optimize its performance in real-world scenarios. Through comprehensive performance investigation and analysis, the project aims to enhance renewable energy integration, improve power quality, increase grid resilience, and optimize system performance.

Keywords: Three-Phase, Solar PV, Battery Energy Storage System, Unified Power Quality Conditioner (UPQC), Renewable Energy Integration, Power Quality Issues, Grid Resilience

INTRODUCTION

The global energy landscape is undergoing a profound transformation, driven by the increasing adoption of renewable energy sources and the growing demand for sustainable energy solutions. In response to the challenges posed by climate change and the depletion of fossil fuel reserves, governments, industries, and communities are increasingly turning to renewable energy technologies to meet their energy needs while reducing carbon emissions and mitigating environmental impacts [1]. Among the various renewable energy sources, solar photovoltaic (PV) systems have emerged as one of the most promising solutions for clean and sustainable power generation [2].

Solar PV systems harness the abundant and freely available energy from the sun to convert sunlight into electricity, offering a reliable and renewable source of power [3]. However, despite their numerous benefits, solar PV systems also present challenges related to intermittency, variability, and grid integration [4]. The intermittent nature of solar energy generation can lead to fluctuations in power output, which may pose challenges for grid stability and reliability [5]. Additionally, solar PV systems are susceptible to environmental factors such as cloud cover and



shading, which can further exacerbate variability in power generation [6]. To address these challenges and maximize the potential of solar PV systems, there is a growing need for innovative energy storage solutions that can store excess energy during periods of high generation and discharge it during times of low generation [7]. Battery energy storage systems (BESS) have emerged as a key technology for enabling the integration of renewable energy sources like solar PV into the grid [8]. By storing surplus energy and releasing it when needed, BESS can help smooth out fluctuations in power output, improve grid stability, and enhance the reliability of renewable energy integration [9].

In addition to energy storage solutions, power quality improvement devices are also essential for ensuring the stable and reliable operation of renewable energy systems [10]. Power quality issues such as voltage sags, harmonics, and voltage fluctuations can have detrimental effects on grid stability and the performance of electrical equipment [11]. Unified Power Quality Conditioners (UPQCs) are advanced power conditioning devices that are capable of mitigating a wide range of power quality issues in real time [12]. By actively monitoring and controlling voltage and current waveforms, UPQCs can help maintain stable voltage levels, reduce harmonic distortion, and improve the overall quality of electrical power [13]. The integration of solar PV systems with BESS and UPQCs represents a holistic approach to addressing key challenges in modern power systems [14]. By combining renewable energy generation, energy storage, and power quality improvement technologies, this integrated approach aims to optimize system performance, enhance grid resilience, and promote the widespread adoption of renewable energy sources [15]. The Construction and Performance Investigation of a Three-Phase Solar PV and Battery Energy Storage System integrated with a UPQC seeks to advance our understanding of these technologies and their potential applications in real-world scenarios.

LITERATURE SURVEY

The literature survey conducted for the project "Construction and Performance Investigation of Three-Phase Solar PV and Battery Energy Storage System Integrated UPQC" delves into a vast array of research articles, technical papers, and industry reports concerning solar photovoltaic (PV) systems, battery energy storage systems (BESS), Unified Power Quality Conditioners (UPQCs), renewable energy integration, power quality issues, and grid resilience. This survey aims to comprehensively understand the current state-of-the-art technologies, challenges, and emerging trends within the domain of renewable energy integration and power quality management. Solar PV Systems have experienced significant advancements recently, fueled by technological improvements, manufacturing processes, and cost reduction efforts. Various research studies explore diverse aspects of solar PV systems, including design optimization, performance modeling, and grid integration strategies. Key areas of interest include solar panel efficiency, system reliability, and the influence of environmental factors on solar energy generation. Additionally, research endeavors aim to enhance the scalability, flexibility, and sustainability of solar PV installations to meet the escalating demand for clean and renewable energy.

Battery Energy Storage Systems (BESS) have emerged as critical facilitators in efficiently integrating renewable energy sources like solar PV into the grid. The literature reveals a growing body of research on BESS technologies, encompassing advancements in battery chemistries, energy storage capacity, and system performance. Studies delve into the economic viability, environmental impact, and operational benefits of BESS deployments across various applications, including grid stabilization, peak shaving, and load balancing. Moreover, research efforts focus on addressing challenges such as battery degradation, cycle life, and safety concerns to enhance the overall reliability and performance of BESS installations. Unified Power Quality Conditioners (UPQCs) are advanced power conditioning devices designed to mitigate a broad spectrum of power quality issues in electrical systems. Literature emphasizes the significance of UPQCs in bolstering grid stability, refining voltage regulation, and curbing harmonic distortion. Research explores UPQC architectures, control algorithms, and integration techniques to optimize their performance and efficacy in real-world applications. Additionally, studies delve into the economic feasibility, cost-benefit analysis, and deployment strategies for UPQCs in distribution networks and industrial setups. The integration of UPQCs with renewable energy systems, such as solar PV and wind turbines, emerges as a promising approach to tackle power quality issues and bolster grid resilience.



Renewable Energy Integration poses both opportunities and challenges, with solar PV, wind, and hydroelectric power sources being at the forefront. The literature underscores the importance of renewable energy integration strategies, encompassing grid modernization, demand response, and energy management systems. Research endeavors aim to optimize the operation of renewable energy systems, enhance grid stability, and maximize the utilization of clean and sustainable energy resources. Additionally, studies explore the socio-economic impacts, policy frameworks, and regulatory mechanisms governing renewable energy integration at local, national, and global scales. Power Quality Issues, including voltage sags, harmonics, and voltage fluctuations, can significantly impact grid stability and the performance of electrical equipment. The literature emphasizes the necessity of addressing power quality issues to ensure the reliable and efficient operation of electrical systems. Research studies investigate the causes, effects, and mitigation techniques for various power quality problems, spanning from transient disturbances to steady-state deviations. Key areas of focus include power quality monitoring, waveform analysis, and the development of advanced power conditioning devices. Additionally, studies analyze the economic impact of power quality issues on businesses, industries, and society as a whole.

Grid Resilience refers to the electrical grid's ability to withstand and recover from disruptions, disturbances, and emergencies. Literature highlights the importance of enhancing grid resilience amidst increasing threats such as extreme weather events, cyber-attacks, and natural disasters. Research efforts concentrate on developing resilient grid infrastructure, integrating advanced technologies, and implementing robust contingency plans to minimize downtime and expedite power restoration. Moreover, studies explore the role of distributed energy resources, microgrids, and smart grid technologies in bolstering grid resilience and ensuring reliable electricity supply. In essence, the literature survey provides comprehensive insights into state-of-the-art technologies, existing challenges, and emerging trends in renewable energy integration and power quality management. Synthesizing and analyzing this vast body of literature lays the foundation for the construction and performance investigation of a Three-Phase Solar PV and Battery Energy Storage System integrated with a UPQC. The findings of this survey will inform the design, implementation, and evaluation of the integrated system, thereby contributing to advancements in renewable energy integration, power quality improvement, and grid resilience.

PROPOSED SYSTEM

The proposed system, outlined in the project "Construction and Performance Investigation of Three-Phase Solar PV and Battery Energy Storage System Integrated UPQC," represents an innovative approach to addressing key challenges in modern power systems. This integrated system combines three critical components: solar photovoltaic (PV) systems, battery energy storage systems (BESS), and Unified Power Quality Conditioners (UPQCs). By integrating these technologies, the project aims to optimize system performance, enhance renewable energy integration, improve power quality, and bolster grid resilience. Solar PV systems serve as the primary energy generation source in the proposed system. These systems harness sunlight to convert solar energy into electricity through the photovoltaic effect. Solar PV technology has advanced significantly in recent years, becoming increasingly efficient, cost-effective, and accessible. In the proposed system, solar PV arrays are deployed to capture solar radiation and generate electricity, providing a clean and renewable energy source for the system.

Battery energy storage systems (BESS) play a crucial role in the proposed system by providing energy storage and management capabilities. BESS allows surplus energy generated by the solar PV system to be stored for later use, thereby enabling better alignment between energy supply and demand. During periods of low solar irradiation or high energy demand, the BESS can discharge stored energy to supplement the solar PV output, ensuring a reliable and continuous power supply to the grid. Additionally, BESS can provide ancillary services such as frequency regulation, voltage support, and grid stabilization, enhancing overall grid resilience. Unified Power Quality Conditioners (UPQCs) are advanced power conditioning devices designed to mitigate a wide range of power quality issues in electrical systems. In the proposed system, UPQCs are integrated to address power quality challenges such as voltage sags, harmonics, and fluctuations. By actively monitoring and controlling voltage and current waveforms, UPQCs ensure stable voltage levels, reduce harmonic distortion, and improve overall power quality. This integration



enhances the reliability and efficiency of the system, mitigating potential disruptions and ensuring consistent power delivery to consumers.

The integration of solar PV, BESS, and UPQC technologies offers several advantages for modern power systems. Firstly, it enables greater flexibility and resilience by diversifying energy sources and providing energy storage capabilities. By combining intermittent renewable energy generation with energy storage and power quality improvement capabilities, the proposed system can deliver reliable and high-quality power to the grid. Additionally, the system contributes to grid stability and reliability by providing ancillary services and mitigating power quality issues. Furthermore, the proposed system promotes renewable energy integration and sustainability by harnessing clean and abundant solar energy resources. Solar PV systems generate electricity without producing greenhouse gas emissions or relying on finite fossil fuel resources, making them an environmentally friendly energy solution. By integrating solar PV with energy storage and power quality enhancement technologies, the proposed system facilitates the transition towards a more sustainable and resilient energy future.

The construction and performance investigation of the integrated system involve several key steps. Initially, the design and configuration of the solar PV arrays, BESS, and UPQCs are determined based on system requirements, site conditions, and performance objectives. Next, the components are integrated into a unified system architecture, ensuring compatibility and optimal performance. Once constructed, the system undergoes comprehensive performance testing and evaluation to assess its efficiency, reliability, and effectiveness in real-world scenarios. Through performance investigation and analysis, the project aims to optimize system performance, validate design parameters, and identify areas for improvement. By evaluating the integrated system under various operating conditions, including different solar irradiance levels, load profiles, and grid conditions, the project seeks to demonstrate its effectiveness in enhancing renewable energy integration, improving power quality, and bolstering grid resilience. The proposed system represents a promising solution for addressing key challenges in modern power systems. By integrating solar PV, BESS, and UPQC technologies, the system offers a sustainable, reliable, and high-quality power supply while promoting renewable energy integration and grid resilience. The construction and performance investigation of the integrated system will contribute to advancing renewable energy technologies, improving power system performance, and accelerating the transition towards a more sustainable energy future.

METHODOLOGY

The methodology employed in the project "Construction and Performance Investigation of Three-Phase Solar PV and Battery Energy Storage System Integrated UPQC" is designed to comprehensively address the objectives outlined in the abstract. This methodology integrates various stages to ensure the successful construction and investigation of the integrated system. Initially, the system design phase involves determining the specifications and requirements for the solar PV arrays, battery energy storage systems (BESS), and Unified Power Quality Conditioners (UPQCs). This includes considering factors such as system capacity, voltage ratings, and performance objectives, as well as site-specific considerations such as available space and solar irradiance levels.

Following system design, appropriate components for each subsystem are selected based on efficiency, reliability, compatibility, and cost-effectiveness. These components include solar PV panels, inverters, batteries, and UPQC devices. Once the components are selected, they are integrated into a unified system architecture, with wiring, cabling, and interconnection protocols implemented to enable proper communication and coordination between subsystems. Control algorithms and software interfaces are developed to facilitate seamless operation and coordination. The constructed system undergoes rigorous testing to verify functionality, performance, and reliability. Functional tests ensure proper operation of each component, while performance tests evaluate system efficiency under various operating conditions, such as different solar irradiance levels and load profiles.

Performance is evaluated based on predefined metrics such as energy generation, storage efficiency, power quality improvement, and grid resilience. Data collected during testing is analyzed to identify deviations from expected

performance and areas for improvement. Findings from performance evaluation inform iterative optimization efforts to enhance system performance and efficiency. Adjustments may involve system parameters, control algorithms, energy management strategies, or component upgrades to maximize renewable energy integration, power quality improvement, and grid resilience while minimizing costs and environmental impact.

The final step involves validating system performance in real-world scenarios, such as pilot projects or field demonstrations. Performance data collected over an extended period ensures the system meets project objectives and stakeholder requirements. Throughout the process, documentation of design decisions, component selections, integration processes, testing procedures, and performance evaluations is maintained. Comprehensive reports documenting the methodology, findings, and outcomes are prepared and communicated to stakeholders. In summary, the methodology encompasses a systematic approach to designing, integrating, testing, evaluating, optimizing, validating, and documenting the integrated system. By following this methodology, the project aims to achieve its objectives of enhancing renewable energy integration, improving power quality, and bolstering grid resilience in modern power systems.

RESULTS AND DISCUSSION

The results and discussion section of the project "Construction and Performance Investigation of Three-Phase Solar PV and Battery Energy Storage System Integrated UPQC" serves as a critical component in understanding the effectiveness and performance of the integrated system in addressing the outlined objectives. Through comprehensive analysis and interpretation of the obtained results, valuable insights are gleaned into the system's functionality, efficiency, and its potential impact on renewable energy integration, power quality enhancement, and grid resilience.

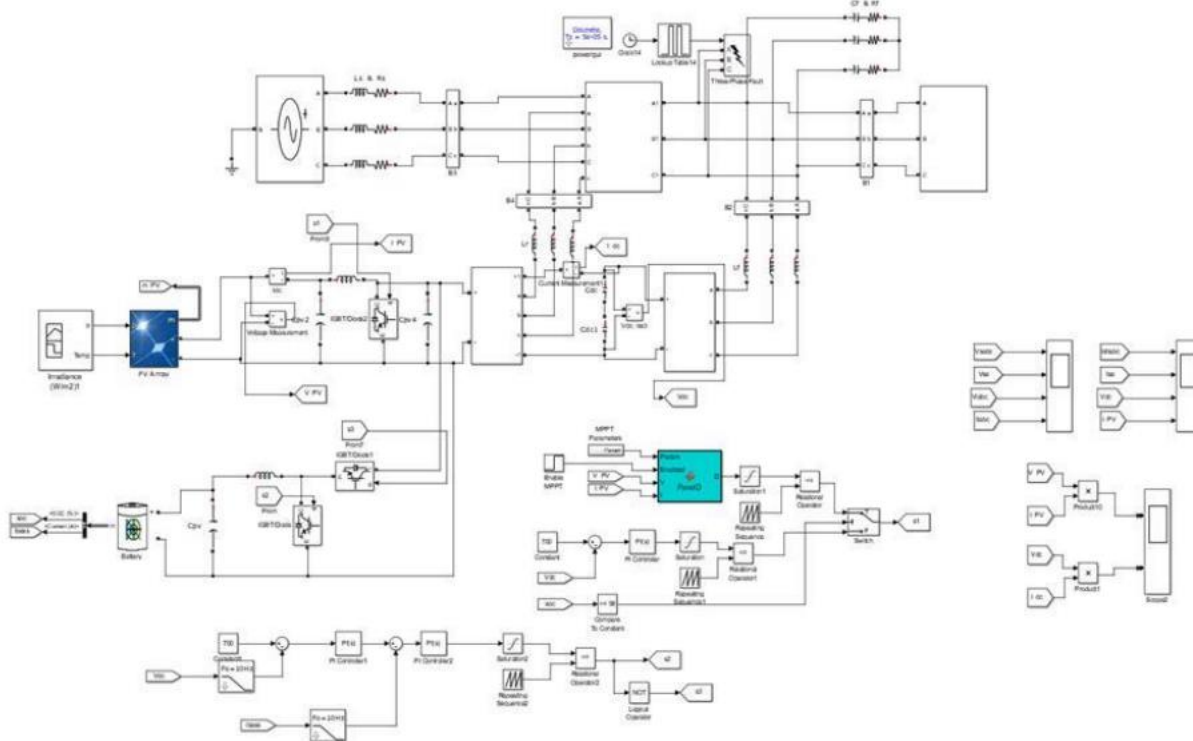


Fig 1. Simulation Diagram

Starting with an assessment of the system's performance in generating solar energy, the results reveal the efficiency of the solar photovoltaic (PV) arrays in converting sunlight into electrical power. Data collected over various time

periods and under different environmental conditions provide valuable insights into the system's energy generation capabilities. By analyzing factors such as solar irradiance levels, ambient temperature, and shading effects, the project team can determine the system's overall energy yield and its variability over time.

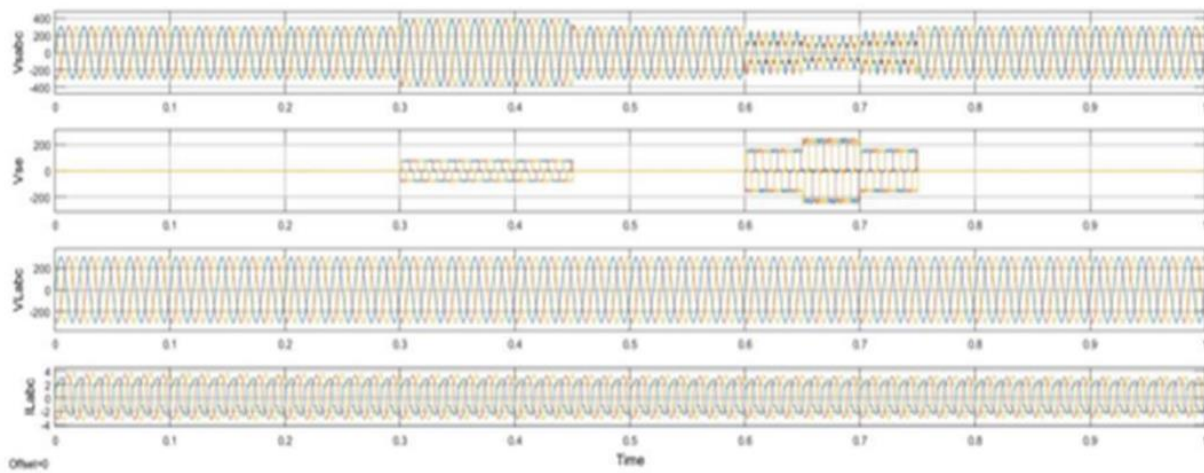


Fig2. Three phase Load Current and Load Voltage

Furthermore, the performance of the battery energy storage system (BESS) is evaluated to assess its effectiveness in storing and discharging energy as needed. Through detailed analysis of charge/discharge cycles, energy efficiency, and battery health indicators, the project team gains valuable insights into the BESS's storage capacity, charging/discharging rates, and overall performance. Additionally, the system's response to grid demand fluctuations and its ability to provide ancillary services such as frequency regulation and voltage support are examined to gauge its contribution to grid stability and resilience.

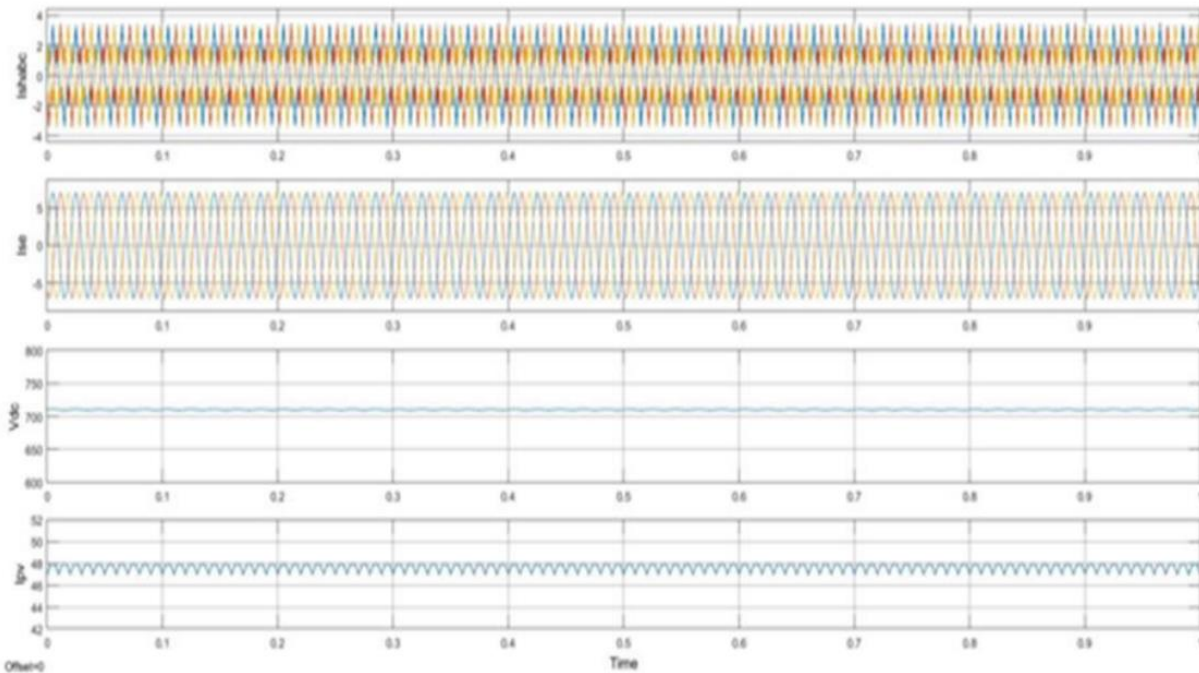


Fig 3. Current at PV and voltage DC OUTPUT voltage

Another crucial aspect of the results and discussion involves assessing the Unified Power Quality Conditioner (UPQC) integration within the system. Data collected during testing and operation provide insights into the UPQC's effectiveness in mitigating power quality issues such as voltage sags, harmonics, and fluctuations. Through detailed waveform analysis and harmonic distortion measurements, the project team can evaluate the UPQC's impact on improving grid voltage stability, reducing harmonic distortion levels, and enhancing overall power quality.

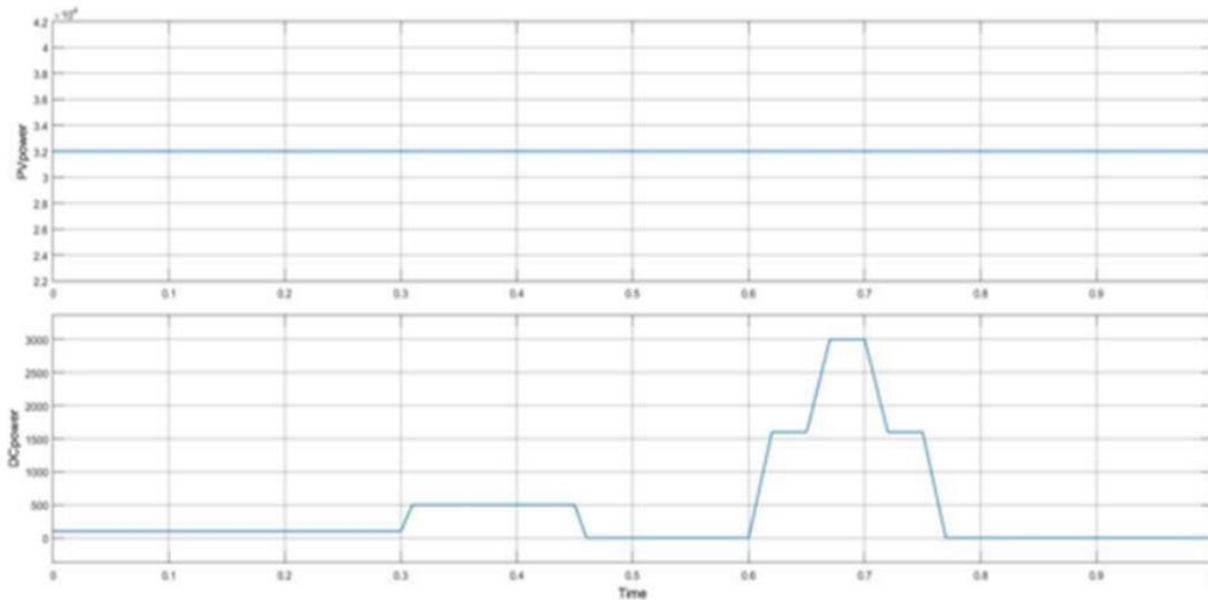


Fig 4. PV power and DC power

Moreover, the results shed light on the system's overall performance in real-world scenarios, including its ability to seamlessly integrate renewable energy sources, manage energy storage efficiently, and enhance grid resilience. By comparing performance metrics such as energy generation, storage efficiency, power quality indices, and grid stability measures against predefined benchmarks and industry standards, the project team can assess the system's effectiveness and identify areas for improvement.

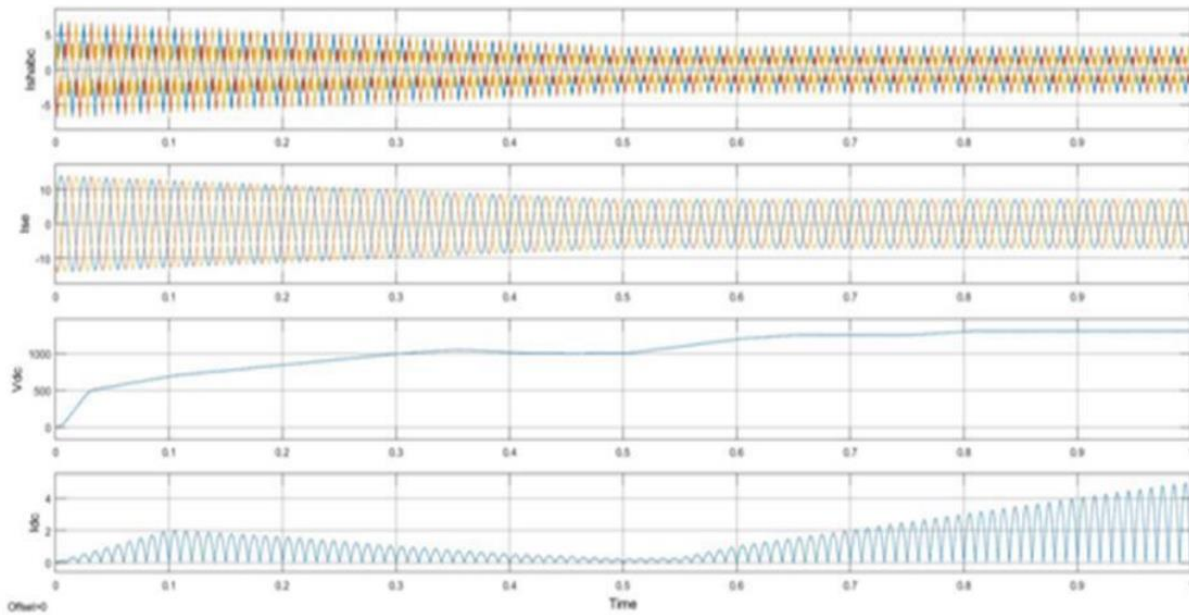


Fig 5. DC voltage and current

Furthermore, the discussion delves into the implications of the obtained results in the context of renewable energy integration, power quality enhancement, and grid resilience. Key findings are analyzed, and their significance in addressing the project objectives is explored. Insights into the system's strengths, weaknesses, opportunities, and threats are discussed, along with potential strategies for optimization and further improvement.

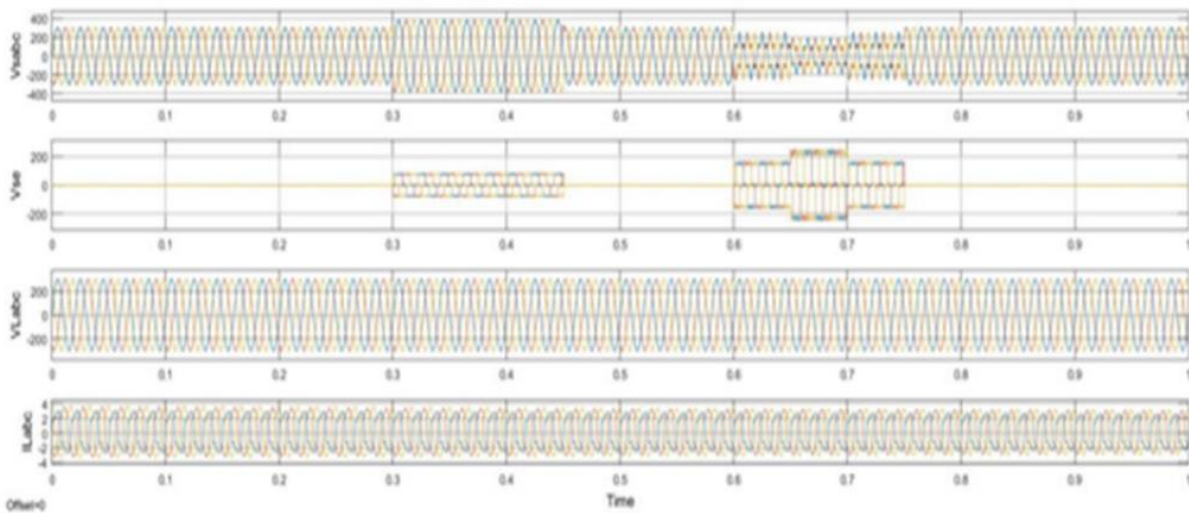


Fig 6. Load currents and load voltages

Moreover, the discussion addresses the broader implications of the integrated system in the context of the evolving energy landscape and the transition towards a more sustainable and resilient power infrastructure. By highlighting the system's potential benefits in terms of reducing carbon emissions, enhancing energy security, and promoting grid stability, the discussion underscores its importance in supporting the transition to a clean, renewable energy future.

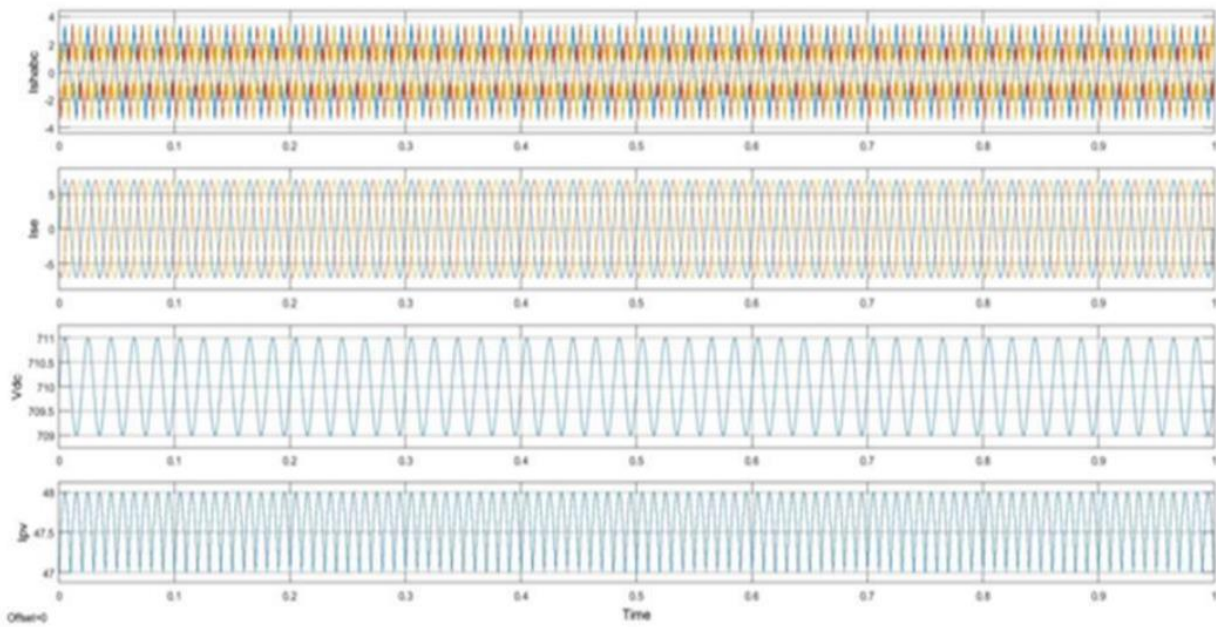


Fig 7. PV currents and DC voltages

Furthermore, the discussion examines the scalability and replicability of the integrated system, considering factors such as cost-effectiveness, technological feasibility, and regulatory considerations. Insights into potential barriers and challenges to widespread adoption are discussed, along with strategies for overcoming them and accelerating the deployment of similar integrated systems in diverse settings.

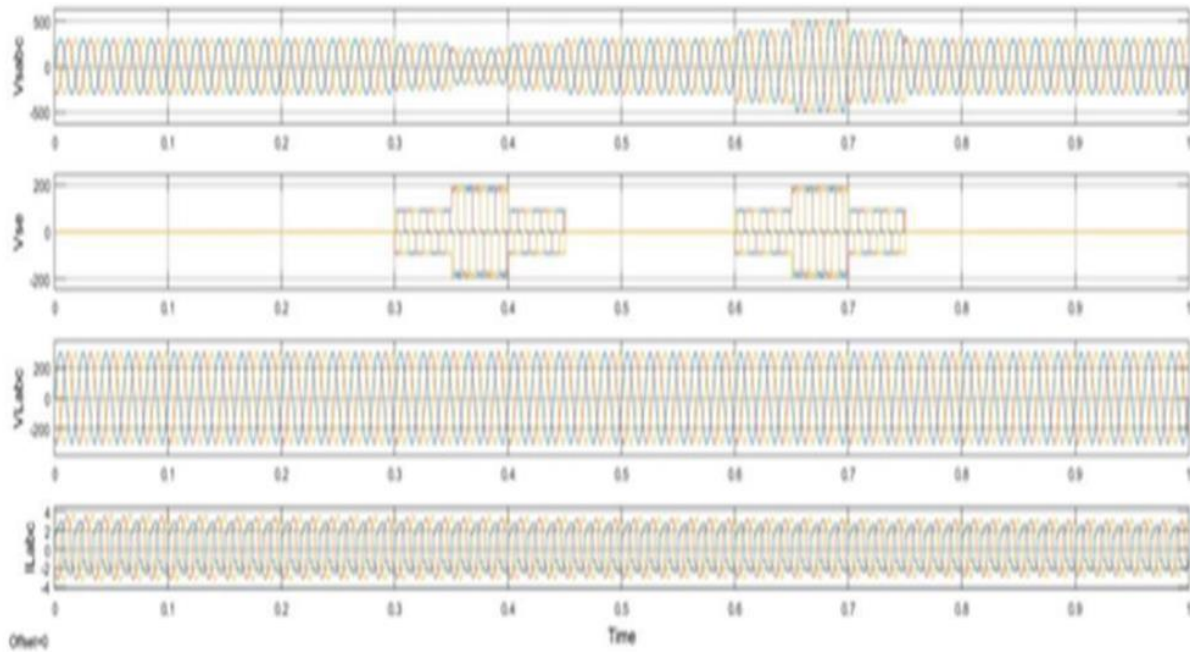


Fig 8. Load currents and load voltages

Additionally, the discussion explores potential areas for future research and development, including advancements in solar PV technology, battery storage systems, power electronics, and grid integration strategies. By identifying emerging trends, technological innovations, and research gaps, the discussion sets the stage for further exploration and innovation in the field of renewable energy integration and power system resilience.

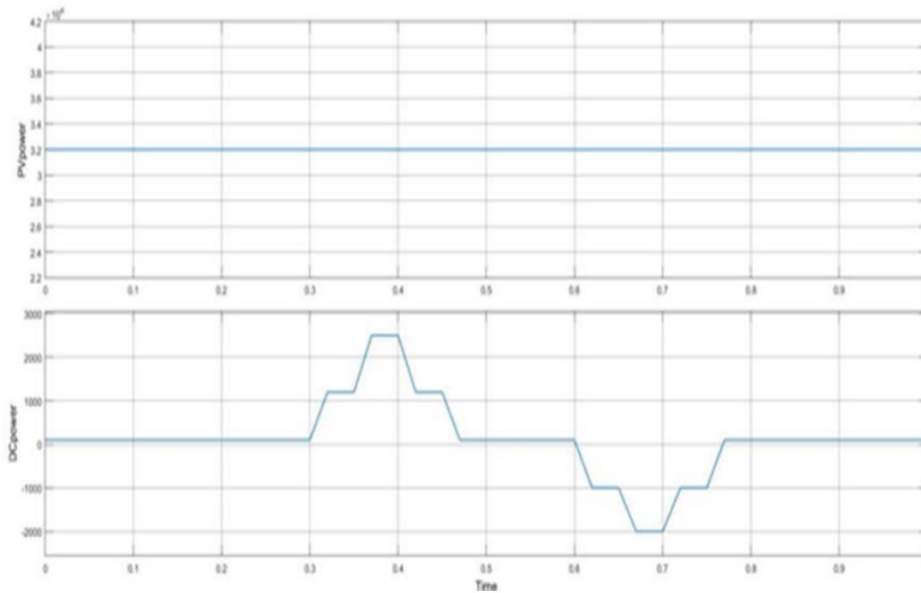


Fig 9. DC power and PV power

In conclusion, the results and discussion section provides a comprehensive analysis of the performance investigation of the three-phase solar PV and battery energy storage system integrated with UPQC. By examining the system's performance metrics, discussing key findings, and exploring their implications, valuable insights are gained into the system's effectiveness, challenges, and potential for contributing to renewable energy integration, power quality enhancement, and grid resilience.

CONCLUSION

The construction of three phase UPQC has been investigated considering the condition of complex power quality problems which are an amalgamation of harmonics, voltage swell, and sags, and voltage interruption under unbalanced and distorted voltage grid condition. Integrating the BESS and PV with the UPQC provides active power capability to the network. The main benefit of BESS integrated with UPQC is that it makes the system capable of supplying and absorbing active power from the PV. Since renewable energy is not completely reliable because of its environment-dependent feature, integrating a BESS will solve the lack of renewable energy resources. Finally, it can be figured that the BESS and PV attached with UPQC can be a good alternative in the distributed generation to upgrade the power quality of the contemporary distribution system. The DC-link voltage is stable because of the continuous supply from the PV-BESS system. Therefore, it can reduce the complexity of the DC-link voltage regulation algorithm. The STF-UVG technique for synchronization phases is applied successfully in the shunt and series APF compensator to generate reference current and voltage. Thus, the UPQC is designed without relying on the PLL components, and mitigation of current and voltage are achieved successfully following the grid condition to ensure the system stability and to achieve almost unity power factor. The implementation of the proposed technique has confirmed that the grid current harmonics follow the IEEE519 standard. Finally, it is worth mentioning that the proposed system can enhance the overall efficiency of the grid power system.

REFERENCES



- [1]. D. Sera, R. Teodorescu, M. Kerekes, and F. Blaabjerg, "Design and Control of Three-Phase Inverter for Grid-Connected Photovoltaic Systems," in IEEE Transactions on Industrial Electronics, vol. 55, no. 7, pp. 2610-2621, July 2008.
- [2]. N. A. Rahim, S. Mekhilef, and J. Selvaraj, "Recent Advances in Solar Photovoltaic Power Conversion Systems," in Renewable and Sustainable Energy Reviews, vol. 19, pp. 255-271, February 2013.
- [3]. P. H. Le, T. K. Nguyen, D. Q. Hung, and T. D. Tuan, "Battery Energy Storage System: Overview and its Applications," in IOP Conference Series: Earth and Environmental Science, vol. 272, no. 5, 2021.
- [4]. M. Rizwan, S. Mekhilef, N. A. Rahim, "Battery Energy Storage System: A Review of Sustainable Technologies," in Energies, vol. 13, no. 3, 2020.
- [5]. J. Guerrero, M. Chandorkar, T. Lee, P. Mattavelli, and R. Teodorescu, "Advanced Control Architectures for Intelligent Microgrids—Part I: Decentralized and Hierarchical Control," in IEEE Transactions on Industrial Electronics, vol. 60, no. 4, pp. 1254-1262, April 2013.
- [6]. L. Yao, J. Li, W. Wu, and M. Yu, "A Review of Power Quality Improvement Techniques for Microgrid System," in Energy Procedia, vol. 17, pp. 216-223, 2012.
- [7]. B. Singh, K. Al-Haddad, and A. Chandra, "A Review of Active Filters for Power Quality Improvement," in IEEE Transactions on Industrial Electronics, vol. 46, no. 5, pp. 960-971, October 1999.
- [8]. H. Karimi, S. M. Mousavi, M. A. S. Masoum, and E. Afjei, "Review of Power Quality Improvement Methods in Microgrids Considering Storage Systems," in Renewable and Sustainable Energy Reviews, vol. 98, pp. 299-316, August 2018.
- [9]. M. Bollen, "Understanding Power Quality Problems: Voltage Sags and Interruptions," in IEEE Press, 2000.
- [10]. S. Chowdhury and P. Crossley, "Understanding FACTS: Concepts and Technology of Flexible AC Transmission Systems," in IEEE Press, 2002.
- [11]. M. Noroozian and J. M. Guerrero, "Unified Power Quality Conditioner (UPQC): Topologies, Modeling, Control, and Applications," in IEEE Transactions on Power Electronics, vol. 29, no. 5, pp. 2488-2506, May 2014.
- [12]. N. Ghaffarzadeh and J. M. Guerrero, "Optimal Design and Placement of Unified Power Quality Conditioner in a Power Distribution System: A Comprehensive Review," in Energies, vol. 14, no. 6, 2021.
- [13]. M. Ferdowsi, H. Lesani, S. S. Mortazavi, and J. M. Guerrero, "Optimal Sizing and Placement of UPQC in Distribution Systems Considering Energy Losses and Voltage Sag Severity," in IEEE Transactions on Smart Grid, vol. 10, no. 4, pp. 4276-4286, July 2019.
- [14]. T. Esram and P. L. Chapman, "Comparison of Photovoltaic Array Maximum Power Point Tracking Techniques," in IEEE Transactions on Energy Conversion, vol. 22, no. 2, pp. 439-449, June 2007.
- [15]. M. O. Balogun, P. Pillay, and D. G. Dorrell, "MPPT Strategies for Photovoltaic Systems: A Review," in Renewable and Sustainable Energy Reviews, vol. 50, pp. 1004-1016, December 2015.
- [16]. Renewable energy system based stand alone system for dc-ac converter fed BLDC motor, Authors: T Rushi Santhosh Singh G Sirisha, MD Kouser, Publication date: 2016/12, Journal-IJR, Volume-3, Issue-18



International Journal For Advanced Research In Science & Technology

A peer reviewed international journal

www.ijarst.in

ISSN: 2457-0362

IJARST

Certificate

This is to Certify that Prof./Dr./Mr./Ms./ **Mrs. E Gowthami** from Rise Krishna Sai Prakasam Group of Institutions.Presented a paper Construction and Performance Investigation of Three -Phase Solar PV and Battery Energy Storage System Integrated UPQC In the Organizing Committee of Asian Science Research

Published in International Journal For Advanced Researchs In Science & Technology. Research (IJARST), Vol-14, Issue-04 Apr-2024




Editor In Chief
N.C KARNAKARAN



IJARST

International Journal For Advanced Research In Science & Technology

A peer reviewed international journal

www.ijarst.in

ISSN: 2457-0362

Certificate

This is to Certify that Prof./Dr./Mr./Ms./ **G. Jahnavi** from Rise Krishna Sai Prakasam Group of Institutions.Presented a paper Construction and Performance Investigation of Three -Phase Solar PV and Battery Energy Storage System Integrated UPQC In the Organizing Committee of Asian Science Research

Published in International Journal For Advanced Research In Science & Technology. Research (IJARST), Vol-14, Issue-04 Apr-2024




Editor In Chief
N.C KARNAKARAN



International Journal For Advanced Research In Science & Technology

A peer reviewed international journal

www.ijarst.in

ISSN: 2457-0362

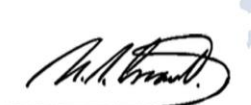
IJARST

Certificate

This is to Certify that Prof./Dr./Mr./Ms./ **J. Anitha** from Rise Krishna Sai Prakasam Group of Institutions.Presented a paper Construction and Performance Investigation of Three -Phase Solar PV and Battery Energy Storage System Integrated UPQC In the Organizing Committee of Asian Science Research

Published in International Journal For Advanced Researchs In Science & Technology. Research (IJARST), Vol-14, Issue-04 Apr-2024




Editor In Chief

N.C KARNAKARAN



International Journal For Advanced Research In Science & Technology

A peer reviewed international journal

www.ijarst.in

IJARST

ISSN: 2457-0362

Certificate

This is to Certify that Prof./Dr./Mr./Ms./ **K. Venkatesh** from Rise Krishna Sai Prakasam Group of Institutions. Presented a paper Construction and Performance Investigation of Three -Phase Solar PV and Battery Energy Storage System Integrated UPQC In the Organizing Committee of Asian Science Research

Published in International Journal For Advanced Researchs In Science & Technology. Research (IJARST), Vol-14, Issue-04 Apr-2024




Editor In Chief
N.C KARNAKARAN



International Journal For Advanced Research In Science & Technology

A peer reviewed international journal

www.ijarst.in

IJARST

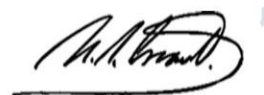
ISSN: 2457-0362

Certificate

This is to Certify that Prof./Dr./Mr./Ms./ **P. Madhan Mohan** from Rise Krishna Sai Prakasam Group of Institutions.Presented a paper Construction and Performance Investigation of Three -Phase Solar PV and Battery Energy Storage System Integrated UPQC In the Organizing Commitee of Asian Science Research

Published in International Journal For Advanced Researchs In Science & Technology. Research (IJARST), Vol-14, Issue-04 Apr-2024




Editor In Chief
N.C KARNAKARAN



International Journal For Advanced Research In Science & Technology

A peer reviewed international journal

www.ijarst.in

ISSN: 2457-0362

IJARST

Certificate

This is to Certify that Prof./Dr./Mr./Ms. **L.Chadrakanth Naidu** from Rise Krishna Sai Prakasam Group of Institutions.Presented a paper Construction and Performance Investigation of Three -Phase Solar PV and Battery Energy Storage System Integrated UPQC In the Organizing Committee of Asian Science Research

Published in International Journal For Advanced Researchs In Science & Technology. Research (IJARST), Vol-14, Issue-04 Apr-2024



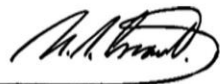

Editor In Chief
N.C KARNAKARAN

TABLE OF CONTENTS

ABSTRACT	I
LIST OF FIGURES	II
LIST OF ABBREVIATIONS	III
CHAPTER 1: INTRODUCTION	1-20
1.Photo voltaic (PV) power system & solar power generator	1
1.1: Principle of solar electricity	2
1.2: Application of solar electricity	2
1.3: Stand alone or off solar electricity	4
1.4: Grid tie solar power station	4
1.5: Grid tie with power backup solar power generation	6
1.6: grid fall back solar power generation	6
1.7: Constitution of solar cells	8
1.8: Working principle of solar cells	8
1.9: Materials used in solar cells	9
1.10: Characteristics and parameters of solar cell	9
1.11: Short circuit of solar cells	10
1.12: Solar cell manufacturing technology	12
CHAPTER 2: LITERATURE SURVEY	21-24
CHAPTER 3: BATTERY ENERGY STORAGE SYSTEM	25-28
3.1: Energy storage system over view	25
3.2: BLOCK DIAGRAM OF BESS	26
3.3: Types of BESS system	27
CHAPTER 4: SYSTEM CONSTRUCTION	29-33
CHAPTER 5: PROPOSED METHOD	34-36
5.1: Objectives	34
5.2: System Design	34
5.3: Construction Plan	35
5.4: Performance Monitoring and Control	35
5.5: Environmental Impact Assessment	35
5.6: Economic Analysis	35
5.7: Regulatory Compliance	35
5.8: Block Diagram	36

5.9: Conclusion	36
5.10: References	36
5.11: Appendices	36
CHAPTER 6: MATLAB HISTORY	37-40
6.1: MATLAB Uses	37
6.2: Key features	38
6.3: Basic MATLAB Commands	39
6.4: Applications	39
6.5: Conclusion	40
CHAPTER 7: MATLAB SIMULATION	41-47
7.1: Key simulation features	41
7.2: Optimization and parameter estimation	42
7.3: Basic simulation workflow	42
7.4: Applications	42
7.5: Simulation block diagram	43
7.6: Conclusion of simulation matlab	47
CONCLUSION	48
REFERENCES	49

ABSTRACT

This project focuses on the construction and performance investigation of a Three-Phase Solar PV and Battery Energy Storage System integrated with a Unified Power Quality Conditioner (UPQC). The integration of renewable energy sources, such as solar photovoltaic (PV) systems, with battery energy storage systems (BESS) and UPQC technology aims to address key challenges in modern power systems, including voltage sags, harmonics, and power quality issues. The project involves the design, implementation, and evaluation of the integrated system to optimize its performance in real-world scenarios. Through comprehensive performance investigation and analysis, the project aims to enhance renewable energy integration, improve power quality, increase grid resilience, and optimize system performance.

LIST OF FIGURE

Fig. No.	Figure Name	Page No.
1.1	PV power systems and solar power Generation	1
1.2	Solar Module	2
1.3	Application of Solar Electricity	3
1.4	Stand Alone or Off Grid Solar Power Station	4
1.5	Grid Tie Solar Power Station	5
1.6	Solar Panels	7
1.7	Construction of Solar Cell	8
1.8	V-I Characteristics of a Photovoltaic Cell	8
1.9	V-I Characteristics of Current at Maximum Power Point	11
1.10	Solar Cells	13
1.11	PV cell waveforms at 25 °C and irradiance variation	16
1.12	PV cell waveforms at different temperature and designated irradiance	17
1.13	Flow Chart of Perturb & Observe Algorithm	18
1.14	PV DC-DC Boost Converter Control Scheme	19
3.1	BESS Block diagram	26
4.1	UPQC system configuration	29
4.2	PV-BESS system configuration	33
4.3	Single-diode PV cell equivalent circuit	33
5.1	Proposal method of PV and BESS integrated UPQC	36
7.1	Simulation Diagram	43
7.2	Three phase Load Current and Load Voltage	43
7.3	Current at PV and voltage DC OUTPUT voltage	44
7.4	PV power and DC power	44
7.5	DC voltage and current	45
7.6	Load currents and load voltages	45
7.7	PV currents and DC voltages	46
7.8	Load currents and load voltages	46
7.9	DC power and PV power	47

LIST OF ABBREVIATIONS

PV	Photovoltaic
BESS	Battery Energy Storage System
UPQC	Unified Power Quality Conditioner
PLL	Phase Locked Loop
STF	Self Tuning Filter
UVG	Unit vector generator
APF	Active power filter
SRF	Synchronous reference frame
MPPT	Maximum power point tracking
PWM	Pulse width modulation
PI Control	Proportional Integral
MATLAB	Matrix Laboratory

CHAPTER -1

INTRODUCTION

The integration of renewable energy sources, such as solar photovoltaic (PV) systems, with energy storage technologies has become increasingly important in modern power systems. This integration enables better utilization of renewable energy resources, enhances grid stability, and facilitates the transition towards a sustainable energy future. In our main project, we focus on the construction and performance investigation of a Three- Phase Solar PV and Battery Energy Storage System integrated with a Unified Power Quality Conditioner (UPQC). The project aims to address key challenges in power systems, including voltage sags, harmonics, and power quality issues, by combining solar PV generation with battery energy storage and UPQC technology. By integrating these components, we seek to achieve multiple objectives, including enhancing renewable energy integration, improving power quality, increasing grid resilience, and optimizing system performance. In this introduction, we provide an overview of the main project objectives, highlighting the significance of integrating solar PV, battery energy storage, and UPQC technologies for enhancing power system performance and sustainability. Through this project, we contribute to the advancement of renewable energy technologies and the transition towards a cleaner and more resilient energy future.

1. Photovoltaic (PV) power systems and solar power Generation

Solar power generation:

When sunlight strikes on photovoltaic solar panels solar electricity is produced. That is why this is also referred to as photovoltaic solar, or PV solar.

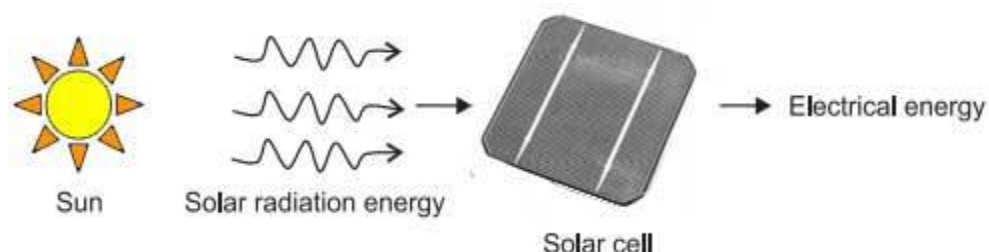


Fig.1.1 photovoltaic (pv) power systems and solar generation

1.1: Principles of Solar Electricity

Generation of electricity by using solar energy depends upon the photovoltaic effect in some specific materials. There are certain materials that produce electric current when these are exposed to direct sun light. This effect is seen in combination of two thin layers of semiconductor materials. One layer of this combination will have a depleted number of electrons. When sunlight strikes on this layer it absorbs the photons of sunlight ray and consequently the electrons are excited and jump to the other layer. This phenomenon creates a charge difference between the layers and resulting to a tiny potential difference between them. The unit of such combination of two layers of semiconductor materials for producing electric potential difference in sunlight is called solar cell. Silicon is normally used as the semiconductor material for producing such solar cell. For building cell silicon material is cut into very thin wafers. Some of these wafers are doped with impurities. Then the un-doped and doped wafers are then sandwiched together to build solar cell. Metallic strip is then attached to two extreme layers to collect current. Conductive metal strips attached to the cells take the electrical current. One solar cell or photovoltaic cell is not capable of producing desired electricity instead it produces very tiny amount of electricity hence for extracting desired level of electricity desired number of such cells are connected together in both parallel and series to form a solar module or photovoltaic module.

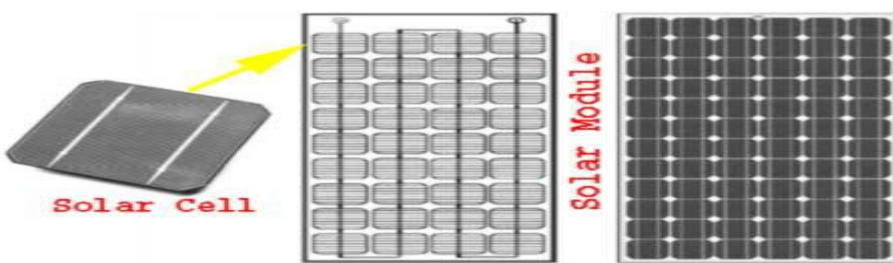


Fig.1.2. Solar Module

1.2.APPLICATION OF SOLAR ELECTRICITY

Solar electric power generation system is useful for producing moderate amount of power. The system works as long as there is a good intensity of natural sunlight. The place where solar modules are installed should be free from obstacles such as trees and buildings otherwise there will be shade on the solar panel which affects the

performance of the system. It is a general view that solar electricity is an impractical alternative of conventional source of electricity and should be used when there is no traditional alternative of conventional source of electricity available. But this is not the actual case. Often it is seem that solar electricity is more money saving alternative than other traditional alternatives of conventional electricity.

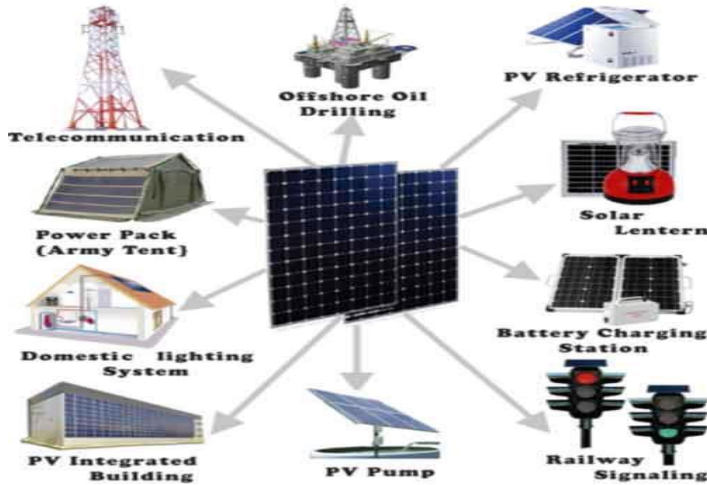


Fig.1.3 Applications of solar electricity

It is always economical to install a solar light or a solar power source where it is difficult and costly to get point from local electric supply authority such as in remote garden, shed or garage where standard electric supply point is not available. Solar electricity system is more reliable and uninterrupted as it does not suffer from unwanted power cut from electric supply company. For constructing a mobile electric power source, for moderate power requirements solar module is good choice. It can be useful whilst camping, working on outdoor sites. It is most effective means for creating green energy for our own purpose and may be for selling surplus energy to customers but for producing electricity in commercial scale the investment and volume of the system becomes large enough. In that case area of the project will be much larger than conventional one. Although for running few lights and low power electrical gadgets such as laptop computer, portable sized television, mini fridge etc. solar electricity system is quite suitable provided there is sufficient free space on ground or on roof top for installing solar panels. But it is not at all economical to run high-power consuming electric equipment like high speed fans, heaters, washing machines, air conditioners and power tools with the help of solar electricity as the cost of production such high energy is quite higher that it is expected. More over there may be lack of space availability in your premises for

installation of large solar panel. Ideal uses of low-cost solar panels are charging batteries in caravans and recreational vehicles or on boats when these are not in movement provided there should be tickle charging facility from dynamo during movement of these vehicles.

TYPES OF SOLAR POWER STATION

There are mainly four types of solar power stations.

1. Stand Alone or Off Grid type Solar Power Plant
2. Grid Tie type Solar Power Plant
3. Grid Tie with Power Backup or Grid Interactive type Solar Power Plant
4. Grid Fallback type Solar Power Plant.

Let us discuss a brief introduction of each type of solar power plant.

1.3: STAND ALONE OR OFF GRID SOLAR POWER STATION

This is most commonly used photovoltaic installation used to provide localized electricity in absence of conventional source of electric power at certain location. As the name prefers this system does not keep any direct or indirect connection with any grid type network. In standalone system the solar modules produce electric energy which is utilized to charge a storage battery and this battery delivers electricity to the connected load. Standalone systems are normally small system with less than 1 kilo watt generation capacity.



Fig.1.4 stand alone or off grid solar power station

1.4: GRID TIE SOLAR POWER STATION

In some countries facility is available of selling power to the local or national grid. This is gaining popularity in Europe and the United States. This system facilitates both electric utility companies as well as the consumers. Here consumers can generate electricity by their own plant and can sell the surplus to the electricity utility company through grid connected to their plant. As the consumers sell the power they can earn money as return of their investment for installation of captive

power plant on the other hand electric utility companies can reduce their capital investment on their own plant for power generation. In a grid-tie solar system, consumers consume electricity produced by solar captive power plant during sunny day time and also export surplus energy to grid but at night while solar plant does not produce energy, they import electric energy from grid for consumption. The main disadvantage of this system is that if there is a power cut in the grid, the solar modules should be disconnected from the grid.

Grid tie solar systems are of two types one with single macro central inverter and other with multiple micro inverters. In the former type of solar system, the solar panels as well as grid supply are connected to a common central inverter called grid tie inverter as shown below. The inverter here converts the DC of the solar panel to grid level AC and then feeds to the grid as well as the consumer's distribution panel depending upon the instant demand of the systems. Here grid-tie inverter also monitors the power being supplied from the grid. If it finds any power cut in the grid, it actuates switching system of the solar system to disconnect it from the grid to ensure no solar electricity can be fed back to the grid during power cut. There is an energy meter connected in the main grid supply line to record the energy export to the grid and energy import from the grid.

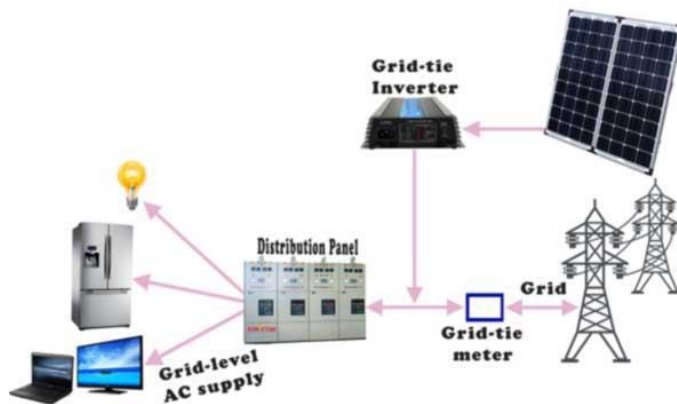


Fig.1.5 Grid tie solar power station

As we already told there is another type of grid-tie system where multiple micro-inverters are used. Here one micro inverter is connected for each individual solar module. The basic block diagram of this system is very similar to previous one except the micro inverters are connected together to produce desired high AC voltage. In previous case the low direct voltage of solar panels is first converted to alternating

voltage then it is transformed to high alternating voltage by transformation action in the inverter itself but in this case the individual alternating output voltage of micro inverters are added together to produce high alternating voltage.

1.5: GRID TIE WITH POWER BACKUP SOLAR POWER GENERATION

It is also called grid interactive system. This is a combination of a grid-tie solar power generation unit and storage battery bank. As we said, the main drawback of grid tie system is that when there is any power cut in the grid the solar module is disconnected from the system. For avoiding discontinuity of supply during power cut period one battery bank of sufficient capacity can be connected with the system as power backup.

1.6: GRID FALBACK SOLAR POWER GENERATION

Grid fallback is most reliable and stable system mainly used for electrifying smaller households. Here solar modules charge a battery bank which in turn supplies distribution boards through an inverter. When the batteries are discharged to a pre-specified level, the system automatically switches back to the grid power supply. The solar modules then recharge the batteries and after the batteries are being charged up to a pre-specified level again the system switches back to solar power. We do not sell electricity back to the electricity utility companies through this system. All the power that we produce is utilized for ourselves only. Although we do not have any direct earning benefit from this system but the system has its own big advantages. This system is most popular where there is no facility of selling power to the grid. Grid fallback system has all advantages of grid interactive system except power selling, but it adds benefit of using own power whenever it is required irrespective of position and condition of sun in the sky. Components of a Solar Electric Generating System

1.6.1: SOLAR PANELS

The main part of a solar electric system is the solar panel. There are various types of solar panel available in the market. Solar panels are also known as photovoltaic solar panels. Solar panel or solar module is basically an array of series and parallel connected solar cells. The potential difference developed across a solar cell is about 0.5 volt and hence desired number of such cells to be connected in series to achieve 14 to 18 volts to charge a standard battery of 12 volts. Solar panels are

connected together to create a solar array. Multiple panels are connected together both in parallel and series to achieve higher current and higher voltage respectively.

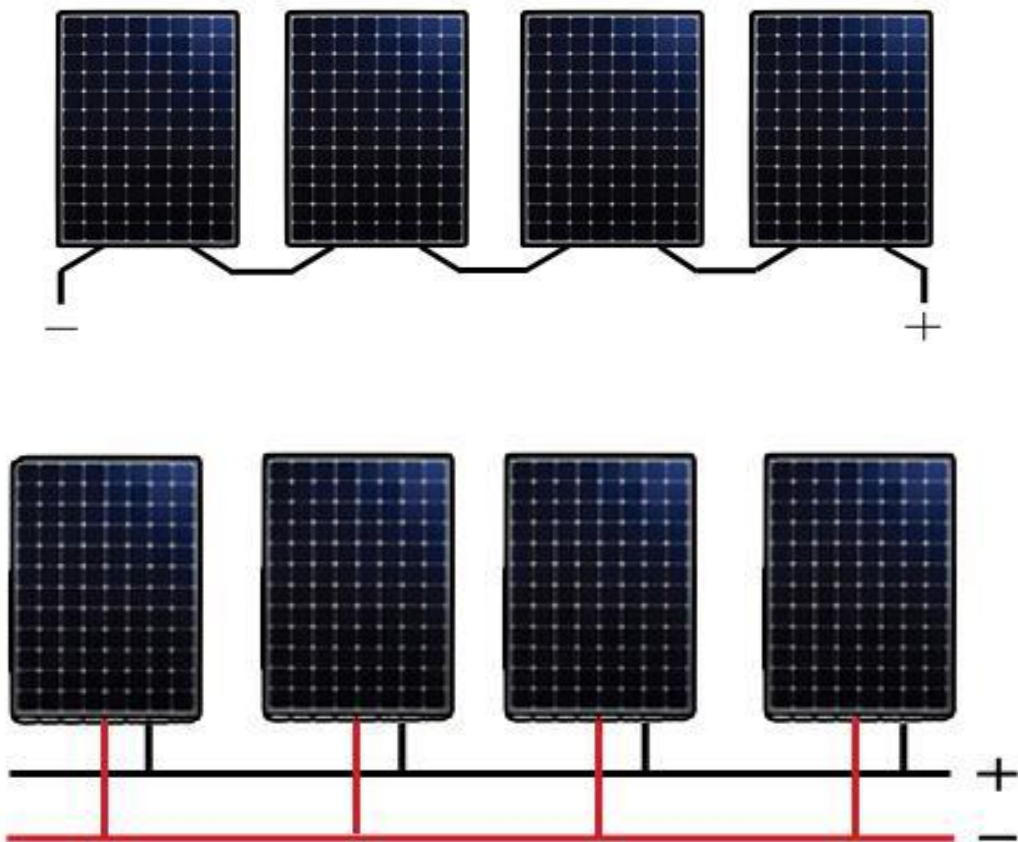


Fig.1.6. Solar Panels

1.6.2: SOLAR CELL

The name “solar cell” means that it is a cell or a plate which converts solar energy into the useful electrical energy. The energy which we get from sun is enormous and it is a great source of energy. Its energy will never finish so this is also known as as the main source of renewable energy. With the scarcity of non-renewable energy it is of utmost importance to find a way out to solve the energy problem by some means within a very short period of time. So there is a way out which is now developing. That is we are now able to convert the sun energy to electrical by some means and that is why the importance of solar cell comes into play. Though it is developing but if it is developed completely, then every household may produce the energy of its own. The solar cell is a device which is made of p-n junction diode which effect photovoltaic effect to convert light energy into electrical energy.

1.7: CONSTRUCTION OF SOLAR CELL

The junction diode is made of SI OR GaAS. A thin layer of p-type is grown on the n-type semiconductor. Top of the p-layer is provided with a few finer electrodes which leaves open space for the light to reach the thin p-layer and it under lays p-n junction. Bottom of the n-layer is provided with a current collecting electrode.

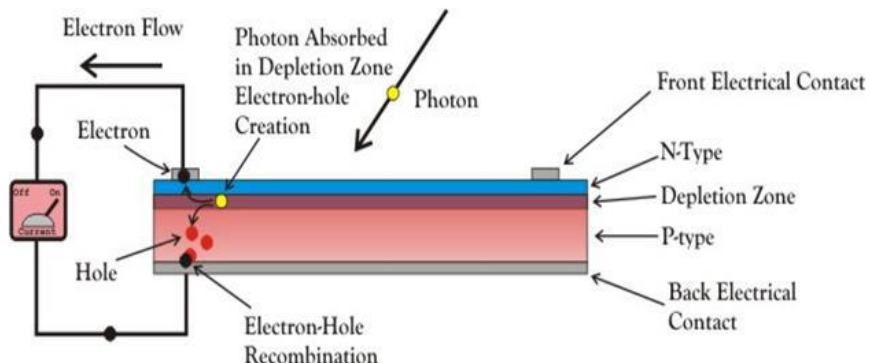


Fig.1.7 Construction of solar cells

1.8: WORKING PRINCIPLE OF SOLAR CELL

When light reaches the p-n junction, electron is excited to the valance band under the condition that light energy is higher than the band gap energy; it generates the electron and holes which are equal in number in the valance and conduction band respectively. These electron hole pairs move in opposite directions to the barrier field. Electrons move towards the n-side and the hole is moved towards the p-side. So a voltage is set up which is known as photo voltage and when a load is connected, the current flows.

1.8.1: V-I Characteristics of a Photovoltaic Cell

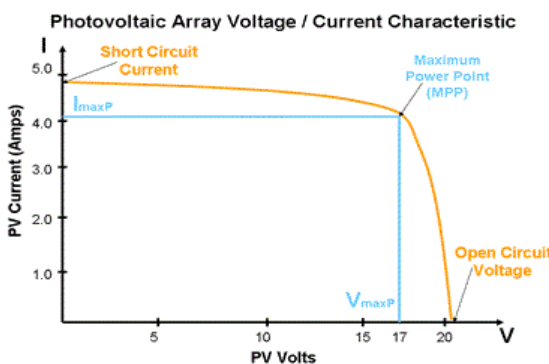


Fig.1.8. V-I Characteristics of a Photovoltaic Cell

1.9: MATERIALS USED IN SOLAR CELL

The materials which are used for this purpose must have band gap close to 1.5ev.

Commonly used materials are-

- Silicon
- GaAs
- CdTe
- CuInSe₂

1.9.1: CRITERIA FOR MATERIALS TO BE USED IN SOLAR CELL

- Must have band gap from 1ev to 1.8ev.
- It must have high optical absorption.
- It must have high electrical conductivity.
- The raw material must be available in abundance and the cost of the material must be low.

1.9.2: ADVANTAGES OF SOLAR CELL

- No pollution associated with it
- It must last for a long time
- No maintenance cost

1.9.3: DISADVANTAGES OF SOLAR CELL

- It has high cost of installation.
- It has low efficiency.
- During cloudy day, the energy cannot be produced and also at night we will not get solar energy.

1.9.4: USES OF SOLAR GENERATION SYSTEMS

- It may be used to charge batteries
- Used in light meters
- It is used to power calculators and wrist watches

1.10: CHARACTERISTICS AND PARAMETERS OF A SOLAR CELL

Solar cell is the basic unit of solar energy generation system where electrical energy is extracted directly from light energy without any intermediate process. The working of a solar cell solely depends upon its photovoltaic effect hence a solar cell also known as photovoltaic cell. A solar cell is basically a semiconductor device. The solar cell produce electricity while light strikes on it and the voltage or potential difference established across the terminals of the cell is fixed to 0.5 volt and it is

nearly independent of intensity of incident light whereas the current capacity of cell is nearly proportional to the intensity of incident light as well as the area that exposed to the light. Each of the solar cells has one positive and one negative terminal like all other type of battery cells. Typically a solar or photovoltaic cell has negative front contact and positive back contact. A semiconductor p-n junction is in the middle of these two contacts. While sunlight falling on the cell the some photons of the light are absorbed by solar cell. Some of the absorbed photons will have energy greater than the energy gap between valence band and conduction band in the semiconductor crystal. Hence one valence electron gets energy from one photon and becomes excited and jumps out from the bond and creates one electron – hole pair. These electrons and holes of e-h pairs are called light-generated electrons and holes. The light – generated electrons near the p-n junction are migrated to n-type side of the junction due to electrostatic force of the field across the junction. Similarly the light generated holes created near the junction are migrated to p – type side of the junction due to same electrostatic force. In this way a potential difference is established between two sides of the cell and if these two sides are connected by an external circuit current will start flowing from positive to negative terminal of the solar cell. This was basic working principle of a solar cell now we will discuss about different parameters of a solar or photovoltaic cell upon which the rating of a solar panel depends. During choosing a particular solar cell for specific project it is essential to know the ratings of a solar panel. These parameters tell us how efficiently a solar cell can convert the light to electricity.

1.11: SHORT CIRCUIT CURRENT OF SOLAR CELL

The maximum current that a solar cell can deliver without harming its own constriction. It is measured by short circuiting the terminals of the cell at most optimized condition of the cell for producing maximum output. The term optimized condition I used because for fixed exposed cell surface the rate of production of current in a solar cell also depends upon the intensity of light and the angle at which the light falls on the cell. As the current production also depends upon the surface area of the cell exposed to light, it is better to express maximum current density instead maximum current. Maximum current density or short circuit current density rating is nothing but ration of maximum or short circuit current to exposed surface area of the cell.

$$J_{sc} = \frac{I_{sc}}{A}$$

Where, I_{sc} is short circuit current, J_{sc} maximum current density and A is the area of solar cell.

1.11.1: OPEN CIRCUIT VOLTAGE OF SOLAR CELL

It is measured by measuring voltage across the terminals of the cell when no load is connected to the cell. This voltage depends upon the techniques of manufacturing and temperature but not fairly on the intensity of light and area of exposed surface. Normally open circuit voltage of solar cell nearly equal to 0.5 to 0.6 volt. It is normally denoted by V_{oc} .

1.11.2: MAXIMUM POWER POINT OF SOLAR CELL

The maximum electrical power one solar cell can deliver at its standard test condition. If we draw the v-i characteristics of a solar cell maximum power will occur at the bend point of the characteristic curve. It is shown in the v-i characteristics of solar cell by P_m .

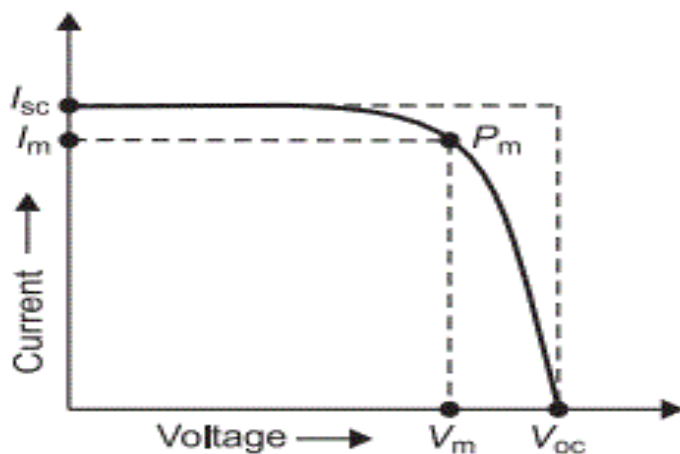


Fig.1.9.VI Characteristics of a solar cell

CURRENT AT MAXIMUM POWER POINT

The current at which maximum power occurs. Current at Maximum Power Point is shown in the v-i characteristics of solar cell by I_m .

VOLTAGE AT MAXIMUM POWER POINT

The voltage at which maximum power occurs. Voltage at Maximum Power Point is shown in the v-i characteristics of solar cell by V_m .

FILL FACTOR OF SOLAR CELL

The ratio between product of current and voltage at maximum power point to the product of short circuit current and open circuit voltage of the solar cell.

$$\text{Fill Factor} = \frac{P_m}{I_{sc} \times V_{oc}}$$

EFFICIENCY OF SOLAR CELL

It is defined as the ratio of maximum electrical power output to the radiation power input to the cell and it is expressed in percentage. It is considered that the radiation power on the earth is about 1000watt/square meter hence if the exposed surface area of the cell is A then total radiation power on the cell will be 1000A watts. Hence the efficiency of a solar cell may be expressed as

$$\text{Efficiency}(\eta) = \frac{P_m}{P_{in}} \approx \frac{P_m}{1000A}$$

1.12: SOLAR CELL MANUFACTURING TECHNOLOGY

There are different types of solar of photovoltaic cells available in the market. Each of them has its own technical and commercial advantages as well as disadvantages. The solar cells are mainly categorized on the basis of the materials used as semiconductor in the cell. Different types of solar cell have different technical parameters but they can be chosen for use in different applications depending upon the optimum conditions of the services. The main raw material used to construct a solar cell is semiconductor material and silicon is widely used semiconductor for that. There is plenty of availability of silicon on the earth. Silicon is available in normal sand. But extracting pure silicon from the natural sources is quite expensive. Lots of efforts are required for that work. In the process silicon is purified, melted, and crystallized. Continuous researches and developments are going on to reduce the quantity of silicon used in the solar cell without affecting its performance. This ensures the availability of cheaper solar cells. Two most common techniques of producing silicon wafers are the chzrolaski (CZ) and floating zone (FZ) techniques.

1.12.1: CRYSTALLINE SILICON SOLAR CELL

Crystalline Silicon Solar Cell has most advantageous against other available technologies of solar cell manufacturing. But these cells require purified silicon as raw material which is quite expensive. Here naturally available silicon quartzes

are melted, purified and then crystallized in ingots. Then these ingots then further cut into smaller sized ingots and then these ingots are sliced into number of thin silicon wafers. These wafers were generally made 0.3 mm thick in early days, but now technology has developed to make them about 0.15mm thick. This thickness of the silicon crystal wafer is important in the view of cost optimization of the cell. Then these wafers are chemically treated for doping with impurities to create p-n-junction across them. Then negative and positive metallic contacts are fabricated on top and bottom the cells by screen printing techniques. The cells typically produce 0.5 to 0.6 volts across them at standard working conditions hence numbers of such cells are wired in series to produce standard 6 or 12 volts. Numbers of such series combinations are then arrayed in parallel on a glass substrate or some kind of insulated reinforced base substrate to increase the power capacity of the module. Then the module is covered with none conducting transparent encapsulating resin and then a protective transparent film. The whole module is then framed with aluminum channel to provide ultimate reinforcement to it. The required power output is achieved by interconnecting suitable number of such modules in an array.

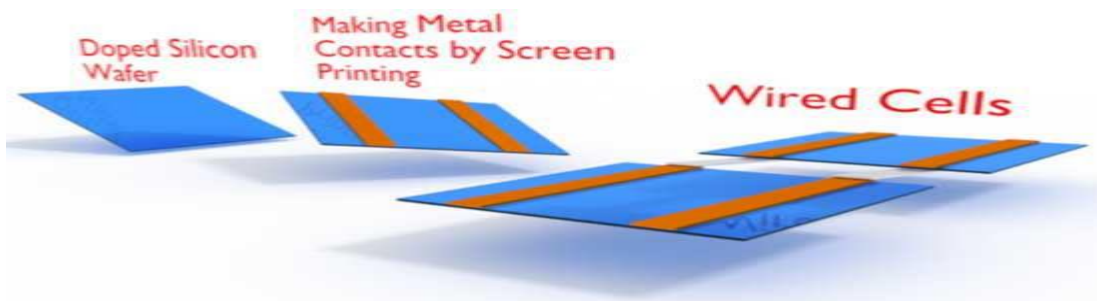


Fig.1.10. Solar Cells

PV SYSTEM MODELLING

The PV model consists of some strings of PV modules connected in parallel. Besides, series PV modules are included on each string as well to achieve the required current, voltage and power ratings. In a module, each PV cells can be modelled by utilizing single-diode equivalent circuit as displayed in Fig. 3. The construction of the single-diode equivalent circuit consists of a current source parallelly connected with a forward diode, a series connected resistance and a resistance connected in parallel. Whenever the PV cell detect the sunlight, it starts producing current. Utilizing Kirchhoff's current law, PV cell output current is derived as:

$$i_{pv} = i_{ph} - i_d - i_{sh} \quad (8)$$

Here, i_{ph} denotes the photocurrent, i_d indicates the current flowing across the forward diode and i_{sh} denotes the current flowing across the shunt resistance. Substituting relevant expressions for i_d and i_{sh} in (9) can be described as follows:

$$i_{pv,c} = i_{ph} - i_s \left[\exp\left(\frac{Q(V_{pv} + i_{pv,c}R_s)}{\eta k T_c}\right) - 1 \right] - \frac{V_{pv,c} + i_{pv,c}R_s}{R_{sh}} \quad (9)$$

Where i_s denotes the leakage current or reverse saturation of the diode (A), Q denotes the electron charge (1.602×10^{-19} C), η denotes the diode ideality factor following the type of PV cell technology (Si-mono) which is 1.2 used in this work, k denotes the Boltzmann's constant (1.381×10^{-23} J/K), T_c denotes the actual temperature of the cell ($^{\circ}$ C), V_{pv} denotes the cell output voltage (V), $i_{pv,c}$ denotes the cell output current (A), R_s denotes the shunt resistance of the cell (Ω) and R_{sh} denotes the cell series resistance (Ω). Furthermore, when the PV cells are attached in series to create a module, the output voltage and output current relationship expressed in (10) can be rewritten as:

$$i_{pv,m} = i_{ph} - i_s \left[\exp\left(\frac{Q(V_{pv} + N_s i_{pv,m} R_s)}{N_s \eta k T_c}\right) - 1 \right] - \frac{V_{pv,m} + N_s i_{pv,m} R_s}{N_s R_{sh}} \quad (10)$$

Where N_s indicates the module current (A), $V_{pv,m}$ indicates the module voltage (V) and N_p indicates the series connected PV cells number for a module. Moreover, the PV modules can be attached in parallel or in series to attain the required output voltage and power. The array is formed by the series and/or parallel connected PV modules. The modification of (10) builds the PV array as follows:

$$i_{pv,m} = i_{ph} N_p - i_s N_p \left[e^{\left(\frac{Q(V_{pv,m} + \frac{N_s}{N_p}(i_{pv,m} R_s))}{N_s \eta k T_c}\right)} - 1 \right] - \frac{V_{pv,m} + \frac{N_s}{N_p} i_{pv,m} R_s}{\frac{N_s}{N_p} (R_{sh})} \quad (11)$$

Where denotes the number of cell strings in parallel. From (8), the photocurrent, i_{ph} relies on the solar irradiation G , the actual cell temperature, and on the surface of the PV cell. Thus, the i_{ph} can be expressed as:

$$i_{ph} = (i_{ph,n} + K_1 \Delta T_c) \frac{G}{G_n} \quad (12)$$

Where G denotes the solar irradiance(W/m²), G_n denotes the solar irradiance at STC (W/m²), i_{ph} denotes the photocurrent (A) at STC, K_1 denotes the temperature coefficient of short circuit current (A/°C), ΔT_c denotes the variation of the actual cell temperature (°C) and T_c denotes the cell temperature at STC (°C).From (9)-(11), the diode saturation current, i_s relies on the cell temperature and it can be stated as:

$$i_s = i_{s,n} \left(\frac{T_c}{T_{c,n}} \right)^3 \exp \left[\frac{Q(E_{go})}{\eta k} \left(\frac{1}{T_{c,n}} - \frac{1}{T_c} \right) \right] \quad (13)$$

Where $Q(E_{go})$ denotes the energy band gap of the material (eV) and 1.12eV is selected as the value according to the category of semiconductor material utilized in this work and $i_{s,n}$ denotes the diode saturation current at STC. The i_s , can be expressed as follows:

$$i_{s,n} = i_{ph,n} \exp \left[\frac{Q(V_{oc,n})}{N_s \eta k T_c} \right] \quad (14)$$

The shunt resistance R_{sh} and series resistance R_s enhance the cell performance by managing the slope of voltage and current relationship. The R_{sh} and R_s can be approximated as follows in (15) and (16). Where V_{oc} denotes the open circuit voltage (V) and i_{sh} denotes the short circuit current (A).

$$R_{sh} > \frac{10 V_{oc}}{i_{sh}} \quad (15)$$

$$R_s < \frac{0.1 V_{oc}}{i_{sh}} \quad (16)$$

The construction of the PV system model follows the parameter of PV panel specified to acquire the desired current, voltage and power ratings that is desired by the UPQC system in MATLAB Simulink. The parameter utilized for the PV system in this work is tabulated in Table I. The parameters of cell and array of the PV model is developed to follow SunPower SPR-215-WHT-U PV module. The PV characteristic curve with specified temperature (25 °C) for the PV module and varying irradiance is displayed

in Fig. 4. The I-V characteristic illustrates in Fig. 4(A) and the P-V characteristics is shown in Fig. 4(B) for solar array.

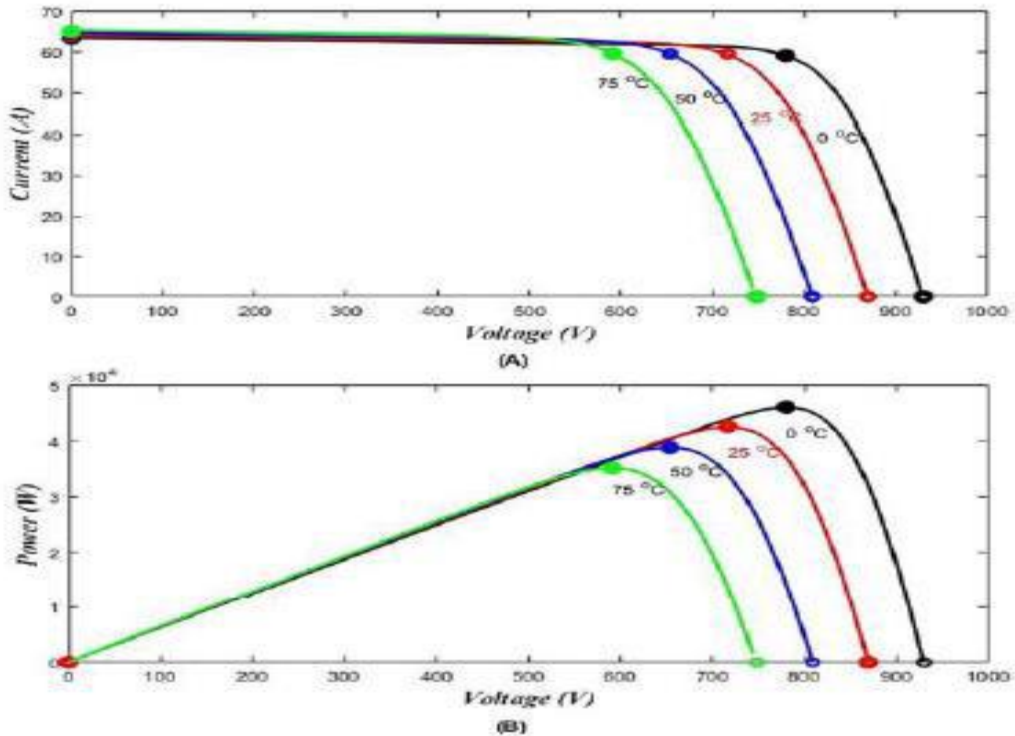


Fig. 1.11. PV cell waveforms at 25 °C and irradiance variation (A) I-V (B) P-V
The characteristic curve with specified irradiance (1000 W/m²) and varying temperature is shown in Fig. 5. I-V characteristic illustrates in Fig. 5(A) and the P-V characteristics is shown in Fig. 5(B) for solar array.

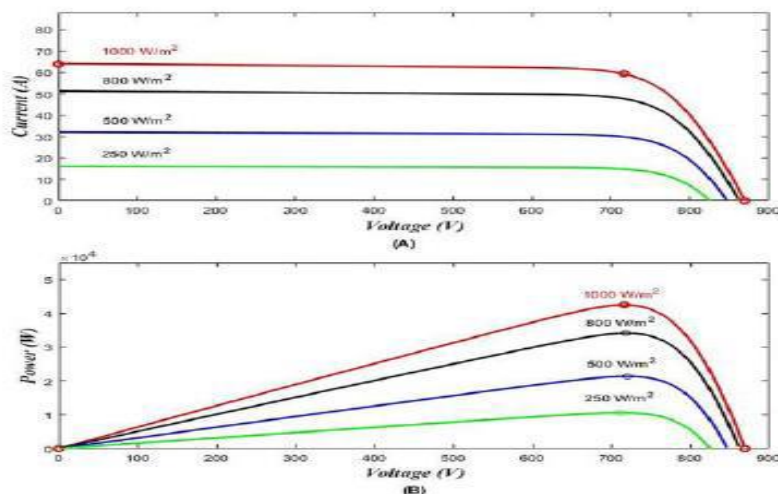


Fig.12. PV cell waveforms at different temperature and designated irradiance (1000 W/m²) (A) I-V (B) P-V.

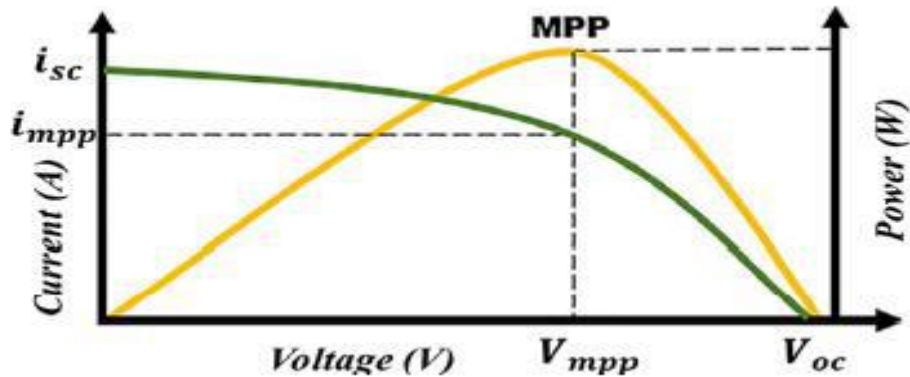


Fig.1.12. Solar PV module I-V and P-V feature.

Next, the solar radiations achieved by the solar panel are varied continuously which results in low quality performance of the solar panel. Likewise, higher temperatures are also responsible for lowering the performance quality of the solar module. The Variation in insolation modifies all the parameters of the solar module illustrated in the PV cell characteristics curves in Fig. 6. Maximum power point tracking (MPPT) can be utilized to improve the efficiency of a PV module under a specified irradiance and temperature. The DC-DC boost converter duty cycle is regulated to maintain the algorithm of the MPPT. In this work, a simple method named Perturb and observe (P & O) is selected and this method can track the MPP more accurately. The P & O algorithm is easy to implement and demonstrated as the flowchart in Fig. 7. PV module output voltage and output current are the input of the MPPT algorithm. To execute this method, the current and voltage of PV modules need to be measured initially to determine the power of PV modules,. The observation and perturbation process is continued until the operating point reaches the MPP. The algorithm compares the voltages and power of time with the sample at a time (-1) and estimates the time to reach to MPP. The P & O algorithm traces by increasing or reducing the voltage at the MPPT regularly of the PV module. When the positive power alteration occurs, a slight voltage perturbation can change the power of solar panel and voltage perturbation is maintained in similar track. Whereas when negative delta power occurs, it shows that the MPP is at far distance and the perturbation is reduced to attain the MPP. The P & O algorithm is summarized in Table II. Therefore, the complete PV curve is examined by small-scale perturbations to locate the MPP that extend the response time of the algorithm. On the other hand, if the perturbation size is expanded, it produces steady-state oscillations about the

MPP. The P & O algorithm output is the approximated MPPT voltage . The MPPT voltage is employed to regulate the DC-DC converter to achieve the PV open-circuit voltage continuously. The PV system output power, is boosted by the DC-DC boost converter that control by controller shows in Fig. 8. The controller of the DC-DC boost converter is operating by getting DC voltage error. The voltage error is calculated by comparing the given reference voltage, which is 700V.

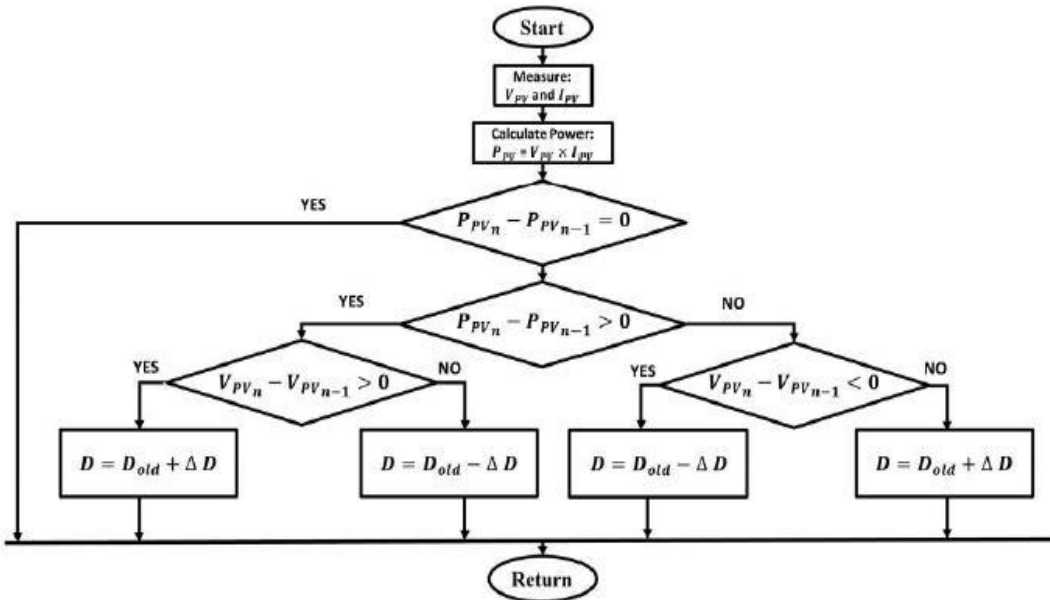


Fig.1.13. Flow Chart of Perturb & Observe Algorithm

The reference voltage is assigned with instantaneous DC-DC Boost converter output DC voltage. Afterwards,* is approximated by reducing the , using a PI controller. In mathematic terms, the approximation can be explained as found from (17) and (18):

$$\begin{aligned} V_{DC,error}^* &= k_{p,1}(V_{DC,error}(t)) \\ &+ k_{i,1} \int_0^t (V_{DC,error}(t)) dt \end{aligned} \quad (17)$$

$$V_{DC,error}(t) = V_{ref} + V_{DC}(t) \quad (18)$$

where ,1 and ,1 indicates the two fixed values that denotes as proportional gain and integral gains of the controller PI1. The values are allocated as 0.1 and 0.1, consecutively. However, the controller of the DC-DC Boost converter will break off the PV system output power, during battery's state of charge is over or equal to 98% of battery capacity. The reason is to keep away the battery from being overcharged

and unstable. Moreover, the lifetime of the battery can be reduced due to overcharging.

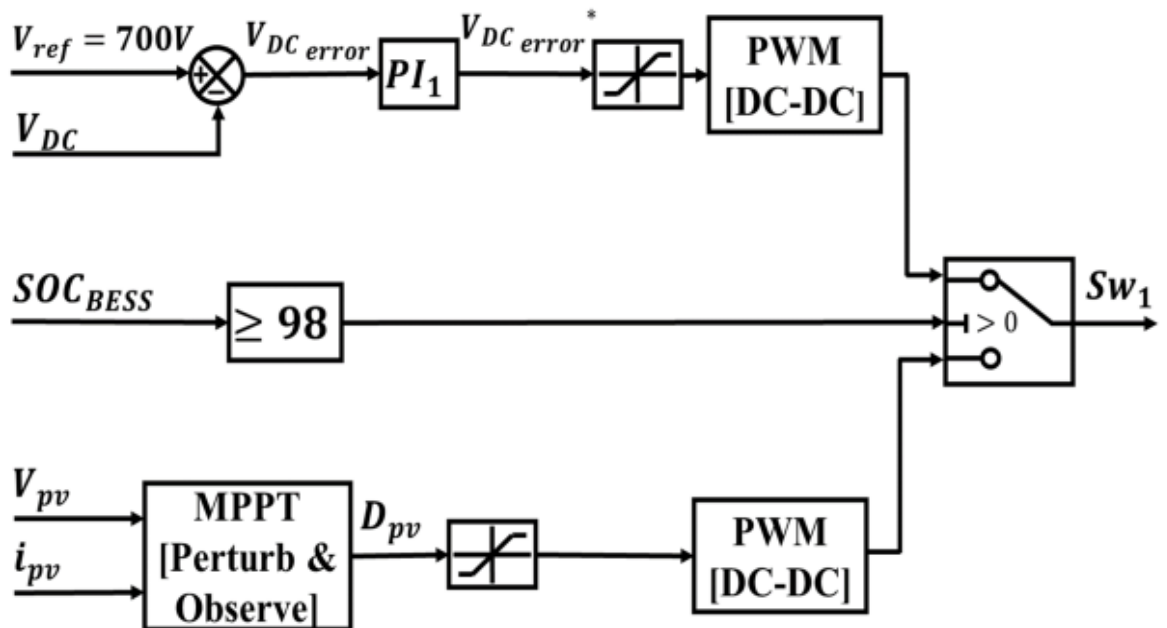


Fig 1.14. PV DC-DC Boost Converter Control Scheme

MPPT:

Maximum Power Point Tracking, is a technique used in solar power systems to maximize the efficiency of solar panels by continuously adjusting the operating point to ensure they're producing maximum power output. It's achieved through algorithms that dynamically track changes in environmental conditions, adjusting the voltage or current to maintain peak power production. Common MPPT algorithms include Perturb and Observe (P&O), Incremental Conductance (Inc Cond), and Fractional Open-Circuit Voltage (FOCV). MPPT systems can significantly increase energy harvest and system efficiency, making them essential components of solar power installations.

Need for MPPT:

Solar panels are non-linear devices, meaning their output power does not increase linearly with incident light. Therefore, simply connecting the panels to a load or battery without adjusting the operating voltage may not utilize them efficiently. MPPT algorithms are used to dynamically adjust the operating point of the panels to track the MPP, ensuring maximum power output.

MPPT Algorithms:

There are several MPPT algorithms, each with its own approach to tracking the MPP. Some common algorithms include Perturb and Observe (P&O), Incremental Conductance (Inc Cond), and Fractional Open-Circuit Voltage (FOCV). These algorithms continuously monitor the output voltage and current of the solar panels and adjust the operating voltage to maximize power output.

Perturb and Observe (P&O):

This is one of the simplest MPPT algorithms. It perturbs (slightly increases or decreases) the operating voltage and observes the change in power output. If the power increases, it continues in that direction; if it decreases, it changes direction. This iterative process continues until the MPP is reached.

Incremental Conductance (Inc Cond):

This algorithm compares the ratio of change in power to the change in voltage with the conductance (di/dv) of the panel. It adjusts the operating voltage based on this comparison to track the MPP.

Benefits of MPPT:

MPPT algorithms maximize the efficiency of solar power systems by ensuring that the panels operate at their MPP under varying environmental conditions. This leads to increased energy harvest and improved overall system performance. MPPT is essential for optimizing the performance of solar power systems by dynamically adjusting the operating point of solar panels to track their maximum power point under changing environmental conditions.

CHAPTER-2

LITERATURE SURVEY

Pradeep Kumar and Asheesh K. Singh,:

Electric power has always been one of the driving forces for progress in human life. This has popularized electric energy as the most utilized form of energy. However, dispersed locations of energy resources and continuously increasing demand of electricity have led to a large electric power transmission network across the landscape. To operate the system effectively, a large number of components, such as protection systems, monitoring systems, operational procedures, etc. are required to work in a synchronized and efficient manner; otherwise, contingencies may arise in the system. Development and integration of renewable energy sources into the existing power system has enhanced the complexity in the network. Efficient operation of this complex network is a tedious task for the authorities. Thus, to simplify the planning, operational, and other tasks, grid codes have been developed. Grid codes are the rules laid by the authorities for all its stakeholders, i.e., the users and power generating stations for connecting to the network and operate as per the standards. These grid codes implement the regulations for smooth operation of the grid and its connected components. It implies to the existing and future plants. This chapter gives an overview of the grid codes, its various components and their development considering integration of renewable energy into the grid. Various aspects, such as classification and specifications of the grid codes, the anomalies that exist between the grid codes developed and standards used in conventional power plants are discussed in this chapter.

Singh, Girish Kumar(IIT Roorkee).

The various forms of solar energy – solar heat, solar photovoltaic, solar thermal electricity, and solar fuels offer a clean, climate-friendly, very abundant and in-exhaustive energy resource to mankind.

Solar power is the conversion of sunlight into electricity, either directly using photovoltaic (PV), or indirectly using concentrated solar power (CSP). The research has been underway since very beginning for the development of an affordable, in-exhaustive and clean solar energy technology for longer term benefits. This paper, therefore, reviews the progress made in solar power generation research and development since its inception. Attempts are also made to highlight the current

and future issues involved in the generation of quality and reliable solar power technology for future applications. For the generation of electricity in far flung area at reasonable price, sizing of the power supply system plays an important role. Photovoltaic systems and some other renewable energy systems are, therefore, an excellent choices in remote areas for low to medium power levels, because of easy scaling of the input power source. The main attraction of the PV systems is that they produce electric power without harming the environment, by directly transforming a free inexhaustive source of energy, the solar energy into electricity. Also, the continuing decrease in cost of PV arrays and the increase in their efficiency imply a promising role for PV generating systems in the near future [8], [9]. Unfortunately, the technologies associated with photovoltaic (PV) power systems are not yet fully established, and therefore, the price of an energy unit generated from a PV system is an order of magnitude higher than conventional energy supplied to city areas, by means of the grid supply.

M. D. Anderson(Electrical & Computer Engineering Department University of Missouri Rolla, USA):

Battery energy storage systems, comprising lead-acid batteries, power conversion systems, and control systems, are discussed. They are used by power generating utilities power distributing utilities, and major power consumers (such as electric furnace foundries). The principal advantages that battery energy storage systems offer generating utilities are described, including load levelling, frequency control, spinning reserve, modular construction, convenient siting, absence of emissions, and investment deferral for new generation and transmission equipment. Power distributing utilities and major power consumers can avoid costly demand changes by discharging their batteries at peak periods and then recharging with lower cost off-peak power (say, at night). Battery energy storage systems are most cost- effective when designed for discharge periods of less than 5 h; other systems (for example, pumped water storage) are better suited for longer discharges. It is estimated that by the year 2000 there will be a potential need for 4000 MW of battery energy storage.

Recent Advances in Energy Storage Systems for Renewable Source Grid Integration: Dr. Muhammed Worku

The reduction of greenhouse gas emissions and strengthening the security of electric energy have gained enormous momentum recently. Integrating intermittent renewable energy sources (RESs) such as PV and wind into the existing grid has

increased significantly in the last decade. However, this integration hampers the reliable and stable operation of the grid by posing many operational and control challenges. Generation uncertainty, voltage and angular stability, power quality issues, reactive power support and fault ride-through capability are some of the various challenges. The power generated from RESs fluctuates due to unpredictable weather conditions such as wind speed and sunshine. Energy storage systems (ESSs) play a vital role in mitigating the fluctuation by storing the excess generated power and then making it accessible on demand.

This paper presents a review of energy storage systems covering several aspects including their main applications for grid integration, the type of storage technology and the power converters used to operate some of the energy storage technologies. This comprehensive review of energy storage systems will guide power utilities; the researchers select the best and the most recent energy storage device based on their effectiveness and economic feasibility.

OPTIMIZED COMPLEX POWER QUALITY CLASSIFIER USING ONE VS. REST SUPPORT VECTOR MACHINES: David De Yong:

Power quality issues are becoming a significant research topic because of the increasing inclusion of very sensitive devices and considerable renewable energy sources. In general, most of the previous power quality classification techniques focused on single power quality events and did not include an optimal feature selection process. This paper presents a classification system that employs Wavelet Transform and the Root Mean Square profile to extract the main features of the measured waveforms containing either single or complex disturbances. A data mining process is designed to select the optimal set of features that describe each disturbance. Support Vector Machine binary classifiers organized in a “One Vs Rest” architecture are individually optimized to classify single and complex disturbances. The parameters that rule the performance of each binary classifier are also individually adjusted using a grid search algorithm that helps them achieve optimal performance. This specialized process significantly improves the total classification accuracy. Several single and complex disturbances are simulated in order to train and test the algorithm. The results show that the classifier is capable of identifying >99% of single disturbances and >98% of complex disturbances.

DYNAMIC VOLTAGE RESTORER (DVR) IN A COMPLEX VOLTAGE**DISTURBANCE COMPENSATION: Muhammad Murtadha Othman:**

A distribution network is operating in a stressful manner because of a complex voltage disturbance stirred by its nonlinear, intensified, sensitive and complex loading condition with vast proliferation of electronic equipment required for the integration of renewable energy. A distribution network that mostly inflicted by the complex voltage disturbance can be referred to as the merge of stationary voltage disturbances with a short duration voltage disturbance under a nonlinear loading condition. Therefore, the dynamic voltage restorer (DVR) integrating with the battery bank will have enough energy storage to overcome long and deep complex voltage disturbance that occurs in a distribution network installed with the photovoltaic (PV) system. The results are obtained with satisfactorily findings in compensating the complex voltage disturbance using DVR.

CHAPTER -3

BESS SYSTEM

INTRODUCTION

A Battery Energy Storage System is a technology that stores electrical energy in batteries for later use. BESS plays a crucial role in modern energy systems by helping to balance supply and demand, smooth out fluctuations in renewable energy sources, and enhance grid reliability. It is employed in various applications, including renewable energy integration, peak shaving, and grid stabilization. BESS can also stand for a Bachelor's degree program in Environmental and Sustainability Studies. This academic discipline focuses on understanding and addressing environmental challenges, promoting sustainable practices, and exploring solutions for a more sustainable and resilient future. Students in BESS programs often study topics such as environmental science, policy, conservation, and sustainable development. Battery Energy Storage System

3.1:Battery Energy Storage System Overview:

3.1.1:Definition:

A Battery Energy Storage System (BESS) is a technology that stores electrical energy in batteries for later use. It consists of rechargeable batteries, power conversion systems, and control systems.

3.1.2:Functionality:

BESS serves as a crucial component in managing and optimizing energy resources within power systems. It can store excess energy when supply exceeds demand and release stored energy during periods of high demand or when renewable energy sources are not generating power.

3.1.3:Applications:

Renewable Energy Integration: BESS helps mitigate the intermittency of renewable energy sources like solar and wind by storing excess energy produced during peak times and supplying it during low production periods.

Grid Stabilization: BESS contributes to grid stability by providing fast-response capabilities, regulating frequency, and supporting voltage control.

Peak Shaving: BESS can be used to reduce peak demand on the electrical grid by supplying stored energy during periods of high electricity consumption.

3.1.4:Components:

- **Batteries:** The heart of the BESS, rechargeable batteries store and release electrical energy.
- **Power Conversion Systems:** These systems convert the direct current (DC) stored in batteries to alternating current (AC) for use in the electrical grid.
- **Control Systems:** Smart control systems manage the charging, discharging, and overall operation of the BESS.

3.1.5:Types of Batteries Used:

- Various types of batteries are used in BESS, including lithium-ion, lead-acid, flow batteries, and more. The choice of battery technology depends on factors such as application, cost, and performance requirements.

3.2 BLOCK DIAGRAM OF BESS

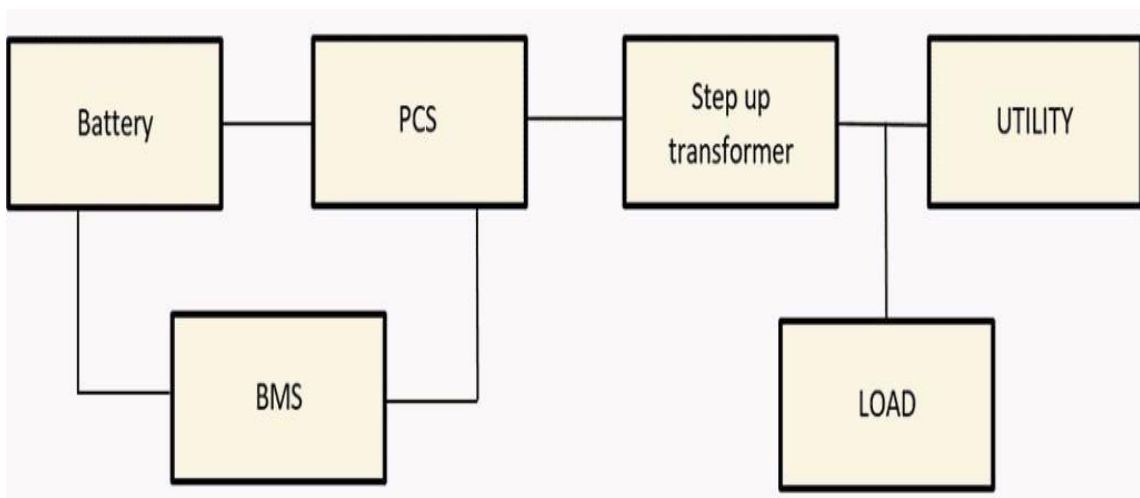


Fig.3.1. BESS block diagram

Battery: A battery is a device that stores and releases electrical energy through electrochemical reactions. It typically consists of one or more electrochemical cells, each composed of positive and negative electrodes, an electrolyte, and a separator. When a battery is connected to an external circuit, a chemical reaction occurs within the cells, leading to the conversion of chemical energy into electrical energy. This process allows batteries to store energy during periods of charging and deliver it as electrical power when needed.

PCS (Power Conversion System): A Power Conversion System (PCS) is a set of components and devices that convert electrical power from one form to another, often changing the voltage, frequency, or phase of the electrical energy. These systems play a crucial role in various applications, including renewable energy integration, energy storage, and electrical grid management.

BMS (Battery Management System): A Battery Management System (BMS) is a critical component in Battery Energy Storage Systems (BESS) and electric vehicles. It is designed to monitor, control, and protect the batteries, ensuring their safe and efficient operation. The BMS performs various functions to optimize the performance, lifespan, and safety of the battery pack. Here are the key aspects of a Battery Management System.

Step Up Transformer: A step-up transformer is a type of transformer that increases the voltage of an alternating current (AC) electrical circuit while decreasing the current. This is achieved through electromagnetic induction.

The primary coil (input side) and the secondary coil (output side) of the transformer are wound around a shared magnetic core.

Utility: "Utility BESS" typically refers to Battery Energy Storage Systems utilized by utility companies in the electricity grid infrastructure. These systems are designed to enhance grid performance, provide ancillary services, and support the integration of renewable energy sources. Here are key aspects of Utility Battery Energy Storage Systems.

Load: "Load BESS" typically refers to Battery Energy Storage Systems that are specifically designed and deployed to address load-related challenges and demands in electrical systems. These systems are employed to manage and optimize the energy consumption of various loads within a given system. Here are key aspects related to Load Battery Energy Storage Systems.

3.3: Types Of BESS System:

It seems there might be a slight error in your question, as you mentioned "bess system." I assume you are referring to "BESS" or "Battery Energy Storage System." If you intended to ask about types of battery energy storage systems, here are some common types:

3.3.1: Lithium-ion Battery Systems:

Lithium-ion (Li-ion) batteries are widely used in various applications, including electric vehicles and stationary energy storage systems. They offer high energy density, long cycle life, and relatively low self-discharge rates.

3.3.2: Lead-Acid Battery Systems:

Lead-acid batteries have been used for many years and are known for their reliability. They are commonly used in uninterruptible power supply (UPS) systems and smaller-scale energy storage applications.

3.3.3: Flow Battery Systems:

Flow batteries store energy in liquid electrolytes, which are pumped through electrochemical cells to generate electricity. Flow batteries are known for their scalability and potential for longer cycle life.

3.3.4: Sodium-Ion Battery Systems:

Sodium-ion batteries are an emerging technology with potential applications in energy storage. They are similar to lithium-ion batteries but use sodium ions instead of lithium ions.

3.3.5: Nickel-Cadmium (NiCd) Battery Systems:

- a) Although less common today due to environmental concerns related to cadmium, nickel
- b) cadmium batteries have been historically used in certain stationary applications.

CHAPTER-4

SYSTEM CONSTRUCTION

The construction of PV-BESS-UPQC is displayed in Fig. 1. The three-phase system is designed for the PV-BESS-UPQC model. The PV-BESS-UPQC comprises of series and shunt APF compensator linked with DC-link split capacitor. The battery and the PV array are linked parallelly to the DC-link. The PV is linked through a boost converter to the DC-link. Moreover, the BESS is linked through a buck-boost converter to the DC-link. The series compensator works like a controlled voltage source manner and mitigates for the supply voltage sags, swells, interruption, and voltage harmonic. On the other hand, the shunt compensator mitigates the current harmonics for the load. Both the series and shunt APF compensator are attached through interfacing inductors.

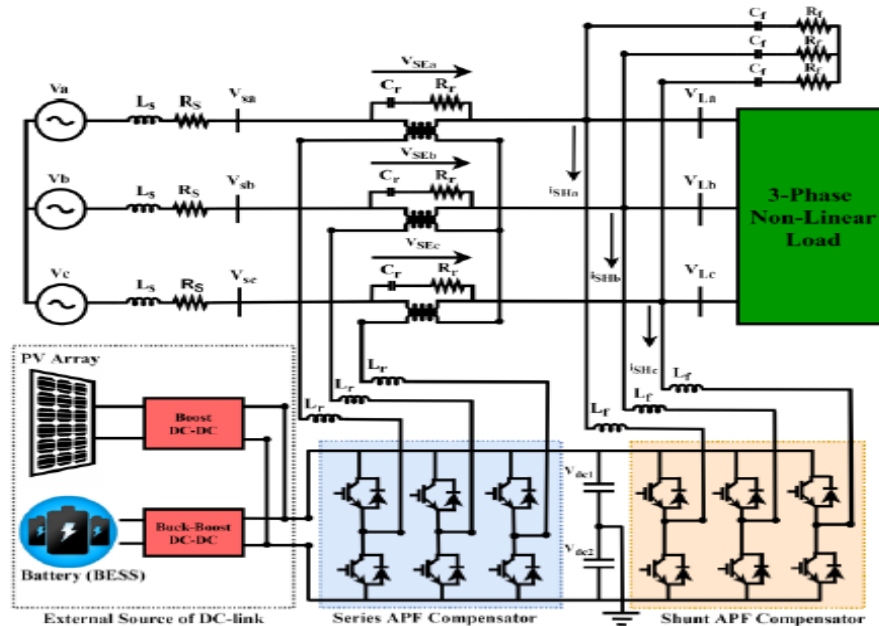


Fig.4.1 UPQC system configuration

Due to the converter switching action harmonics are generated and therefore, ripple filter is utilized to filter out harmonics. The series compensator uses a series injection transformer to insert voltage to the grid. In this work, a three-phase non-linear load is utilized. The PV-BESS- UPQC design procedure starts with the accurate measurement of PV array, split capacitor, reference voltage of DC-link etc. The design of the shunt compensator follows the way that apart from mitigating

current harmonics it controls the peak output power from PV array. Since the PV array is connected to the UPQC DC-link directly, the PV array is constructed in a way such that the maximum power point (MPP) voltage is equivalent to the reference DC-link voltage. During nominal conditions, the rating of PV array ensures that the load active power is delivered by the PV array and power is supplied to the grid and charging BESS by the PV array as well. Besides, the BESS is designed in a way that, when the PV array generate less power than the DC-link load demand, the BESS provides the insufficient power equivalent to the decrease in DC-link voltage. Moreover, when there is no power produced by PV array, the BESS will supply the total load demand.

A: DESIGN OF UPQC

1) DC-LINK VOLTAGE MAGNITUDE

The minimum value of DC-link voltage, relies on phase-voltage of the system. The voltage magnitude of the DC-link needs to be nearly twice the peak value of the phase-voltage of the supply. The equation of is given as follows:

$$V_{dc,min} = \frac{2\sqrt{2}(V_{LL,rms})}{\sqrt{3} (m)} \quad (1)$$

Where, indicates the index of modulation depth that assigned as 1 and ,indicates the phase-voltage of the grid which is selected as considered by Malaysia Energy Commission following IEC standard. Therefore, is obtained as for a of . DC-link voltage, is chosen as 700 V after considering the value of PV-BESS as external source of DC-link.

2) DC-LINK CAPACITOR VALUE

The equation of the DC-link capacitor is presented as follows:

$$C_{dc,min} = \frac{3V_{ph} i_{sh} a_f k_e t}{1/2 (V_{dc,set}^2 - V_{dc,min}^2)} \quad (2)$$

Here, h indicates the phase-voltage, h indicates the phase-current for shunt APF, indicates the overloading factor, indicates the time to achieve the steady-state, indicates the variation of energy during dynamic condition, indicates the voltage which is equivalent to the reference voltage and , indicates the minimum required

voltage of the DC-link. The calculated minimum voltage of the DC link, = 677.69 , = 700 , $h= 230.9 \text{ V}$, $h= 57.5 \text{ A}$, = 30 ms, =1.2, and energy variation during dynamics = 10% ($= 0.1$), the measured value of ,is 9330.28 μF and it is approximated as 9400 μF . Then, two split capacitors are set on 4700 μF each.

3)INDUCTOR RIPPLE FILTER FOR SHUNT APF

The shunt APF is attached through an inductor with the network as a passive filter which relies on the switching frequency denoted as a_f denotes ripple current and V_{dc} denotes the DC-link voltage. The interfaced inductor equation is shown as follows:

$$L_{f,min} = \frac{(\sqrt{3})(m)(V_{dcset})}{12(a_f)(f_{SH})(I_{cr,pp})} \quad (3)$$

Here, m indicates the modulation depth, indicates the maximum overload value in pu unit,

indicates the ripple current for the inductor which measured as 20% of Shunt APF rms phase current. f_{SH} indicates the switching frequency. Considering $=20\%$, $f_s=10 \text{ kHz}$, $m=1$, $V_{DC}=700 \text{ V}$, and $a=1.5$, the value of is measured as 1.79 mH. Here, the set value is considered which is 3mH in this investigation

4)SERIES INJECTION THREE-PHASE ISOLATION TRANSFORMER

The injection transformer is considered for attaching the VSC of a series APF in series with the grid. The transformer voltage rating relies on the voltage that need to be injected and the DC-link voltage. For compensating a voltage variation of $\pm 60\%$, the voltage to be injected, VSE is calculated as 138.54V. In that case the modulation index becomes low for the series compensator at 700V DC-link voltage. The maximum value turns ratio of the injection transformer for the series APF is expressed as follows:

$$K_{SE} = \frac{V_{LLrms}}{\sqrt{3}(V_{SE})} \quad (4)$$

Where the is calculated was 1.667 approximate to 2. The VA rating of the injection transformer is expressed as follows:

$$S_{SE} = 3(V_{SE})(i_{SE(under sag)}) \quad (5)$$

The current across the series APF is equivalent to the grid current. During the voltage sag condition of 0.6 pu, the supply current is measured as 36A. Therefore, the achieved injection transformer VA rating is 15 kVA.

5)INDUCTOR RIPPLE FILTER FOR SERIES APF

The series APF is attached through an inductor with the network as a passive filter which relies on the DC-link voltage, ripple current and switching frequency. The interfaced inductor equation is shown as follows:

$$L_{r,min} = \frac{(\sqrt{3})(m)(V_{dc,set})(K_{SE})}{12(a_f)(f_{SE})(I_r)} \quad (6)$$

Here, m denotes the modulation depth, a denotes the maximum overload value in per unit,

denotes the ripple current for the inductor which computed as 20% of Series APF rms phase current. a_f denotes the switching frequency. Where, $m = 1, = 1.5, = 10$ kHz, 20% ripple current and $V_{dc} = 700$ V, so the measured inductor value is 3.6 mH.

DESIGN OF UPQC CONNECTING WITH PV-BESS AS EXTERNAL SUPPORT OF DC-LINK

The suggested model displayed in Fig. 2 comprises the PV system, BESS, boost converter, buck-boost converters, and controller. The BESS is attached parallelly to the DC-link capacitor utilizing buck-boost converter, so the stability of the UPQC is improved for compensating power quality problem. In the model, the total power flow is expressed in the (7). Furthermore, the PV system parameters and the parameters of Li-ion battery implemented in this paper are tabulated in the Table I.

$$P_{total} = P_{pv} + P_{BESS} - P_{Load_{DC-link}} \quad (7)$$

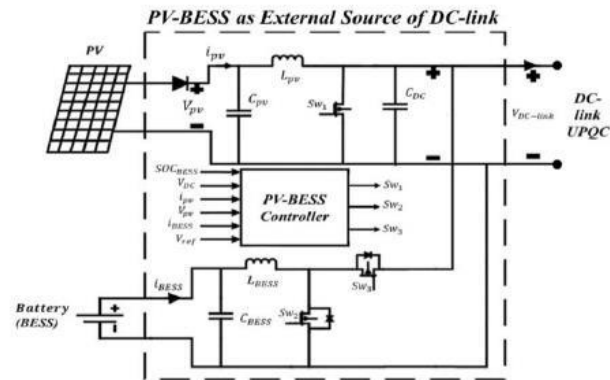


Fig.4.2. PV-BESS system configuration

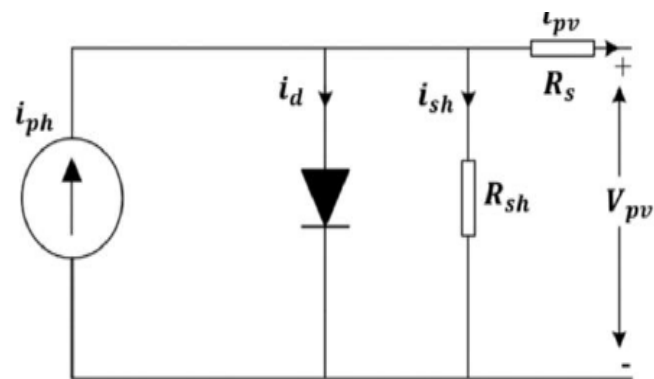


Fig.4.3 Single-diode PV cell equivalent circuit

CHAPTER 5

PROPOSED METHODOLOGY

INTRODUCTION

In the face of global climate challenges and the increasing demand for sustainable energy sources, the integration of renewable energy technologies has become imperative. This proposal outlines a comprehensive approach for the construction and investigation of a cutting-edge 3-phase solar photovoltaic (PV) system seamlessly integrated with Battery Energy Storage System (BESS) and Unified Power Quality Conditioner (UPQC). This innovative system aims not only to harness solar energy efficiently but also to enhance power quality and grid stability. Background information on solar PV, BESS, and UPQC technologies. Rationale for integrating these technologies. Importance of the project in the context of renewable energy and power quality.

5.1: Objectives

The primary objectives of this proposal are as follows:

- Design and construct a 3-phase solar PV system tailored to local energy demand. Integrate BESS to store surplus energy and facilitate grid balancing.
- Implement UPQC technology to enhance power quality by compensating for voltage and current disturbances.
- Investigate the performance and synergies of the integrated system under various operating conditions
 - a. Clearly define the specific objectives of the project.
 - b. Specify performance metrics for the integrated system

5.2: System Design

5.2.1: Solar PV System

- a. Overview of the solar PV array design.
- b. Selection of solar panels, inverters, and other components.
- c. Sizing of the system based on energy demand.

5.2.2: Battery Energy Storage System (BESS)

- a. Description of the BESS components (batteries, inverters, etc.).

- b. Sizing and capacity planning.
- c. Control and management strategies.

5.2.3:Unified Power Quality Conditioner (UPQC)

- a. Explanation of UPQC functionalities.
- b. Selection of UPQC components.

5.2.4: System Integration

- a. Detailed plan for integrating the three subsystems.
- b. Communication protocols and interfaces.

5.3: Construction Plan

- a. Phased construction approach.
- b. Timeline for each phase.
- c. Resource allocation and procurement plan.

5.4: Performance Monitoring and Control

- a. System monitoring tools and sensors.
- b. Control algorithms for optimizing energy production and power quality.
- c. Contingency plans for system failures.

5.5: Environmental Impact Assessment

- a. Evaluation of the environmental impact of the integrated system.
- b. Strategies for minimizing environmental footprint.

5.6: Economic Analysis

- a. Cost estimation for construction.
- b. Financial benefits analysis (savings, incentives, etc.).
- c. Return on investment (ROI) calculations.

5.7: Regulatory Compliance

- a. Compliance with local and national regulations.
- b. Permitting and licensing requirements.

5.8: BLOCK DIAGRAM

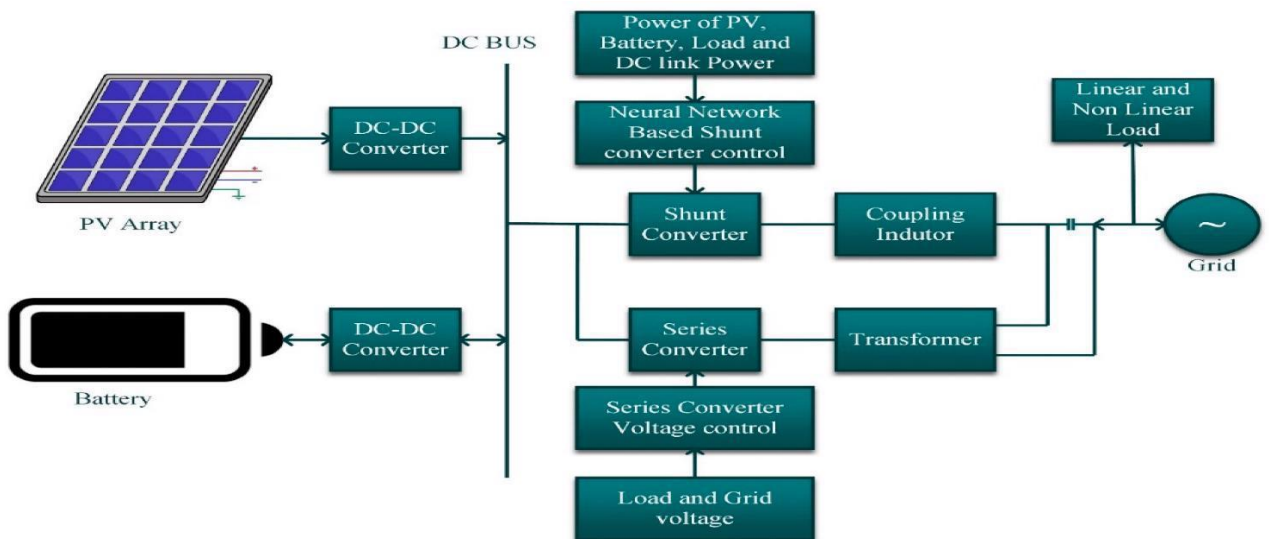


fig.5.1.block diagram of proposed method of pv and bess integrated upqc

5.9: Conclusion

- a. Recap of the project objectives and design.
- b. Emphasize the potential impact and benefits of the integrated system.

5.10: References

- a. Citations for relevant literature, standards, and regulations.

5.11: Appendices

- a. Additional technical details, charts, graphs, etc.
- b. Remember that this is a general framework, and the specific details will depend on the unique requirements of your project, location, and stakeholders. It's crucial to engage with experts in solar PV, energy storage, and power quality to ensure the success of the integrated system.

CHAPTER 6

MATLAB HISTORY

INTRODUCTION

Since it was initially known as the matrix programming language, MATLAB is an acronym for "Matrix Laboratory." It is a programming language of the fourth generation. It is a multi-paradigm, MATLAB. Therefore, it can be used with a variety of programming paradigms, including functional, Visual, and Object-Oriented. Like other well-known programming languages like Java, C#, etc., MATLAB has its own Integrated Development Environment (IDE) and collection of libraries. Since it was initially known as the matrix programming language, MATLAB is an acronym for "Matrix Laboratory." It is a programming language of the fourth generation. It is a multi-paradigm, MATLAB. Therefore, it can be used with a variety of programming paradigms, including functional, Visual, and Object-Oriented.

Cleve Moler, the department head of computer science at the University of New Mexico at the time, made the initial discovery. He wanted to develop a different approach for his students to do linear algebra and numerical computations without needing to utilize Fortran. Cleve Molar, Steve Bangart, and Jack Little founded MathWorks in 1984 after seeing MATLAB's economic potential.

6.1: MATLAB Uses

The built-in functions of MATLAB offer top-notch resources for performing calculations, including optimization, linear algebra, numerical solution of ordinary differential equations (ODEs), data analysis, quadrate, signal processing, and many other scientific tasks. Modern algorithms are used for the majority of these functions. There are many of these for both animations and 2-D and 3-D graphics. MATLAB also supports an external interface. The user can create their own functions in the MATLAB language. Thus they are not restricted to using only the built-in functions. Additional toolboxes are provided by MATLAB. These toolboxes were created for common uses such as neural networks, symbolic computations, image processing, control system design, and statistics.

The various uses of MATLAB are:

1. Developing algorithms
2. Performing linear algebra that is linear

3. Graph plotting for larger data sets
4. Data visualization and analysis
5. Numerical Matrix Computation

Now that we have explored the uses of MATLAB, we will now be going through its various advantages.

Become a Data Scientist with Hands-on Training!

6.2: Key Features:

6.2.1: Matrix-Based Programming:

1. MATLAB is designed around the concept of matrices, making it particularly powerful for linear algebra operations.
2. Matrix manipulation is intuitive and efficient, simplifying the implementation of mathematical algorithms.

6.2.2: Interactivity:

1. MATLAB provides an interactive environment where users can execute commands and see immediate results.
2. This interactivity is valuable for exploration, testing, and debugging.

6.2.3: Extensive Functionality:

1. MATLAB comes with a vast set of built-in functions and toolboxes for various applications, including signal processing, image processing, control systems, and more.
2. Users can also create their own functions to extend the functionality.

6.2.4: Data Visualization:

1. Powerful plotting and visualization tools enable users to create a wide range of 2D and 3D plots to analyze and present data.
2. Customization options allow for the creation of publication-quality graphics.

6.2.5: Simulink Integration:

1. Simulink, MATLAB's companion product, provides a graphical environment for modeling, simulating, and analyzing multidomain dynamical systems.

6.2.6: Community and Support:

1. A large and active user community facilitates knowledge sharing and troubleshooting.

2. MathWorks provides comprehensive documentation, tutorials, and online forums for support.

6.3: Basic MATLAB Commands:

Variables and Assignment:

Matlab Copy code

```
x = 10; % Assigning a value to a variable y = sin(x); % Performing a mathematical operation
```

Matrix Operations:

Matlab Copy code

```
A = [1, 2; 3, 4]; % Creating a matrix B = eye(2); % Creating an identity matrix C = A * B; % Matrix multiplication
```

Plotting:

Matlab Copy code

```
t = line space(0, 2*pi, 100); y = sin(t); plot(t, y); % Plotting a sine wave
```

Functions:

Matlab Copy code

```
function result = square(x) result = x^2; end
```

6.4: Applications:

Engineering and Science:

1. MATLAB is widely used in engineering disciplines, physics, and other scientific fields for numerical simulations, data analysis, and modeling.

Signal and Image Processing:

MATLAB is a go-to tool for processing and analyzing signals and images due to its rich set of functions and toolboxes.

Control System Design:

Engineers use MATLAB for designing and analyzing control systems, utilizing the Simulink environment.

Machine Learning:

With the introduction of the MATLAB Deep Learning Toolbox, MATLAB has become popular for developing and implementing machine learning algorithms.

6.5: Conclusion:

MATLAB's versatility, ease of use, and extensive functionality make it a powerful tool for a wide range of applications. Whether you are a student, researcher, or professional, MATLAB provides a flexible environment for tackling diverse computational challenges.

CHAPTER 7

MATLAB SIMULATION

Introduction to MATLAB for Simulations

Simulation in MATLAB:

MATLAB is a versatile platform for conducting simulations, allowing users to model and analyse complex systems. The simulation capabilities of MATLAB, combined with its rich set of functions and toolboxes, make it a preferred choice for researchers, engineers, and scientists engaged in diverse fields.

7.1: Key Simulation Features:

7.1.1: Mathematical Modelling:

1. MATLAB provides a powerful environment for creating mathematical models to represent real-world systems.
2. Users can define equations, algorithms, and mathematical relationships to simulate dynamic processes.

7.1.2: Simulation Toolbox:

1. The Simulink toolbox in MATLAB offers a graphical environment for modelling, simulating, and analysing multidomain dynamical systems.
2. Block diagrams are used to represent system components, making it easy to visualize and understand complex interactions.

7.1.3: Dynamic System Simulation:

1. MATLAB allows the simulation of dynamic systems, including mechanical, electrical, chemical, and control systems.
2. Users can study system behaviour over time, considering various inputs and parameters.

7.1.4: Monte Carlo Simulations:

1. MATLAB is well-suited for Monte Carlo simulations, enabling the exploration of the impact of random variations and uncertainties in a model.
2. This is particularly useful for risk assessment and sensitivity analysis.

7.2: Optimization and Parameter Estimation:

1. MATLAB provides optimization tools that can be integrated with simulations to find optimal solutions for system parameters.
2. Parameter estimation techniques are used to refine models based on observed data.

7.2.1: Event-Based Simulations:

1. Event-driven simulations can be implemented using MATLAB, allowing users to model systems with discrete events and interactions.
2. This is beneficial for studying systems that involve sudden changes or discrete occurrences.

7.3: Basic Simulation Workflow:

7.3.1: Model Definition:

Define the mathematical model of the system using MATLAB scripts or Simulink block diagrams.

7.3.2: Simulation Configuration:

Configure simulation parameters, including time steps, solver options, and initial conditions.

7.3.3: Execution:

Run the simulation to obtain time-domain or frequency-domain responses of the system.

7.3.4: Analysis:

Analyze simulation results using MATLAB's extensive plotting and visualization tools.

Extract key performance metrics and insights from the simulation data.

7.4: Applications:

7.4.1: Engineering Systems:

Simulate mechanical, electrical, and control systems to analyze performance and optimize designs.

7.4.2: Communication Systems:

Model and simulate communication systems to evaluate signal processing algorithms, channel effects, and performance metrics.

7.4.3: Biological and Medical Systems:

Simulate physiological processes, drug interactions, and medical imaging systems.

7.4.4: Financial Modeling:

Conduct Monte Carlo simulations for risk analysis and pricing of financial instruments.

7.5: SIMULATION DIAGRAM

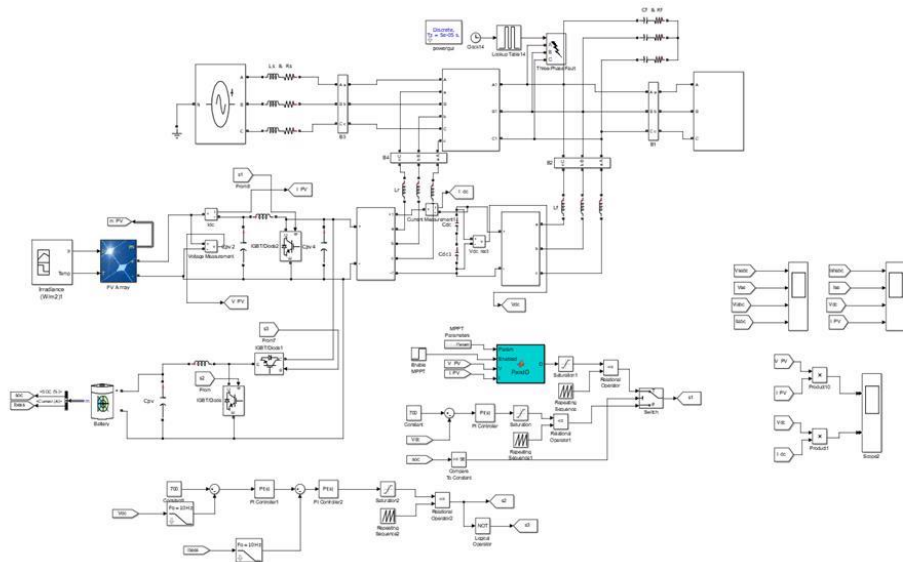


Fig.7.1. simulation Diagram

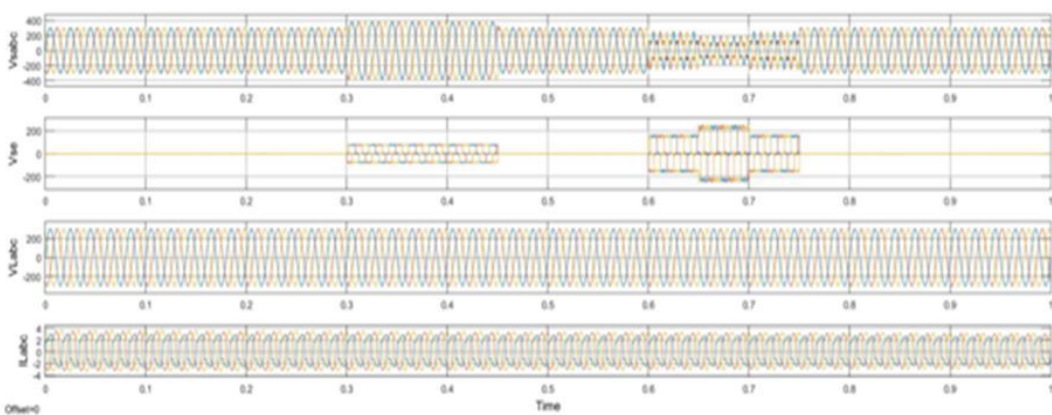


Fig.7.2. Three phase Load Current and Load Voltage

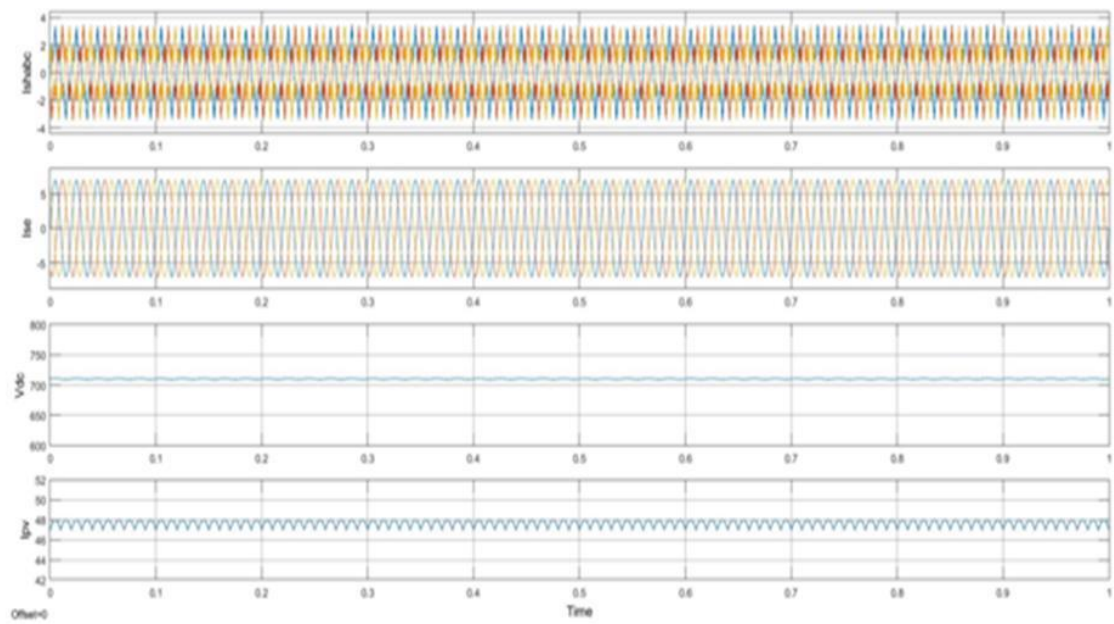


Fig.7.3. Current at PV and voltage DC OUTPUT voltage.

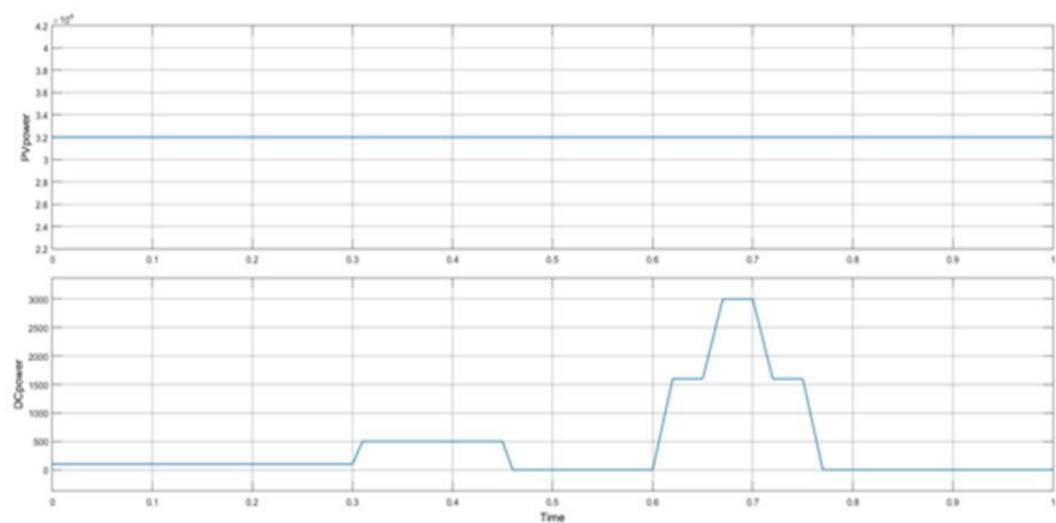


Fig.7.4. PV power and DC power.

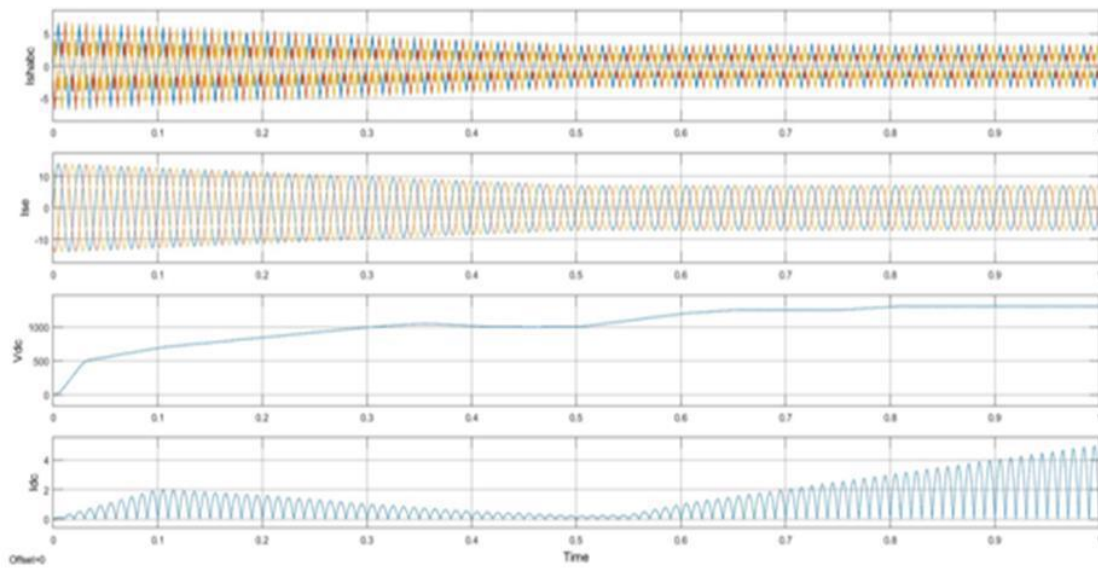


Fig.7.5.DC voltage and current

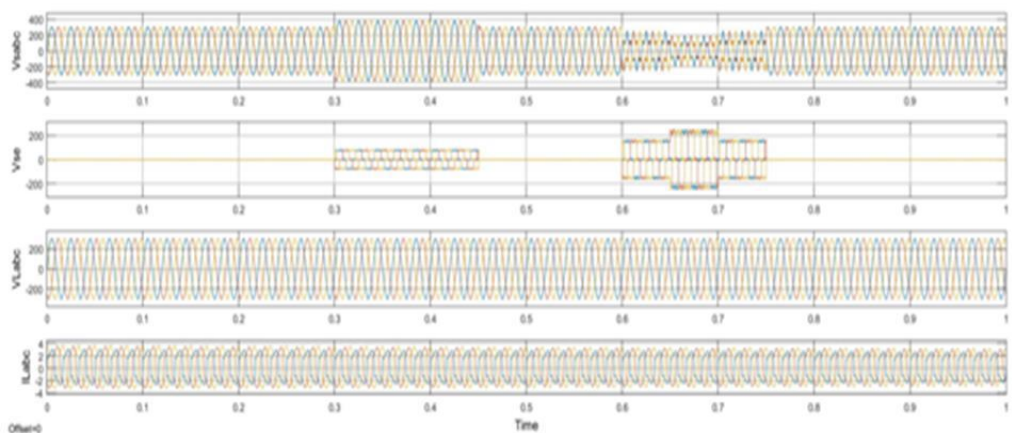


Fig.7.6. Load currents and load voltages

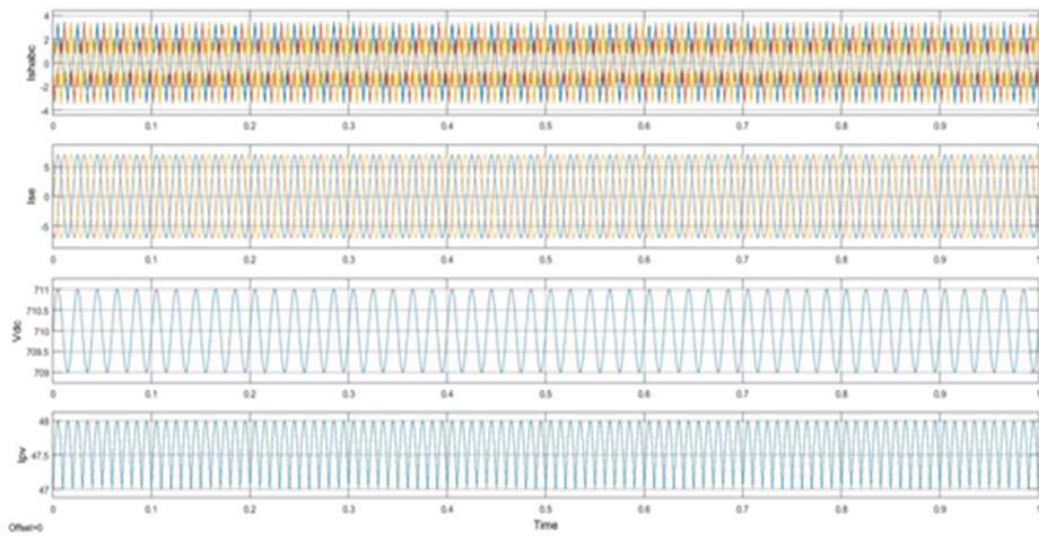


Fig.7.7. PV currents and DC voltages

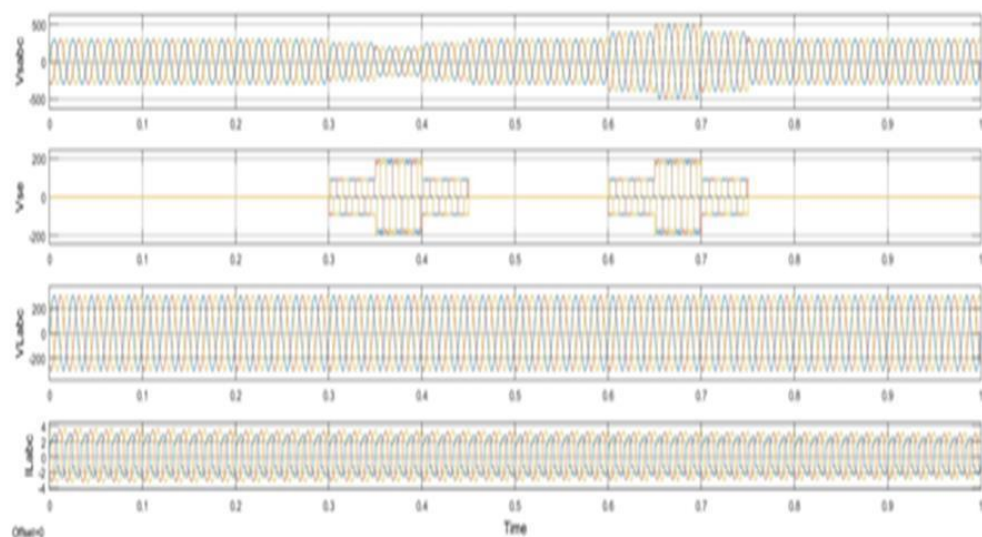


Fig.7.8. Load currents and load voltages

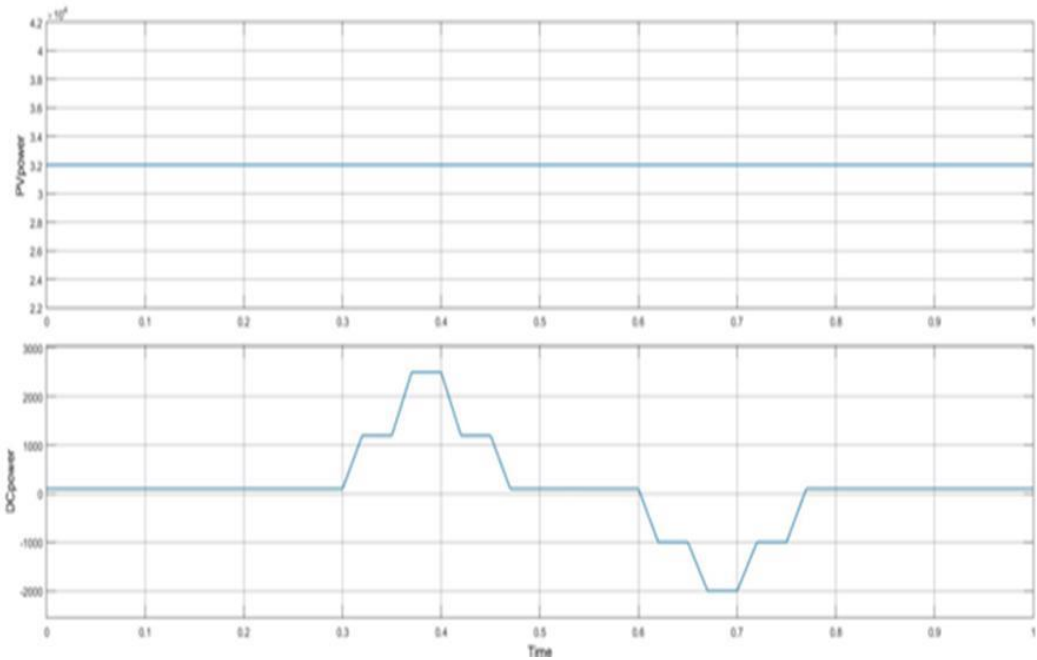


Fig.7.9 DC power and PV power

7.6: CONCLUSION OF SIMULATION MATLAB

MATLAB's simulation capabilities, coupled with its user-friendly interface and extensive documentation, make it an indispensable tool for researchers and engineers involved in understanding, analyzing, and optimizing complex systems. Whether simulating physical processes, exploring statistical scenarios, or optimizing parameters, MATLAB offers a comprehensive environment for a wide range of simulation applications.

CONCLUSION

The construction of three phase UPQC has been investigated considering the condition of complex power quality problems which are an amalgamation of harmonics, voltage swell, and sags, and voltage interruption under unbalanced and distorted voltage grid condition. Integrating the BESS and PV with the UPQC provides active power capability to the network. The main benefit of BESS integrated with UPQC is that it makes the system capable of supplying and absorbing active power from the PV. Since renewable energy is not completely reliable because of its environment-dependent feature, integrating a BESS will solve the lack of renewable energy resources. Finally, it can be figured that the BESS and PV attached with UPQC can be a good alternative in the distributed generation to upgrade the power quality of the contemporary distribution system. The DC-link voltage is stable because of the continuous supply from the PV-BESS system. Therefore, it can reduce the complexity of the DC-link voltage regulation algorithm. The STF-UVG technique for synchronization phases is applied successfully in the shunt and series APF compensator to generate reference current and voltage. Thus, the UPQC is designed without relying on the PLL components, and mitigation of current and voltage are achieved successfully following the grid condition to ensure the system stability and to achieve almost unity power factor. The implementation of the proposed technique has confirmed that the grid current harmonics follow the IEEE-519 standard. Finally, it is worth mentioning that the proposed system can enhance the overall efficiency of the grid power system.

REFERENCES

1. IEEE Standards Coordinating Committee 22 on Power Quality, IEEE Recommended Practice for Monitoring Electric Power Quality, vol. 2009, no. June. 1995.
2. D. De Yong, S. Bhowmik, and F. Magnago, “Optimized Complex Power Quality Classifier Using One vs. Rest Support Vector Machines,” *Energy Power Eng.*, vol. 09, no. 10, pp. 568–587, 2017.
3. A. Javadi, A. Hamadi, L. Woodward, and K. Al-Haddad, “Experimental Investigation on a Hybrid Series Active Power Compensator to Improve Power Quality of Typical Households,” *IEEE Trans. Ind. Electron.*, vol. 63, no. 8, pp. 4849–4859, 2016.
4. A. Javadi, L. Woodward, and K. Al-Haddad, “Real-Time Implementation of a Three-Phase THSeAF Based on a VSC and a P+R Controller to Improve the Power Quality of Weak Distribution Systems,” *IEEE Trans. Power Electron.*, vol. 33, no. 3, pp. 2073–2082, 2018.
5. M. A. Mansor, M. M. Othman, I. Musirin, and S. Z. M. Noor, “Dynamic voltage restorer (DVR) in a complex voltage disturbance compensation,” *Int. J. Power Electron. Drive Syst.*, vol. 10, no. 4, pp. 2222–2230, 2019.
6. A. Ghosh and G. Ledwich, “Compensation of distribution system voltage using DVR,” *IEEE Trans. Power Deliv.*, vol. 17, no. 4, pp. 1030–1036, 2002.
7. S. Jothibasu and M. K. Mishra, “A control scheme for storage less DVR based on characterization of voltage sags,” *IEEE Trans. Power Deliv.*, vol. 29, no. 5, pp. 2261–2269, 2014.
8. A. Farooqi, M. M. Othman, A. F. Abidin, S. I. Sulaiman, and M. A. M. Radzi, “Mitigation of power quality problems using series active filter in a microgrid system,” *Int. J. Power Electron. Drive Syst.*, vol. 10, no. 4, pp. 2245–2253, 2019.
9. C. Kumar and M. K. Mishra, “Operation and Control of an Improved Performance Interactive DSTATCOM,” *IEEE Trans. Ind. Electron.*, vol. 62, no. 10, pp. 6024–6034, 2015.
10. Y. Hoon, M. A. M. Radzi, M. K. Hassan, and N. F. Mailah, “Control algorithms of shunt active power filter for harmonics mitigation: A review,” *Energies*, vol. 10, no. 12, 2017. 3967–3975, 2011.

Received April 10, 2020, accepted May 12, 2020, date of publication May 25, 2020, date of current version June 12, 2020.

Digital Object Identifier 10.1109/ACCESS.2020.2997056

Construction and Performance Investigation of Three-Phase Solar PV and Battery Energy Storage System Integrated UPQC

MUHAMMAD ALIF MANSOR[✉], KAMRUL HASAN[✉], MUHAMMAD MURTADHA OTHMAN, (Member, IEEE), SITI ZALIHA BINTI MOHAMMAD NOOR, (Member, IEEE), AND ISMAIL MUSIRIN

Faculty of Electrical Engineering, Universiti Teknologi MARA, Shah Alam 40450, Malaysia

Corresponding author: Muhammad Murtadha Othman (mamat505my@yahoo.com)

This work was supported by the Long-Term Research Grant (LRGS), Ministry of Education Malaysia for the program titled “Decarbonization of Grid with an Optimal Controller and Energy Management for Energy Storage System in Microgrid Applications” under Grant 600-IRMI/LRGS 5/3 (001/2019).

ABSTRACT This study examines the use of Unified Power Quality Conditioner (UPQC) to mitigate the power quality problems existed in the grid and the harmonics penetrated by the non-linear loads. The UPQC is supported by the Photovoltaic (PV) and Battery Energy Storage System (BESS) in this work. Generally, the PV system supplies the active power to the load. However, if the PV is unable to supply the power then the BESS activates and provides power especially during the longer-term voltage interruption. The standalone PV-UPQC system is less reliable compared to a hybrid PV-BESS system because of its instability and high environment-dependency. Therefore, BESS will improve the voltage support capability continuously in the longer-term, reduce the complexity of the DC-link voltage regulation algorithm, and keep producing clean energy. The phase synchronization operation of the UPQC controller is directed by a self-tuning filter (STF) integrated with the unit vector generator (UVG) technique. Implementation of STF will make sure the UPQC can successfully operate under unbalanced and distorted grid voltage conditions. Thus, the requirement of a phase-locked loop (PLL) is omitted and the STF-UVG is utilized to produce the synchronization phases for the series and shunt active power filter (APF) compensator in UPQC controller. Finally, the proposed STF-UVG method is compared with the conventional synchronous references frame (SRF-PLL) method based UPQC to show the significance of the proposed technique. Several case studies are further considered to validate the study in MATLAB-Simulink software.

INDEX TERMS Battery energy storage system (BESS), power quality, self-tuning filter (STF), solar photovoltaic (PV), unified power quality conditioner (UPQC).

I. INTRODUCTION

Energy is the basic input of life. Electricity is one of the significant energy among the different forms of energy. It ensures the flexibility of life and the demand for this energy is increasing rapidly. In recent decades, the ‘Power Quality’ term has achieved remarkable responses from the researchers, most importantly in the electrical engineering sector. Energy efficiency is maintained by compensating the power quality problems which ensures a smooth generation of electrical energy and to encourage decarbonization of the grid. Under

The associate editor coordinating the review of this manuscript and approving it for publication was Madhav Manjrekar.

different environmental conditions and requirements, the definition of power quality can have several interpretations and significances. For instance, the network can be affected by the harmonics created by non-linear loads which is a great concern for the utility and the disturbances existed in the supplied voltage is a great concern for the consumers. Power losses, undesirable and abnormal characteristics of equipment due to power quality problems can cause interference in neighboring communication lines, and disruption to different consumers. IEEE-1159 [1] stated the behavior of a standard waveform and categorized a different kind of disturbances. A complex power quality scenario is a specific disturbance that consists of an amalgamation of two or more individual disturbances,

for instance, fluctuation or harmonics for a small period distortion such as, sags or surges [2].

The voltage disturbances such as voltage harmonics, swells, and sags are responsible for the tripping of equipment like sensitive loads and the consequences can be detrimental for industrial plants, for instance, termination of the industrial process. These scenarios are familiar in the industry which creates high economical losses. To overcome this situation, mitigation devices of the series APFs are installed by the industrial customers to secure their plant from the disturbances coming from the grid [3]–[8]. The use of power electronics components is growing rapidly in modern plants which results in harmonics generation and sensitive load in the system, and for this reason, shunt APFs are implemented to overcome issues [9]–[12]. Therefore, a new trend is established to fulfill dual purposes, firstly serving the utility, and secondly benefiting the customers. The significance of this trend is to protect simultaneously both the utility and customers so that the sensitive components are protected from the disturbances in the voltage and to minimize the distortion penetrated to the utility by the loads utilized by the customers [13]. Therefore, The UPQC model is formed with series and shunt APF compensator in a back to back configuration that can control both the load voltage and grid current concurrently [14]. The current trend of microgrid and distributed generation increase the interest of the researcher to work on UPQC [15]–[17]. In addition, there has been an increased concern on the utilization of renewable power sources, reduced dependence on depleting sources of fossil fuels, which also caused global warming. There is a necessity for renewable energy systems, which also enhance power quality and also have the potentiality for operation during the unavailability of the grid.

In [19], proposed a fuel cell (FC) integrated with UPQC to mitigate PQ issues effectively on the grid side by providing real power support during voltage interruption. However, in their study, did not give any emphasize on the integration of renewable energy resources with UPQC and also have not encouraged decarbonization of the grid connected system. In [20], [21], proposed a PV integrated with UPQC to produce clean energy and improve the power quality problems. However, long interruption and deep voltage sag were not considered in their study. Furthermore, the dynamic voltage restorer (DVR) connected with superconducting magnetic energy storage system (SMES) to support the load for long term and thus, addressed the issue on long interruption [22]. Nonetheless, the current related harmonics problem was not considered. In such case, energy storage system like BESS can be interfaced with the PV-UPQC and can be a great support for continuously providing real power to the load. When UPQC operating in standalone mode, BESS is most essential for renewable energy systems. The extra cost of the BESS is justified when the system is applied for critical loads such as semiconductor industries, hospitals etc. where an uninterrupted supply of best quality power is of supreme importance. Therefore, The UPQC is supported by the PV

and BESS was design in this work. The PV is attached to the DC-link through DC-DC boost converter and the BESS is connected to the DC-link through DC-DC buck-boost converter [23], [24]. Generally, the PV system supplies the active power to the load but when the PV is unable to supply the power then the BESS activates and provides power especially during the longer-term voltage interruption in order to enhance the stability of the distribution power system. In [19] and [25]–[27], researchers try to design the DC-link voltage regulation algorithm to ensure stable and constant DC-link capacitor voltage. But, the UPQC controller become more complex and computational burden. However, PV-BESS can be considered a better alternative since it can support DC-link capacitor of a UPQC externally and can reduce the burden on the DC-link capacitor.

The synchronization phase is one the most significant parts of the control of an UPQC system. Note that the accurate synchronization phase operation is required for generating reference current and voltage by the shunt and series APF compensator, respectively [28]. The UPQC should be able to perform the synchronization operation effectively by injecting the voltage and current in phase with the grid. In [15]–[21], most of the UPQC controller is developed utilizing a conventional SRF-PLL for the synchronization phase algorithm which is not capable of dealing with unbalanced and distorted voltage grid condition. Moreover, a conventional PLL controller consists of a low pass filter that introduce phase delay in the synchronization operation causing undesired ripples in the reference current and voltage. Furthermore, the PI controller of a PLL increase the control complexity and require fine tuning which is time consuming [29]. A possible solution to the phase detection synchronization is utilizing the STF that have better phase tracking and fundamental component extraction capabilities. In this work, to produce to come up with simple controller structure by its working principle involves generation of unit vectors consisting of sine and cosine function for the process of extracting harmonic current algorithm and voltage error algorithm. Furthermore, the synchronization phases in term of unit vector is apply on the reference current generation in shunt compensator that design with integrating together with strength STF with working concept of the direct-quadrature-zero (STF- $dq0$) that not depending on any components of PLL. In series compensator, the reference voltage generation also will be applying working concept of the $dq0$ with utilizing synchronization phases for in-phase compensation. Most importantly, the proposed technique that will applying on UPQC controller need to be superior and more reliable when dealing with unbalanced and distorted voltage grid condition. It is also can maintaining grid current sinusoidal with regulating the desired load voltage which minimizing the phase difference to achieve almost unity power factor.

In this paper, PV and BESS connected parallelly with UPQC is proposed to solve the complex power quality problems specifically in case of long voltage interruption. Various case study is applied to validate the dynamic performance

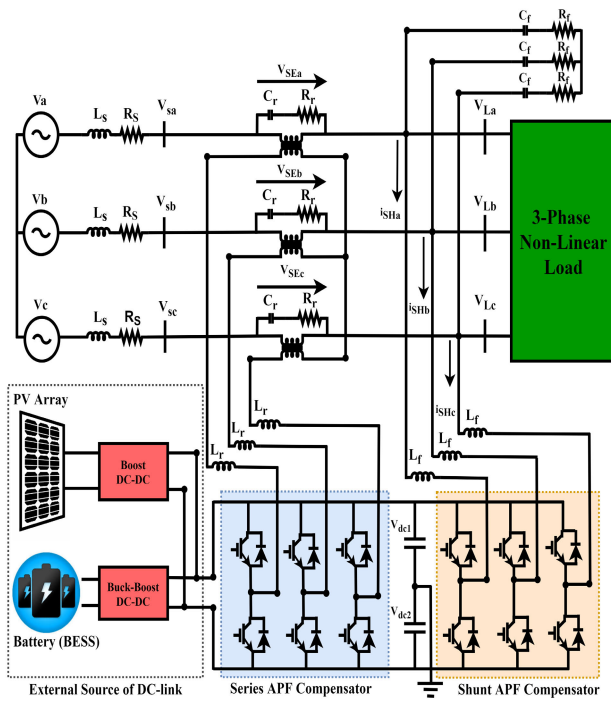


FIGURE 1. UPQC system configuration.

of the suggested UPQC integrated with PV and BESS. The comparison between the performance of UPQC with only DC-link capacitor and the UPQC integrated with PV and BESS is also shown. In addition, the STF integrated with the UVG technique (STF-UVG) is utilized to produce the synchronization phases for the UPQC controller to address the drawbacks of the conventional PLL. The performance comparison of the STF-UVG and a standard SRF-PLL to validate the superiority of the proposed technique. Finally, the performance of the suggested UPQC system is investigated utilizing MATLAB-Simulink software under dynamic condition.

II. SYSTEM CONSTRUCTION

The construction of PV-BESS-UPQC is displayed in Fig. 1. The three-phase system is designed for the PV-BESS-UPQC model. The PV-BESS-UPQC comprises of series and shunt APF compensator linked with DC-link split capacitor. The battery and the PV array are linked parallelly to the DC-link. The PV is linked through a boost converter to the DC-link. Moreover, the BESS is linked through a buck-boost converter to the DC-link. The series compensator works like a controlled voltage source manner and mitigates for the supply voltage sags, swells, interruption, voltage harmonic. On the other hand, the shunt compensator mitigates the current harmonics for the load. Both the series and shunt APF compensator are attached through interfacing inductors.

Due to the converter switching action harmonics are generated and therefore, ripple filter is utilized to filter out harmonics. The series compensator uses a series injection

transformer to insert voltage to the grid. In this work, a three-phase non-linear load is utilized. The PV-BESS-UPQC design procedure starts with the accurate measurement of PV array, split capacitor, reference voltage of DC-link etc. The design of the shunt compensator follows the way that apart from mitigating current harmonics it controls the peak output power from PV array. Since the PV array is connected to the UPQC DC-link directly, the PV array is constructed in a way such that the maximum power point (MPP) voltage is equivalent to the reference DC-link voltage. During nominal conditions, the rating of PV array ensures that the load active power is delivered by the PV array and power is supplied to the grid and charging BESS by the PV array as well. Besides, the BESS is designed in a way that, when the PV array generate less power than the DC-link load demand, the BESS provides the insufficient power equivalent to the decrease in DC-link voltage. Moreover, when there is no power produced by PV array, the BESS will supply the total load demand.

A. DESIGN OF UPQC

1) DC-LINK VOLTAGE MAGNITUDE

The minimum value of DC-link voltage, $V_{dc,min}$ relies on phase-voltage of the system. The voltage magnitude of the DC-link needs to be nearly twice the peak value of the phase-voltage of the supply. The equation of $V_{dc,min}$ is given as follows:

$$V_{dc,min} = \frac{2\sqrt{2}(V_{LL,rms})}{\sqrt{3}(m)} \quad (1)$$

where, m indicates the index of modulation depth that assigned as 1 and $V_{LL,rms}$ indicates the phase-voltage of the grid which is selected as 400 V_{rms} considered by Malaysia Energy Commission following IEC standard. Therefore, $V_{dc,min}$ is obtained as 653.2 V for a $V_{LL,rms}$ of 400 V_{rms} . DC-link voltage, V_{dc} is chosen as 700 V after considering the value of PV-BESS as external source of DC-link.

2) DC-LINK CAPACITOR VALUE

The equation of the DC-link capacitor is presented as follows:

$$C_{dc,min} = \frac{3V_{ph}i_{sh}afk_e t}{1/2(V_{dc,set}^2 - V_{dc,min}^2)} \quad (2)$$

Here, V_{ph} indicates the phase-voltage, i_{sh} indicates the phase-current for shunt APF, a_f indicates the overloading factor, t indicates the time to achieve the steady-state, k_e indicates the variation of energy during dynamic condition, $V_{dc,set}$ indicates the voltage which is equivalent to the reference voltage and $V_{dc,min}$ indicates the minimum required voltage of the DC link. The calculated minimum voltage of the DC link, $V_{dc,min} = 677.69\text{ V}$, $V_{dc,set} = 700\text{ V}$, $V_{ph} = 230.9\text{ V}$, $i_{sh} = 57.5\text{ A}$, $t = 30\text{ ms}$, $a_f = 1.2$, and energy variation during dynamics = 10% ($k_e = 0.1$), the measured value of $C_{dc,min}$ is $9330.28\text{ }\mu\text{F}$ and it is approximated as $9400\text{ }\mu\text{F}$. Then, two split capacitors are set on $4700\text{ }\mu\text{F}$ each.

3) INDUCTOR RIPPLE FILTER FOR SHUNT APF

The shunt APF is attached through an inductor with the network as a passive filter which relies on the switching frequency denoted as f_{SH} , $I_{cr,pp}$ denotes ripple current and $V_{dc,set}$ denotes the DC-link voltage. The interfaced inductor equation is shown as follows:

$$L_{f,min} = \frac{(\sqrt{3})(m)(V_{dc,set})}{12(a_f)(f_{SH})(I_{cr,pp})} \quad (3)$$

Here, m indicates the modulation depth, a_f indicates the maximum overload value in pu unit, $I_{cr,pp}$ indicates the ripple current for the inductor which measured as 20% of Shunt APF rms phase current. f_{SH} indicates the switching frequency. Considering $I_{cr,pp} = 20\%$, $f_s=10$ kHz, $m = 1$, VDC = 700 V, and $a = 1.5$, the value of $L_{f,min}$ is measured as 1.79 mH. Here, the set value is considered which is 3mH in this investigation

4) SERIES INJECTION THREE-PHASE ISOLATION TRANSFORMER

The injection transformer is considered for attaching the VSC of a series APF in series with the grid. The transformer voltage rating relies on the voltage that need to be injected and the DC-link voltage. For compensating a voltage variation of $\pm 60\%$, the voltage to be injected, V_{SE} is calculated as 138.54 V. In that case the modulation index becomes low for the series compensator at 700 V DC-link voltage. The maximum value turns ratio of the injection transformer for the series APF is expressed as follows:

$$K_{SE} = \frac{V_{LL_{rms}}}{\sqrt{3}(V_{SE})} \quad (4)$$

where the K_{SE} is calculated was 1.667 approximate to 2. The VA rating of the injection transformer is expressed as follows:

$$S_{SE} = 3(V_{SE})(i_{SE(\text{undersag})}) \quad (5)$$

The current across the series APF is equivalent to the grid current. During the voltage sag condition of 0.6 pu, the supply current is measured as 36 A. Therefore, the achieved injection transformer VA rating is 15 kVA.

5) INDUCTOR RIPPLE FILTER FOR SERIES APF

The series APF is attached through an inductor with the network as a passive filter which relies on the DC-link voltage, ripple current and switching frequency. The interfaced inductor equation is shown as follows:

$$L_{r,min} = \frac{(\sqrt{3})(m)(V_{dc,set})(K_{SE})}{12(a_f)(f_{SE})(I_r)} \quad (6)$$

Here, m denotes the modulation depth, a denotes the maximum overload value in per unit, I_r denotes the ripple current for the inductor which computed as 20% of Series APF rms phase current. f_{SE} denotes the switching frequency. Where, $m = 1$, $a_f = 1.5$, $f_{SE} = 10$ kHz, 20% ripple current and $V_{dc,set} = 700$ V, so the measured inductor value is 3.6 mH.

B. DESIGN OF UPQC CONNECTING WITH PV-BESS AS EXTERNAL SUPPORT OF DC-LINK

The suggested model displayed in Fig. 2 comprises the PV system, BESS, boost converter, buck-boost converters, and controller. The BESS is attached parallelly to the DC-link capacitor utilizing buck-boost converter, so the stability of the UPQC is improved for compensating power quality problem. In the model, the total power flow is expressed in the (7). Furthermore, the PV system parameters and the parameters of Li-ion battery implemented in this paper are tabulated in the Table 1.

$$P_{total} = P_{pv} + P_{BESS} - P_{Load\ DC-link} \quad (7)$$

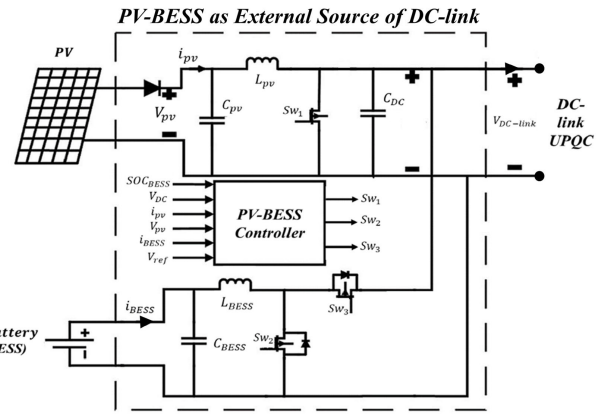


FIGURE 2. PV-BESS system configuration.

TABLE 1. Parameters of devices implemented in the work.

Device	Parameters	Values
PV panel single panel (SunPower SPR-215- WHT-U)	Rated Power	214.92 W
	Open circuit voltage (V_{OC})	48.3 V
	Short circuit current (I_{SH})	5.8 A
	Voltage at maximum power (V_{MP})	39.8 V
	Current at maximum power (I_{MP})	5.4 A
	Number of cells in parallel	11
	Number of cells in series	18
	Temperature	25 °C
	Rated Capacity	350 Ah
	Maximum Capacity	450 Ah
Li-ion battery	Nominal voltage	650 V
	Fully charge voltage	756 V

1) PV SYSTEM MODELLING

In this paper, the PV model is utilized from the Simulink library. The PV model consists of some strings of PV modules connected in parallel. Besides, series PV modules are included on each string as well to achieve the required current, voltage and power ratings. In a module, each PV cells can be modelled by utilizing single-diode equivalent circuit as

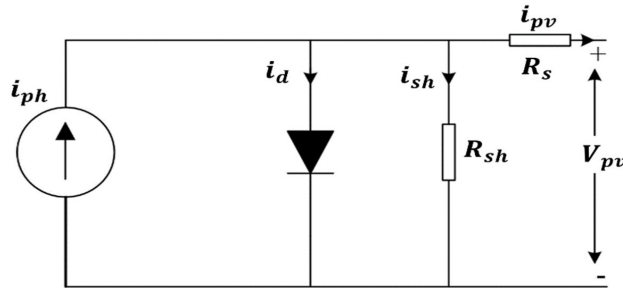


FIGURE 3. Single-diode PV cell equivalent circuit.

displayed in Fig. 3. The construction of the single-diode equivalent circuit consists of a current source parallelly connected with a forward diode, a series connected resistance and a resistance connected in parallel. Whenever the PV cell detect the sunlight, it starts producing current. Utilizing Kirchhoff's current law, PV cell output current is derived as:

$$i_{pv} = i_{ph} - i_d - i_{sh} \quad (8)$$

Here, i_{ph} denotes the photocurrent, i_d indicates the current flowing across the forward diode and i_{sh} denotes the current flowing across the shunt resistance. Substituting relevant expressions for i_d and i_{sh} in (9) can be described as follows:

$$i_{pv,c} = i_{ph} - i_s \left[\exp \left(\frac{Q(V_{pv,c} + i_{pv,c}R_s)}{\eta k T_c} \right) - 1 \right] - \frac{V_{pv,c} + i_{pv,c}R_s}{R_{sh}} \quad (9)$$

where i_s denotes the leakage current or reverse saturation of the diode (A), Q denotes the electron charge (1.602×10^{-19} C), η denotes the diode ideality factor following the type of PV cell technology (Si-mono) which is 1.2 used in this work, k denotes the Boltzmann's constant (1.381×10^{-23} J/K), T_c denotes the actual temperature of the cell (°C), $V_{pv,c}$ denotes the cell output voltage (V), $i_{pv,c}$ denotes the cell output current (A), R_{sh} denotes the shunt resistance of the cell (Ω) and R_s denotes the cell series resistance (Ω). Furthermore, when the PV cells are attached in series to create a module, the output voltage and output current relationship expressed in (10) can be rewritten as:

$$i_{pv,m} = i_{ph} - i_s \left[\exp \left(\frac{Q(V_{pv,m} + N_s i_{pv,m} R_s)}{N_s \eta k T_c} \right) - 1 \right] - \frac{V_{pv,m} + N_s i_{pv,m} R_s}{N_s R_{sh}} \quad (10)$$

where $i_{pv,m}$ indicates the module current (A), $V_{pv,m}$ indicates the module voltage (V) and N_s indicates the series connected PV cells number for a module. Moreover, the PV modules can be attached in parallel or in series to attain the required output voltage and power. The array is formed by the series and/or parallel connected PV modules. The modification of

(10) builds the PV array as follows:

$$i_{pv,m} = i_{ph} N_p - i_s N_p \left[e^{\left(\frac{Q(V_{pv,m} + \frac{N_s}{N_p} (i_{pv,m} R_s))}{N_s \eta k T_c} \right)} - 1 \right] - \frac{V_{pv,m} + \frac{N_s}{N_p} i_{pv,m} R_s}{\frac{N_s}{N_p} (R_{sh})} \quad (11)$$

where N_p denotes the number of cell strings in parallel. From (8), the photocurrent, i_{ph} relies on the solar irradiation G , the actual cell temperature, T_c and on the surface of the PV cell. Thus, the i_{ph} can be expressed as:

$$i_{ph} = (i_{ph,n} + K_1 \Delta T_c) \frac{G}{G_n} \quad (12)$$

where G denotes the solar irradiance (W/m²), G_n denotes the solar irradiance at STC (W/m²), $i_{ph,n}$ denotes the photocurrent (A) at STC, K_1 denotes the temperature coefficient of short circuit current (A/°C), ΔT_c denotes the variation of the T_c actual cell temperature (°C) and $T_{c,n}$ denotes the cell temperature at STC (°C). From (9)-(11), the diode saturation current, i_s relies on the cell temperature and it can be stated as:

$$i_s = i_{s,n} \left(\frac{T_c}{T_{c,n}} \right)^3 \exp \left[\frac{Q(E_{go})}{\eta k} \left(\frac{1}{T_{c,n}} - \frac{1}{T_c} \right) \right] \quad (13)$$

where E_{go} denotes the energy band gap of the material (eV) and 1.12eV is selected as the value according to the category of semiconductor material utilized in this work and $i_{s,n}$ denotes the diode saturation current at STC. The $i_{s,n}$ can be expressed as follows:

$$i_{s,n} = i_{ph,n} \exp \left[\frac{Q(V_{oc,n})}{N_s \eta k T_c} \right] \quad (14)$$

The shunt resistance R_{sh} and series resistance R_s enhance the cell performance by managing the slope of voltage and current relationship. The R_{sh} and R_s can be approximated as follows in (15) and (16). Where V_{oc} denotes the open circuit voltage (V) and i_{sh} denotes the short circuit current (A).

$$R_{sh} > \frac{10V_{oc}}{i_{sh}} \quad (15)$$

$$R_s < \frac{0.1V_{oc}}{i_{sh}} \quad (16)$$

The construction of the PV system model follows the parameter of PV panel specified to acquire the desired current, voltage and power ratings that is desired by the UPQC system in MATLAB Simulink. The parameter utilized for the PV system in this work is tabulated in Table 1. The parameters of cell and array of the PV model is developed to follow SunPower SPR-215-WHT-U PV module. The PV characteristic curve with specified temperature (25 °C) for the PV module and varying irradiance is displayed in Fig. 4. The I-V characteristic illustrates in Fig. 4(A) and the P-V characteristics is shown in Fig. 4(B) for solar array.

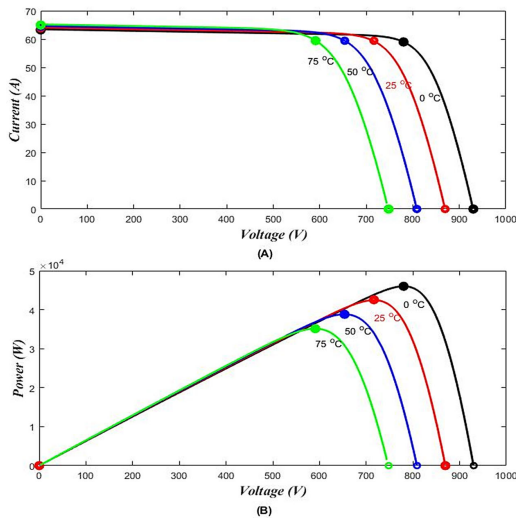


FIGURE 4. PV cell waveforms at 25 °C and irradiance variation (A) I-V (B) P-V.

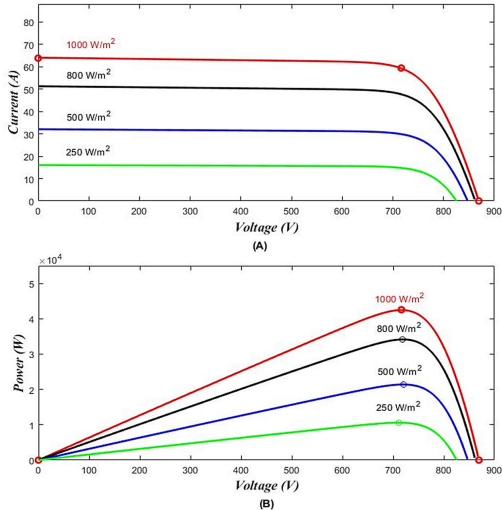


FIGURE 5. PV cell waveforms at different temperature and designated irradiance (1000 W/m²) (A) I-V (B) P-V.

The characteristic curve with specified irradiance (1000 W/m²) and varying temperature is shown in Fig. 5. I-V characteristic illustrates in Fig. 5(A) and the P-V characteristics is shown in Fig. 5(B) for solar array.

Next, the solar radiations achieved by the solar panel are varied continuously which results in low quality performance of the solar panel. Likewise, higher temperatures are also responsible for lowering the performance quality of the solar module. The Variation in insolation modifies all the parameters (P_{max} , V_{max} , i_{max} , V_{oc} , i_{sc}) of the solar module illustrated in the PV cell characteristics curves in Fig. 6. Maximum power point tracking (MPPT) can be utilized to improve the efficiency of a PV module under a specified irradiance and temperature. The DC-DC boost converter duty cycle is regulated to maintain the algorithm of the MPPT. In this work, a simple method named Perturb and observe

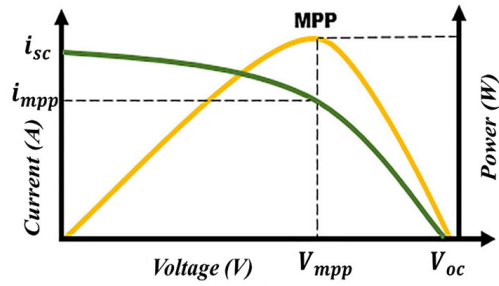


FIGURE 6. Solar PV module I-V and P-V feature.

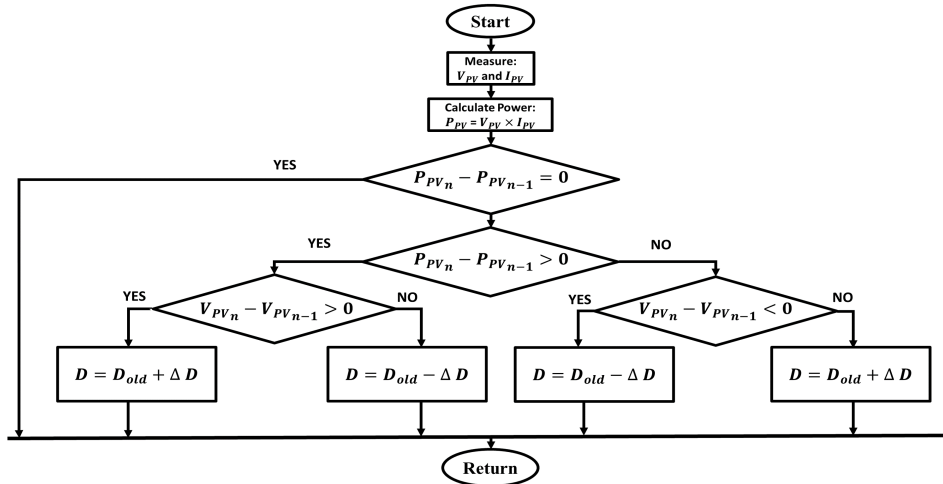
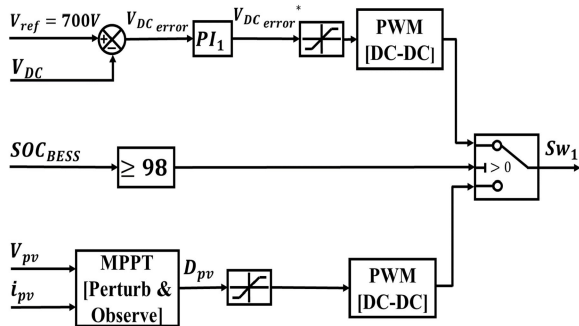
(P & O) is selected and this method can track the MPP more accurately. The P & O algorithm is easy to implement and demonstrated as the flowchart in Fig. 7. PV module output voltage V_{pv} and output current i_{pv} are the input of the MPPT algorithm. To execute this method, the current and voltage of PV modules need to be measured initially to determine the power of PV modules, P_{pv} . The observation and perturbation process is continued until the operating point reaches the MPP. The algorithm compares the voltages and power of time (n) with the sample at a time ($n - 1$) and estimates the time to reach to MPP. The P & O algorithm traces by increasing or reducing the voltage at the MPPT regularly of the PV module. When the positive power alteration occurs, a slight voltage perturbation can change the power of solar panel and voltage perturbation is maintained in similar track. Whereas when negative delta power occurs, it shows that the MPP is at far distance and the perturbation is reduced to attain the MPP. The P & O algorithm is summarized in Table 2. Therefore, the complete PV curve is examined by small-scale perturbations to locate the MPP that extend the response time of the algorithm. On the other hand, if the perturbation size is expanded, it produces steady-state oscillations about the MPP. The P & O algorithm output is the approximated MPPT voltage V_{mpp} . The MPPT voltage is employed to regulate the DC-DC converter to achieve the PV open-circuit voltage continuously. The PV system output power, P_{pv} is boosted by the DC-DC boost converter that control by controller shows in Fig. 8. The controller of the DC-DC boost converter is operating by getting DC voltage error, $V_{DC,error}$. The voltage error is calculated by comparing the given reference voltage, V_{ref} which is 700V.

The reference voltage is assigned with instantaneous DC-DC Boost converter output DC voltage V_{DC} . Afterwards, $V_{DC,error}^*$ is approximated by reducing the $V_{DC,error}(t)$ using a PI controller. In mathematic terms, the approximation can be explained as found from (17) and (18):

$$V_{DC,error}^* = k_{p,1}(V_{DC,error}(t)) + k_{i,1} \int_0^t (V_{DC,error}(t)) dt \quad (17)$$

$$V_{DC,error}(t) = V_{ref} + V_{DC}(t) \quad (18)$$

where $k_{p,1}$ and $k_{i,1}$ indicates the two fixed values that denotes as proportional gain and integral gains of the controller PI₁.

**FIGURE 7.** Flow chart of Perturb & Observe algorithm.**FIGURE 8.** PV DC-DC boost converter control scheme.**TABLE 2.** Scheme of Perturb & Observe algorithm.

Perturbation	ΔP	Perturbation Output
+ve	+ve	+ve
+ve	-ve	-ve
-ve	+ve	-ve
-ve	-ve	+ve

The values are allocated as 0.1 and 0.1, consecutively. However, the controller of the DC-DC Boost converter will break off the PV system output power, P_{pv} during battery's state of charge SOC_{BESS} is over or equal to 98% of battery capacity. The reason is to keep away the battery from being overcharged and unstable. Moreover, the lifetime of the battery can be reduced due to overcharging.

2) BATTERY ENERGY STORAGE SYSTEM MODELLING

Batteries generally consist of one or more electrochemical cells in series and/or parallel to achieve the desired nominal voltage and capacity for the BESS modelling. Generally, the classification of battery models depends on

electrochemical model and electric circuit model, and from these models the other models are normally obtained. For example, using Peukert's equation, the model of a battery is improved by integrating current. Besides, Shepherd's equation which is an electrochemical model. The mathematical model is utilized in this work because of efficient tools like SIMULINK/MATLAB. The Li-ion battery is used in this work due to its high-power density and energy, slow self-discharge and low maintenance cost, comparing to the other batteries. The parameter utilized for the BESS system in this work is tabulated in Table 1.

The equivalent electrical circuit of battery is constructed by a controlled voltage source connected with a constant internal resistance in series. The charging/discharging model of the Li-ion battery is stated in as follows:

$$V_{battery,charge} = E_{f1,2}(i_t, i_l, i) - iR \quad (19)$$

where $V_{battery,charge}$ indicates the battery voltage (V), $E_{f1,2}(i_t, i_l, i)$ indicates the no-load voltage (V), R indicates the internal resistance (Ω), and i indicates the battery current (A). Next, the controlled voltage source can be expressed for charging and discharging in charge model and discharging model. Then, the charging model of Li-ion battery is given as follows:

$$\begin{aligned} E_{f1}(i_t, i_l, i) = E_0 - K \frac{Q}{(0.1)Q + i_t} i_l - K \frac{Q}{Q - \int i_t dt} i_t \\ + A \exp(-B \cdot \int i_t dt) \end{aligned} \quad (20)$$

Then, the discharging model of the Li-ion battery is stated in as follows:

$$\begin{aligned} E_{f2}(i_t, i_l, i) = E_0 - K \frac{Q}{Q + i_t} i_l - K \frac{Q}{Q - \int i_t dt} i_t \\ + A \exp(-B \cdot \int i_t dt) \end{aligned} \quad (21)$$

From the (20) and (21), where E_0 indicates the battery constant voltage (V), K indicates the polarization voltage (Ah^{-1}), Q indicates the battery rated capacity (Ah), $\int i_t dt$ indicates the extracted battery capacity current rate (Ah), A indicates the exponential zone amplitude (V), B indicates the exponential zone time constant inverse (Ah^{-1}) and i_l indicates the low frequency current (A). Next, the term $A_{exp}(-B \cdot \int i_t dt)$ symbolizes the exponential area of the voltage when it is fully charged to the edge of exponential zone of the discharge characteristic curve. Thus, the gain of undetermined parameters of A and B can be specified from the exponential part as follows. The voltage drops during the exponential zone express in as follows.

$$A = E_{full} - E_{exp} \quad (22)$$

where E_{full} indicates the fully charged voltage and E_{exp} indicates the voltage at the boundary of exponential zone. The exponential zone time constant inverse is:

$$B = \frac{3}{Q_{exp}} \quad (23)$$

where Q_{exp} indicates the charge at the boundary of exponential zone. Here, the parameter E_0 utilized in (20) and (21) symbolizes the transition quantity between the starting of voltage when it is fully charged and the boundary of exponential zone. Thus, the value of E_0 can be calculated from the voltage in fully charged condition and it can be stated as follows:

$$E_0 = E_{full} + iR - A \quad (24)$$

The term $-K(Q/Q - \int i_t dt)i_t$ utilized in (20) and (21) indicates the nominal area from the boundary of exponential zone to the boundary of nominal zone of the discharge characteristic curve. Thus, the gain of K can be specified from the nominal part as follows:

$$K = (E_0 - E_{nom} - iR + A_{exp}(-BQ_{nom})) \frac{Q - Q_{nom}}{Q(Q_{nom} + i)} \quad (25)$$

where E_{nom} indicates the end voltage of the nominal zone and Q_{nom} indicates the end voltage of the nominal zone. The value of the completely charged voltage, charge of nominal zone, the end voltage and charge of the exponential zone can be determined from the discharge characteristic curve of that battery.

The Battery State of Charge (SOC) Regarding Charging and Discharging: The SOC presents one of the most important feature for batteries, however it represents many different concerns. Generally, the SOC of a battery is determined as the ratio of its current capacity to the nominal capacity.

The manufacturer provide the nominal capacity and it shows the charge that can be stored in maximum amount in the battery. The counting method by Coulomb estimates the charging current and discharging current of a battery is integrated over time in order to measure the SOC. Coulomb counting technique is done to measure the $SOC(t)_{charge}$ or $SOC(t)_{discharge}$ at time in (%), which is

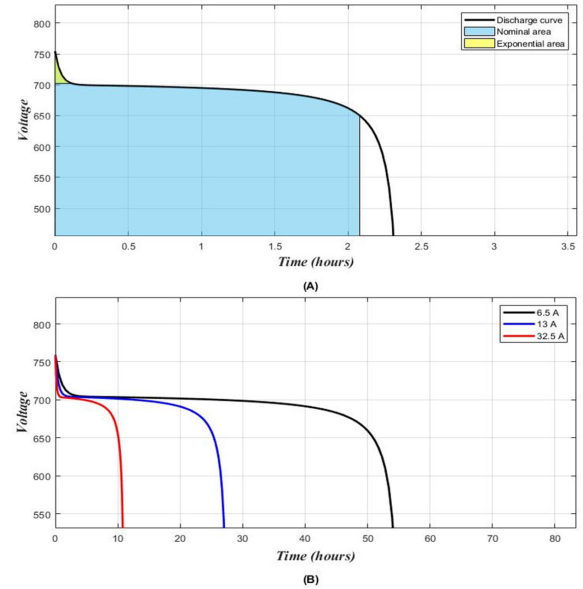


FIGURE 9. Feature of Li-ion battery current discharge.

calculated from the charging current, $i_{BESS,charge}(t)$ or discharging current, $i_{BESS,discharge}(t)$ with battery capacity in (Ah), and prior calculated SOC values, $SOC(t-1)_{charge}$ or $SOC(t-1)_{discharge}$. SOC is measured by the following (26) and (27)

$$SOC(t)_{charge} = SOC(t-1)_{charge} + \frac{1}{C_{BESS}} \int_{t-1}^t i_{BESS,charge}(t) dt \quad (26)$$

$$SOC(t)_{discharge} = SOC(t-1)_{discharge} - \frac{1}{C_{BESS}} \int_{t-1}^t i_{BESS,discharge}(t) dt \quad (27)$$

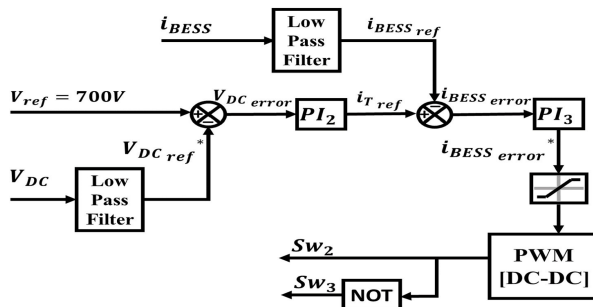
However, there are some factors that affect the perfection of Coulomb counting method involving the battery history, temperature, discharge current, and cycle life.

The discharge featured waveform of Li-ion battery is illustrated in Fig. 9. The discharge features are separated into three sections and which are nominal section, exponential section and the last is discharge curve. Voltage reduced rapidly in the exponential area, whereas the nominal battery voltage is the mid-point voltage throughout the charging and discharging and flatter curve represent minor inequality in voltage in this region. In the fully charged stage the voltage is superior over the nominal voltage. However, when end of life is appeared, the voltage is lower comparing to the mid-point voltage.

3) FREQUENCY SHARING STRATEGY OF A BESS-PV

In Fig. 10, shown the bidirectional converter Buck-Boost DC-DC controller for charging and discharging mode that contains embedded internal control loops and external control loops.

The stability of the frequency is maintained by the provided active power with proper configuration of the external control

**FIGURE 10.** BESS DC-DC Buck-Boost converter controller scheme.**TABLE 3.** Frequency droop features under several working conditions.

Working Conditions	Frequency	Droop features	Power distribution
Solar PV generation > DC-link Load demand	Increases	Regulate the rise in frequency and voltage within the suitable limits.	BESS absorbs the extra power equivalent to the rise in frequency and bus voltage until it attains the maximum charging limit.
Solar PV generation = DC-link Load demand	Stable	Maintain the stable voltage and frequency at its nominal value.	PV system supply the load- demand. BESS function at standby state.
Solar PV generation < DC-link Load demand	Decreases	Controlling the fall in frequency and voltage within the suitable limits.	BESS delivers the insufficient power equivalent to the fall in frequency and bus voltage until it attains the lowest discharging limit.
No Solar PV generation	Decreases	Controlling the fall-in frequency and voltage at a steady state value.	BESS delivers the total load-demand.

with a frequency droop f_{droop} . The design of internal control loop is constructed with a control loop of voltage to stabilize the system voltage and for fast dynamic response the filter output current is adjusted by the current control loop. The BESS active power can be measured as:

$$P_{BESS} = P_{DC-LINK} - P_{pv} \quad (28)$$

Here, $P_{DC-LINK}$ is the DC-link active power, P_{pv} is the total active power supplied by the PV. The active power of BESS, P_{BESS} obtained from (28) present the frequency droop,

$$f_{droop} = f_{atno-load} - m [P_{BESS(atfull-load)} - P_{BESS(atno-load)}] \quad (29)$$

The f_{droop} can be adjusted within their suitable limits to gain system stability. The methodology is suggested based on the frequency stability approach where load is divided between low and high-frequency elements by utilizing of a filter as demonstrated below in (30) and (31).

$$V_{DC,ref}^* = \left(\frac{1}{1 + T.s} \right) (V_{DC}) \quad (30)$$

$$i_{BESS,ref} = \left(\frac{1}{1 + T.s} \right) (i_{BESS}) \quad (31)$$

The PV module DC-link voltage of a, $V_{DC,ref}^*$ is compared with the DC voltage reference, V_{ref} and is then delivered to the voltage controller outer loop using PI₂ controller to generate current reference. Mathematically, the approach can be expressed as obtained from (32) and (33).

$$V_{DC,error}(t) = V_{ref} - V_{DC,ref}^*(t) \quad (32)$$

$$i_{T,ref} = k_{p,2}(V_{DC,error}(t)) + k_{i,2} \int_0^t (V_{DC,error}(t)) dt \quad (33)$$

where $k_{p,2}$ and $k_{i,2}$ are the two fixed values that denotes as proportional gain and integral gains of the controller PI₂. The values are allocated as 1.477 and 3077. Furthermore, the output reference BESS current, $i_{BESS,ref}$ is compared with the reference current from voltage control loop, $i_{T,ref}$ and is then delivered to the inner current loop controller using controller PI₃. The approach can be seen in mathematical term in (34) and (35).

$$i_{BESS,error}^* = k_{p,3}(i_{BESS,error}(t)) + k_{i,3} \int_0^t (i_{BESS,error}(t)) dt \quad (34)$$

$$i_{BESS,error}(t) = i_{T,ref} - i_{BESS,ref}(t) \quad (35)$$

where $k_{p,3}$ and $k_{i,3}$ are the two fixed values that denotes as proportional gain and integral gains of the controller PI₃. The values are allocated as 0.043 and 0.65. When the active power of a PV module increases than the load demand of DC-link for UPQC, then the voltage frequency components is high. But, When the active power of a PV module decreases than the load demand of DC-link for UPQC, then the voltage frequency components is low. The lower frequency components delivered, and the gate signals are generated for the DC-DC converter of a BESS for discharging mode. In Table 3 explains the interpretation of the frequency droop features for power distributing under several working conditions of the PV-BESS-UPQC system.

III. WORKING PRINCIPLE OF THE PROPOSED CONTROL OF PV-BESS-UPQC USING SELF-TUNING FILTER TECHNIQUE

A. STF-UVG SYNCHRONIZATION TECHNIQUE

The proposed STF-UVG technique extract the synchronization phases in a simple method from the supply voltage and the method is non-iterative. In Fig.11 shown the STF technique in UPQC controller scheme. In (36) the matrix form of

the three-phase supply voltage is demonstrated, and Clarke transformation matrix is used to convert the source voltage from $\alpha\beta$ -domain to $\alpha\beta0$ -domain.

$$\begin{bmatrix} V_{S_\alpha} \\ V_{S_\beta} \\ V_{S_0} \end{bmatrix} = \sqrt{\frac{2}{3}} \begin{bmatrix} 1 & -\frac{1}{2} & -\frac{1}{2} \\ 0 & \frac{\sqrt{3}}{2} & -\frac{\sqrt{3}}{2} \\ \frac{1}{2} & \frac{1}{2} & \frac{1}{2} \end{bmatrix} \begin{bmatrix} V_a \\ V_b \\ V_c \end{bmatrix} \quad (36)$$

The distorted supply voltage is separated into fundamental component and harmonic component by considering only two phases in $\alpha\beta$ -domain. The relationship is shown in (37).

$$\begin{bmatrix} V_{S_\alpha} \\ V_{S_\beta} \end{bmatrix} = \begin{bmatrix} V_{S_\alpha(\text{fund})} + V_{S_\alpha(\text{har})} \\ V_{S_\beta(\text{fund})} + V_{S_\beta(\text{har})} \end{bmatrix} \quad (37)$$

Here, $V_{s,\alpha(\text{fund})}$ indicates the fundamental (fund) component and $V_{s,\alpha(\text{har})}$ indicates the harmonic (har) component in $\alpha\beta$ -domain. Both the fundamental component in $\alpha\beta$ -domain is required to produce synchronization phases. The fundamental components are extracted by self-tuning filtering (STF) method. The STF method is applied to suppress the existed harmonic components in the distorted supply voltage. Therefore, the synchronization phases are extracted more perfectly, and the quality of the extraction is improved. The Laplace transformation is performed and a typical STF transfer function is expressed in (38).

$$\begin{bmatrix} V_{S_\alpha(\text{fund})}(s) \\ V_{S_\beta(\text{fund})}(s) \end{bmatrix} = \frac{K_1}{s} \begin{bmatrix} V_{S_\alpha}(s) - V_{S_\alpha(\text{fund})}(s) \\ V_{S_\beta}(s) - V_{S_\beta(\text{fund})}(s) \end{bmatrix} + \frac{2\pi f_{c1}}{s} \begin{bmatrix} -V_{S_\beta(\text{fund})}(s) \\ V_{S_\alpha(\text{fund})}(s) \end{bmatrix} \quad (38)$$

Here, K_1 denotes constant gain parameter and f_{c1} denotes the cut-off frequency. The rating of K_1 can be estimated in between 20 to 80 and the rating of f_{c1} follows the system frequency. In this project, the rating is estimated 20 for K_1 and 50 Hz for f_{c1} . Synchronization phases of $\sin(\omega t)$ and $\cos(\omega t)$ can be attained with the availability of $V_{s,\alpha(\text{fund})}$ and $V_{s,\beta(\text{fund})}$ and demonstrated in the (39).

$$\begin{bmatrix} \sin(\omega t) \\ \cos(\omega t) \end{bmatrix} = \frac{1}{\sqrt{(V_{S_\alpha(\text{fund})})^2 + (V_{S_\beta(\text{fund})})^2}} \begin{bmatrix} V_{S_\alpha(\text{fund})} \\ -V_{S_\beta(\text{fund})} \end{bmatrix} \quad (39)$$

The action of conventional PLL element can be omitted by utilizing (39) as UVG technique and the generation of synchronization phases can be effectively done in the presence of supply voltage distortion in UPQC.

B. CONTROL OF SERIES APF COMPENSATION

The three-phase reference voltage signal, $V_{ref,abc}^*$ in abc -domain is calculated as follows in (40) by utilizing the information of phase and frequency of STF-UVG. Here, the value of maximum peak voltage magnitude, $V_{m,max-peak}$ is obtained from peak amplitude of the fundamental load voltage. The reference voltage signal should be in phase with

supply voltage at PCC, peak amplitude load reference voltage is the d -frames components while the q -frames components should be zero.

$$\begin{bmatrix} V_{ref_a}^* \\ V_{ref_b}^* \\ V_{ref_c}^* \end{bmatrix} = V_{m,max-peak} \begin{bmatrix} \sin(\omega t) \\ \sin(\omega t - \frac{2\pi}{3}) \\ \sin(\omega t + \frac{2\pi}{3}) \end{bmatrix} \quad (40)$$

$$\begin{bmatrix} V_{ref_\alpha}^* \\ V_{ref_\beta}^* \\ V_{ref_0}^* \end{bmatrix} = \sqrt{\frac{2}{3}} \begin{bmatrix} 1 & -\frac{1}{2} & -\frac{1}{2} \\ 0 & \frac{\sqrt{3}}{2} & -\frac{\sqrt{3}}{2} \\ \frac{1}{2} & \frac{1}{2} & \frac{1}{2} \end{bmatrix} \begin{bmatrix} V_{ref_a}^* \\ V_{ref_b}^* \\ V_{ref_c}^* \end{bmatrix} \quad (41)$$

$$\begin{bmatrix} V_{ref_d}^* \\ V_{ref_q}^* \end{bmatrix} = \begin{bmatrix} \cos(\omega t) & \sin(\omega t) \\ -\sin(\omega t) & \cos(\omega t) \end{bmatrix} \begin{bmatrix} V_{ref_\alpha}^* \\ V_{ref_\beta}^* \end{bmatrix} \quad (42)$$

Then, three-phase reference voltage signal demonstrated in matrix form in (41) and Clarke transformation matrix is used to convert the reference voltage signal from abc domain to $\alpha\beta0$ -domain. Next, the fundamental component of the distorted supply voltage at PCC is extracted by using the proposed STF-UVG to generate synchronization phases and frequency that obtained in (39) is used for producing the reference axis in the dq -frames. Considering only two phases, the reference voltage signal is acquired in the dq -frames by using (42) where Park transformation matrix is utilized. Moreover, the Equation (43) is utilized to transform the three-phase load voltage, $V_{L,abc}$ from abc -domain to $\alpha\beta0$ -domain utilizing Clarke-matrix. Then, load voltage signal in $\alpha\beta0$ -domain is converted by considering only two phases in dq -frames by using Park-matrix with the consideration of synchronization phases and frequency from STF-UVG for producing the reference axis in the dq -frames and demonstrated in (44).

$$\begin{bmatrix} V_{L_\alpha} \\ V_{L_\beta} \\ V_{L_0} \end{bmatrix} = \sqrt{\frac{2}{3}} \begin{bmatrix} 1 & -\frac{1}{2} & -\frac{1}{2} \\ 0 & \frac{\sqrt{3}}{2} & -\frac{\sqrt{3}}{2} \\ \frac{1}{2} & \frac{1}{2} & \frac{1}{2} \end{bmatrix} \begin{bmatrix} V_{L_a} \\ V_{L_b} \\ V_{L_c} \end{bmatrix} \quad (43)$$

$$\begin{bmatrix} V_{L_d} \\ V_{L_q} \end{bmatrix} = \begin{bmatrix} \cos(\omega t) & \sin(\omega t) \\ -\sin(\omega t) & \cos(\omega t) \end{bmatrix} \begin{bmatrix} V_{L_\alpha} \\ V_{L_\beta} \end{bmatrix} \quad (44)$$

Next, the Equation (45) is utilized to transform the three-phase supply voltage, $V_{s,abc}$ from abc -domain to $\alpha\beta0$ -domain utilizing Clarke-matrix. Then, supply voltage signal in $\alpha\beta0$ -domain is converted by considering only two phases in dq -frames by using Park-matrix with the consideration of synchronization phases and frequency from STF-UVG for producing the reference axis in the dq -frames and

demonstrated in (46).

$$\begin{bmatrix} V_{S_\alpha} \\ V_{S_\beta} \\ V_{S_0} \end{bmatrix} = \sqrt{\frac{2}{3}} \begin{bmatrix} 1 & -\frac{1}{2} & -\frac{1}{2} \\ 0 & \frac{\sqrt{3}}{2} & -\frac{\sqrt{3}}{2} \\ \frac{1}{2} & \frac{1}{2} & \frac{1}{2} \end{bmatrix} \begin{bmatrix} V_{S_a} \\ V_{S_b} \\ V_{S_c} \end{bmatrix} \quad (45)$$

$$\begin{bmatrix} V_{S_d} \\ V_{S_q} \end{bmatrix} = \begin{bmatrix} \cos(\omega t) & \sin(\omega t) \\ -\sin(\omega t) & \cos(\omega t) \end{bmatrix} \begin{bmatrix} V_{S_\alpha} \\ V_{S_\beta} \end{bmatrix} \quad (46)$$

In the series active power filter controller compensator, the compensation strategies are using the comparison technique between the load voltage, $V_{L,dq}$ and supply voltage, $V_{s,dq}$ at PCC both in the dq frames to give actual voltage error of series compensator. Next, the reference voltage signal, $V_{ref,dq}^*$ that already in phase with supply voltage at PCC is compared with the supply voltage, $V_{s,dq}$ at PCC both in the dq frames to obtain actual reference voltage of series compensator. Moreover, the comparison between actual reference voltage and actual voltage error of series compensator will attain the injection reference voltage, $V_{SE,dq}^*$. Both the equation is demonstrated in (47) and (48).

$$V_{SE_d}^* = (V_{ref_d}^* - V_{S_d}) - (V_{L_d} - V_{S_d}) \quad (47)$$

$$V_{SE_q}^* = (V_{ref_q}^* - V_{S_q}) - (V_{L_q} - V_{S_q}) \quad (48)$$

Then, the $V_{SE,d}^*$ and $V_{SE,q}^*$ is converted from dq -frames to abc -domain and demonstrated in Equations (49) and (50). The injection reference voltage series compensator, $V_{SE,abc}^*$ are passed through in a hysteresis voltage controller to generate appropriate gating pulses for the series converter

$$\begin{bmatrix} V_{SE_\alpha}^* \\ V_{SE_\beta}^* \end{bmatrix} = \begin{bmatrix} \sin(\omega t) & \cos(\omega t) \\ -\cos(\omega t) & \sin(\omega t) \end{bmatrix} \begin{bmatrix} V_{SE_d}^* \\ V_{SE_q}^* \end{bmatrix} \quad (49)$$

$$\begin{bmatrix} V_{SE_a}^* \\ V_{SE_b}^* \\ V_{SE_c}^* \end{bmatrix} = \sqrt{\frac{2}{3}} \begin{bmatrix} 1 & 0 \\ -\frac{1}{2} & \frac{\sqrt{3}}{2} \\ -\frac{1}{2} & -\frac{\sqrt{3}}{2} \end{bmatrix} \begin{bmatrix} V_{SE_\alpha}^* \\ V_{SE_\beta}^* \end{bmatrix} \quad (50)$$

C. CONTROL OF SHUNT APF COMPENSATION

The extraction of the load current harmonic component is done by the suggested STF on $\alpha\beta$ -domain. The (51) is utilized to transform the three-phase load current $i_{L,abc}$ from abc domain to $\alpha\beta 0$ -domain utilizing Clarke-matrix. Emphasizing on $\alpha\beta$ -domain, the signal of load current $i_{L,\alpha\beta}$ can be divided into fundamental component and harmonic component. Therefore, the relationship can be stated in (52).

$$\begin{bmatrix} i_{L_\alpha} \\ i_{L_\beta} \\ i_{L_0} \end{bmatrix} = \sqrt{\frac{2}{3}} \begin{bmatrix} 1 & -\frac{1}{2} & -\frac{1}{2} \\ 0 & \frac{\sqrt{3}}{2} & -\frac{\sqrt{3}}{2} \\ \frac{1}{2} & \frac{1}{2} & \frac{1}{2} \end{bmatrix} \begin{bmatrix} i_{L_a} \\ i_{L_b} \\ i_{L_c} \end{bmatrix} \quad (51)$$

$$\begin{bmatrix} i_{L_\alpha} \\ i_{L_\beta} \end{bmatrix} = \begin{bmatrix} i_{L_{\alpha(fund)}} + i_{L_{\alpha(har)}} \\ i_{L_{\beta(fund)}} + i_{L_{\beta(har)}} \end{bmatrix} \quad (52)$$

Here, $i_{L,\alpha(fund)}$ indicate the fundamental (fund) components and $i_{L,\alpha(har)}$ indicate the harmonic (har) components of load current on α -domain. The representation of load current component in β -domain is same as α -domain. The Laplace transformation is performed and the STF technique is implemented for the extraction of load current fundamental components ($i_{L,\alpha(fund)}$ and $i_{L,\beta(fund)}$) on $\alpha\beta$ -domain. The formula is shown in (53).

$$\begin{bmatrix} i_{L_{\alpha(fund)}}(s) \\ i_{L_{\beta(fund)}}(s) \end{bmatrix} = \frac{K_2}{s} \begin{bmatrix} i_{L_\alpha}(s) - i_{L_{\alpha(fund)}}(s) \\ i_{L_\beta}(s) - i_{L_{\beta(fund)}}(s) \end{bmatrix} + \frac{2\pi f_{c2}}{s} \begin{bmatrix} -i_{L_{\beta(fund)}}(s) \\ i_{L_{\alpha(fund)}}(s) \end{bmatrix} \quad (53)$$

Here, K_2 denotes constant gain parameter and f_{c2} denotes the cut-off frequency. The rating of K_2 can be estimated in between 20 to 80 and the rating of f_{c2} follows the system frequency. In this project, the rating is estimated 20 for K_1 and 50 Hz for f_{c1} . The harmonic components ($i_{L,\alpha(har)}$ and $i_{L,\beta(har)}$) can be achieved by utilizing the fundamental components ($i_{L,\alpha(fund)}$ and $i_{L,\beta(fund)}$). The calculation is expressed in (54):

$$\begin{bmatrix} i_{L_{\alpha(har)}} \\ i_{L_{\beta(har)}} \end{bmatrix} = \begin{bmatrix} i_{L_\alpha} - i_{L_{\alpha(fund)}} \\ i_{L_\beta} - i_{L_{\beta(fund)}} \end{bmatrix} \quad (54)$$

Equation (54) shows the process of extraction of harmonic components. The process follows by the subtraction between the fundamental components (the extraction is done using STF filter) and the load current component $i_{L,\alpha\beta}$ in $\alpha\beta$ -domain. Therefore, the harmonic components are extracted in an indirect manner. Next, the harmonic components attained from (54) and synchronization phases attained from (39) are used to achieve the harmonic components in d -frame following the (55).

$$i_{L_d(har)} = i_{L_{\alpha(har)}} \sin(\omega t) - i_{L_{\beta(har)}} \cos(\omega t) \quad (55)$$

The wave of the original load current in $\alpha\beta$ -domain, $i_{L,\alpha\beta}$ and the identical synchronized phases are implemented to operate the transformation of $\alpha\beta$ -domain into frame- q by utilizing the following approach in (56):

$$i_{L_q} = i_{L_\alpha} \cos(\omega t) + i_{L_\beta} \sin(\omega t) \quad (56)$$

In the $\alpha\beta 0$ -domain, 0-domain does not require to be transformed. However, the DC component of the d -frame denotes the fundamental load current magnitude and the oscillating AC component denotes the harmonic current magnitude. Besides, q -frame carries the phase data of the load current. Noteworthy fact is frame-0 of reference frame $dq0$ which is straightly acquired from the domain- $\alpha\beta 0$ is required to stabilize the dc-link voltage. Likewise, the harmonic component of d -frame loads current $i_{L,d(har)}$, load current $i_{L,q}$ in q -frame and load current $i_{L,0}$, in 0-frame are three different undesirable component of load currents that denote unbalanced, harmonic and reactive currents.

Next, $i_{error,dc}$ is measured by reducing the error $e_1(t)$ obtained between total instantaneous dc-link voltage and

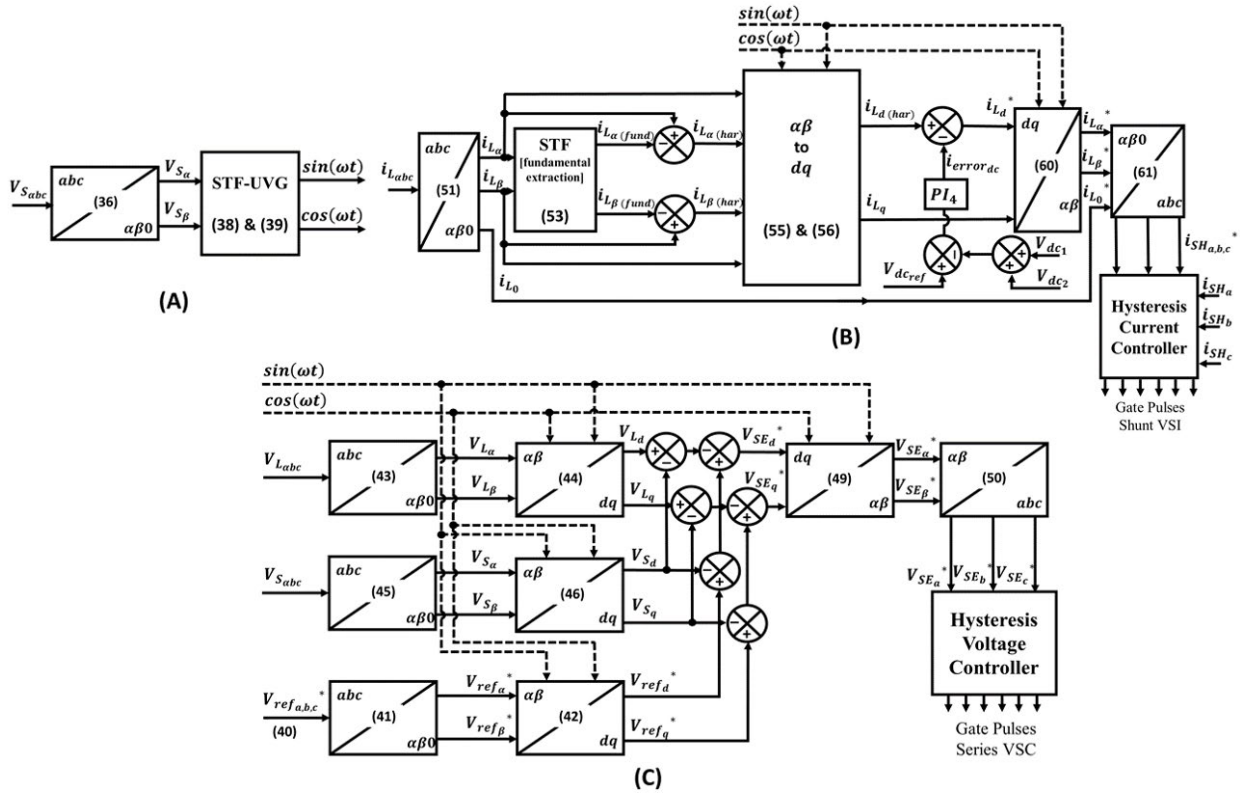


FIGURE 11. Control block diagram of the self-tuning filter (STF) technique in UPQC controller scheme (A) STF-UVG (B) Shunt APF control scheme (C) Series APF control scheme.

reference dc-link voltage $V_{dc,ref}$ with a PI controller. The mathematic calculation is given in (57) and (58):

$$i_{error_{dc}} = k_{p,4}e_1(t) + k_{i,4} \int_0^t e_1(t) dt \quad (57)$$

$$e_1(t) = V_{dc,ref} - (V_{cap_1}(t) + V_{cap_2}(t)) \quad (58)$$

where $k_{p,4}$ and $k_{i,4}$ are two fixed values that denotes as proportional gain and integral gains of the controller PI_4 . The values are allocated as 0.3 and 2 in this study. Therefore, the grid reference current in the d -frame is given as in (59):

$$i_d^* = i_{Ld(har)} - i_{error_{dc}} \quad (59)$$

Then, the signal $i_{L,d}^*$ and $i_{L,q}$ is converted into abc -domain injection reference grid currents. From (60) and (61) are applied to produce the reference current $i_{SH,abc}$. The injection reference supply currents and the measured supply current are compared in a hysteresis current controller to produce the shunt converter gating pulses.

$$\begin{bmatrix} i_{L\alpha}^* \\ i_{L\beta}^* \end{bmatrix} = \begin{bmatrix} \sin(\omega t) & \cos(\omega t) \\ -\cos(\omega t) & \sin(\omega t) \end{bmatrix} \begin{bmatrix} i_{Ld}^* \\ i_{Lq}^* \end{bmatrix} \quad (60)$$

$$\begin{bmatrix} i_{SH\alpha}^* \\ i_{SHb}^* \\ i_{SHc}^* \end{bmatrix} = \sqrt{\frac{2}{3}} \begin{bmatrix} 1 & 0 \\ -\frac{1}{2} & \frac{\sqrt{3}}{2} \\ -\frac{1}{2} & -\frac{\sqrt{3}}{2} \end{bmatrix} \begin{bmatrix} i_{L\alpha}^* \\ i_{L\beta}^* \end{bmatrix} \quad (61)$$

IV. SIMULATION RESULTS

The operation of proposed PV-BESS-UPQC using STF-UVG combine with STF- $dq0$ filter technique (knowns as STF technique) is presented and the operation is analysed using MATLAB-Simulink platform (R2018a). The simulation studies include connection of the proposed PV-BESS-UPQC circuits, design of the PV-BESS-UPQC control system and performance assessment. A standard two-level inverter for the shunt APF compensator and series APF compensator sharing common DC-link which is a combination of the DC link capacitor, PV and BESS. At the shunt APF, standard split DC-link capacitors of $4700 \mu F$ are utilized and each of them stores the reactive power from the unbalance non-linear load. Then, the output of shunt compensator is attached to a 3 mH L -typed filter while by attaching a 3.6 mH L -typed filter to the series APF, switching ripples is minimized. In this study, the DC-link reference capacitor voltage is assigned as 700 V . Meanwhile, unbalance nonlinear loads are considered, and they are comprising of nonlinear loads allocated as three single-phase in unbalanced manner. The unbalance non-linear load parameter is summarized in Table 4. The performance of the proposed model is analysed in a comparative manner, performance simulated by UPQC that connected with PV and BESS (with PV-BESS) as external support of DC-link capacitor is compared with standard conventional UPQC (without PV-BESS) to validate the significance of UPQC after connecting the

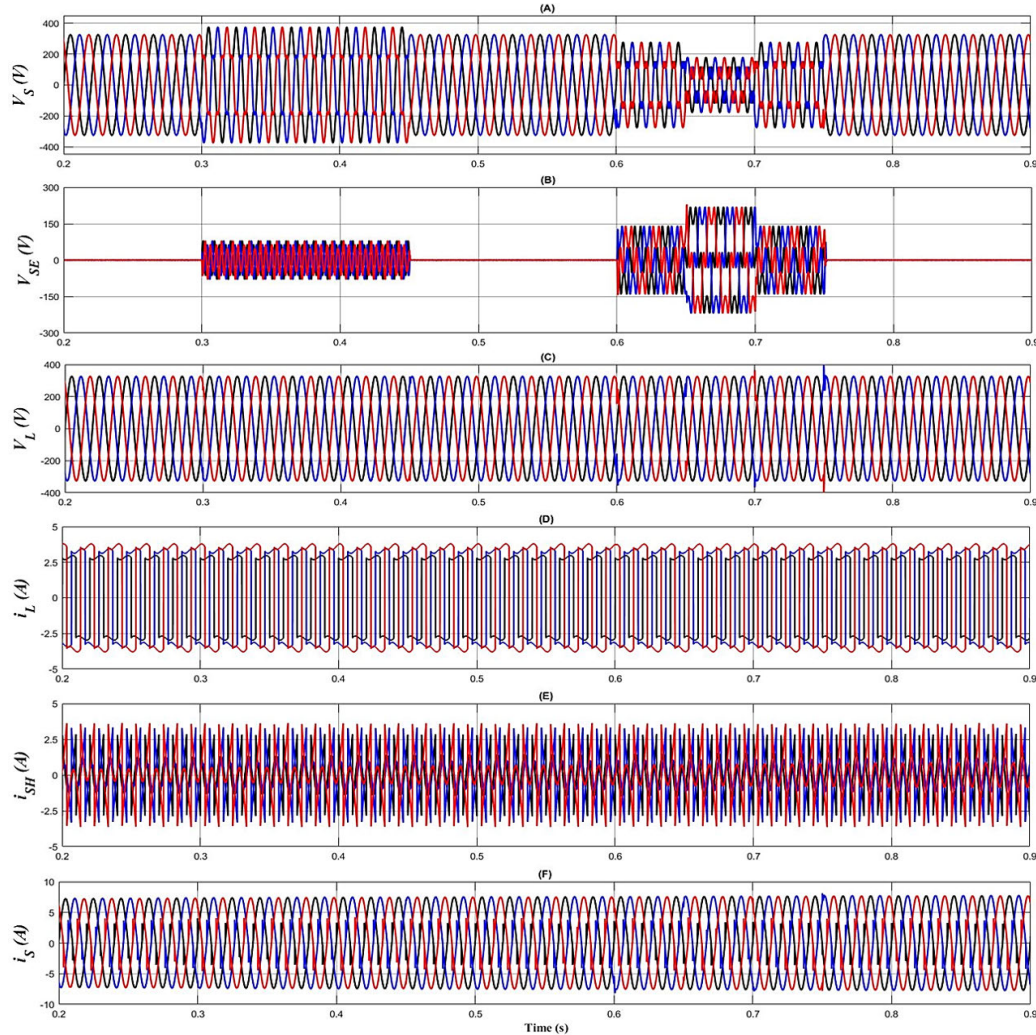


FIGURE 12. Simulation waveform acquired under Case Study 1 for UPQC connecting with PV-BESS, with include (A) three-phase source voltage (B) Injection voltage of Series APF (C) Load Voltage (D) Load Current (E) Injection Current of Shunt APF (F) Source Current.

TABLE 4. Configuration of nonlinear load for simulation studies.

Nonlinear load	Load description
Unbalance Single phase load	Phase- α Single-phase uncontrolled rectifier supplying a series attached 1500 mH inductor and 70 Ω resistor
	Phase- β Single-phase uncontrolled rectifier supplying a series attached 1300 mH inductor and 60 Ω resistor
	Phase- γ Single-phase uncontrolled rectifier supplying a series attached 1100 mH inductor and 55 Ω resistor

external support of DC-link. Furthermore, the PV-BESS-UPQC is tested while applying the proposed STF technique for the compensator controller and compared with the performance of the standard conventional SRF-PLL combine with a reference current generation applying moving average

filter (MAF) filter technique (knowns as SRF-MAF technique). Several case studies are conducted in the steady-state condition where different power quality problems are considered.

A. CASE STUDY 1: UPQC USING STF TECHNIQUE CONNECTING EXTERNAL SOURCE OF PV-BESS

- 1) SCENARIO A: BALANCE HARMONIC SOURCE VOLTAGE WITH NON-LINEAR LOAD AT CONSTANT IRRADIANCE 800 W/M² AT 45° (CONNECTING WITH PV-BESS AS EXTERNAL SOURCE OF DC-LINK)

The performance of PV-BESS-UPQC under context of source voltage harmonics at PCC and the combination of harmonic and sag are displayed in Fig. 12. The irradiation is maintained constant at 800 W/m² and the temperature 45 degree Celsius that follow the Malaysia tropical climate. The different observed signals are grid voltages, series compensated voltages, load voltages, load currents, shunt compensated currents, source currents. From Fig. 12(A), it can be noticed

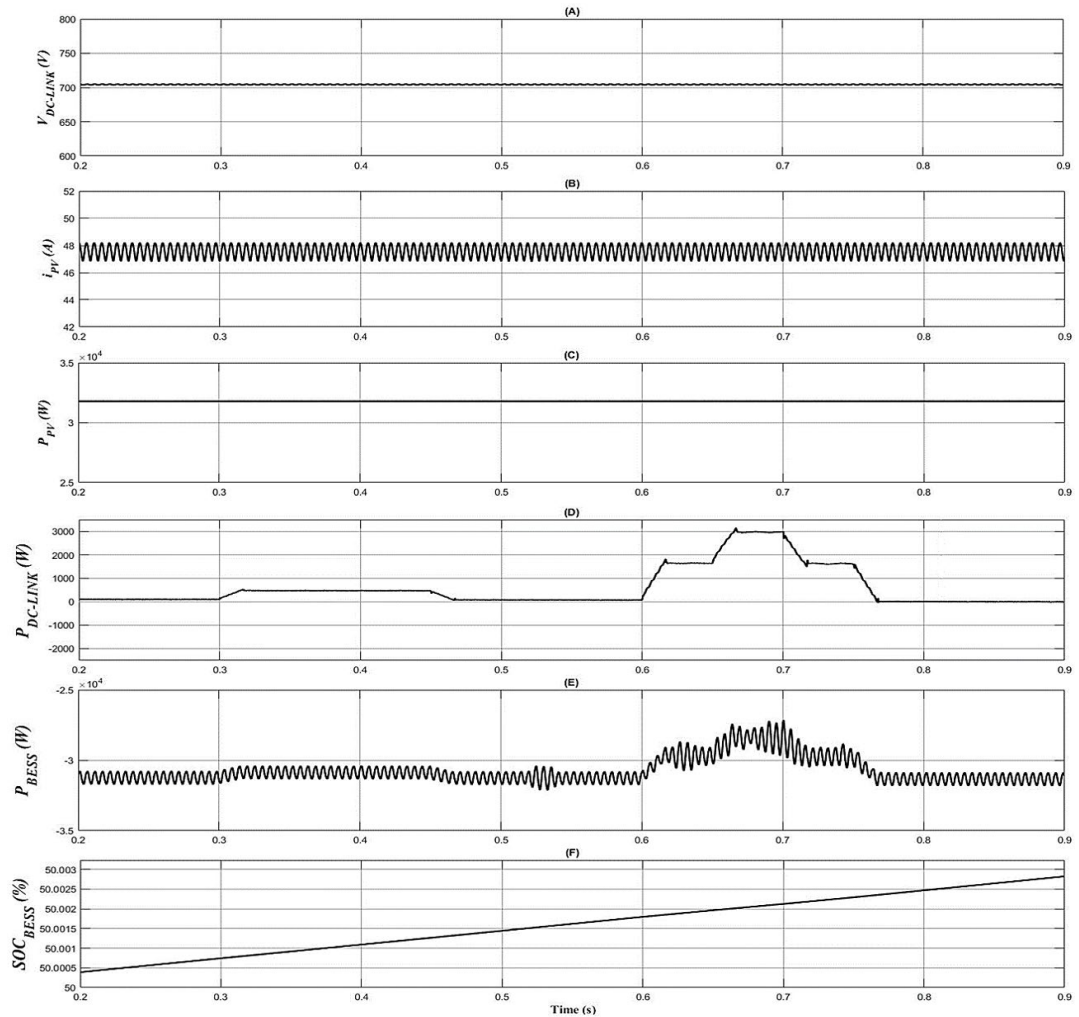


FIGURE 13. Simulation result acquired under Case Study 1 for UPQC connecting with PV-BESS, with include (A) DC-Link Voltage (B) Current of PV (C) Power of PV (D) Output power of DC-Link (E) Power of BESS (F) SOC of BESS.

that during 0.3s to 0.45s, there is voltage harmonics and during 0.6s to 0.65s, there is a combination of voltage harmonic and voltage sag of 0.7 pu and during 0.65s to 0.7s, there is a combination of voltage harmonic and voltage sag of 0.4 pu. An appropriate voltage V_{SE} is injected by the series compensator to mitigate the source voltage, V_S under these contexts during the condition of voltage sag which can be seen in Fig. 12(B) to keep the load voltage, V_L equivalent to the rated voltage. It can be noticed from Fig. 12(C) that the load voltage is sinusoidal and equal to the rated voltage. Fig. 12(D) shows the distorted load current, i_L created by the unbalanced non-linear load. Three-phase unbalance load is considered in this work. Since the non-linear load is utilized, the shunt compensator mitigates for the source current, i_S by injecting a current i_{SH} shown in Fig. 12(E) to keep the grid current sinusoidal. The sinusoidal grid current can be seen from Fig. 12(F). From Fig. 13(A), it can be noticed that the DC link voltage is stable at 700 V during the voltage harmonic and the combination of voltage harmonic and voltage sag. The

PV current is around 46.2 A observed in Fig. 13(B) and the power of the PV can be seen in Fig. 13(C) which is 32 KW. The DC link power can be observed in Fig. 13(D) and it is increased during 0.3s to 0.45s so that the voltage harmonics can be compensated. Moreover, during 0.6s to 0.75s the power of the DC is increased so that the harmonics can be mitigated, and the load can be supported during insufficient voltage supplied from the source as well. The power of the BESS is seen in Fig. 13(E) and it can be observed that during 0.3s to 0.45s the power of the BESS is slightly increased and during 0.6s to 0.75s when the combination of harmonics and sag happened the power of the BESS is increased little high since the current of the BESS is increased. The state of charge (SOC) shows in Fig. 13(F) and can be noticed the charging operation of the BESS throughout the process.

The THD for current under voltage harmonic condition is shown in Fig. 14(A). It can be observed that the THD is very low which is 2.05%. Moreover, Fig. 14(B) shows the THD for current under voltage harmonic with sag condition and can be

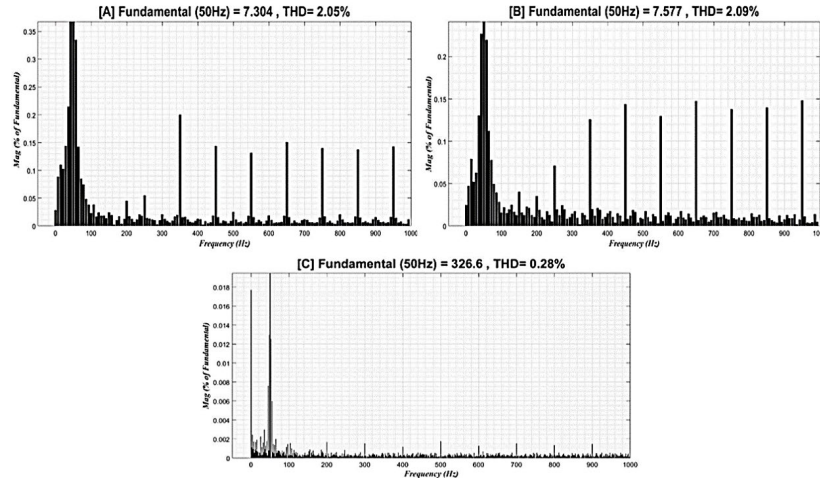


FIGURE 14. Simulation findings acquired under Case Study 1 for UPQC connecting with PV-BESS, (A) THD for current under voltage harmonic condition (B) THD for current under voltage harmonic with sag condition (C) THD for voltage.

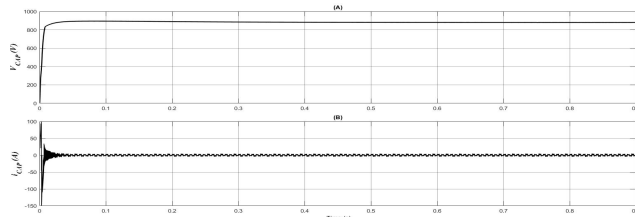


FIGURE 15. Simulation findings obtained under Case Study 1 for UPQC connecting with PV-BESS (A) Total capacitor voltage (B) Total capacitor current.

noticed that the THD is only 2.09%. Furthermore, Fig. 14(C) shows the THD for voltage and can be seen that the THD is only 0.28%. All these THD results fulfil the IEEE standard 519. From Fig. 15, it can be noticed that the rise time of the capacitor voltage is very fast. At 0.01s the capacitor voltage achieved the desired voltage. When the capacitor voltage reaches to the desired voltage faster, rapid compensation by the series compensator and the shunt compensator can be executed. Moreover, the capacitor voltage is stable during 0.3s to 0.45s when the voltage harmonic happened and during 0.6s to 0.75s when the combination of voltage harmonic and sag happened. These results verified that the shunt compensator is working properly since the shunt compensator is responsible for capacitor voltage balancing. The capacitor current is also shown in the Fig. 15. It can be observed from the Fig. 15 that transient response exists until 0.01s in the capacitor current and then it becomes stable throughout the operation. However, the UPQC without PV and BESS does not show quality result like the PV-BESS-UPQC. In the scenario B, UPQC without PV and BESS will be discussed and comparison with PV-BESS-UPQC will be shown in Table 5 and Table 6 in terms of THD.

2) SCENARIO B: BALANCE HARMONIC SOURCE VOLTAGE WITH NON-LINEAR LOAD AT CONSTANT IRRADIANCE 800 W/M² AT 45° (WITHOUT CONNECTING EXTERNAL SOURCE OF PV-BESS)

The performance of UPQC under context of PCC voltage harmonics and the combination of harmonic and sag are displayed in Fig 16. The case study is done without connecting PV and BESS. The irradiation is maintained constant at 800 W/m² and the temperature 45 degree Celsius. The different observed signals are grid voltages, series compensated voltages, load voltages, load currents, shunt compensated currents, source currents. From Fig. 16(A), it can be noticed that during 0.3s to 0.45s, there is voltage harmonics and during 0.6s to 0.65s, there is a combination of voltage harmonic and voltage sag of 0.7 pu and during 0.65s to 0.7s, there is a combination of voltage harmonic and voltage sag of 0.4 pu. The series compensator mitigates for the source voltage under these contexts by injecting an appropriate voltage V_{SE} during voltage sag which can be seen in Fig. 16(B) to keep the load voltage, V_L equivalent to the rated voltage. It can be observed from Fig. 16(C) that the load voltage is sinusoidal and equal to the rated voltage. Fig. 16(D) shows the distorted load current, i_L created by the unbalanced non-linear load. Three phase unbalance loads are considered in this work. Since the non-linear load is utilized in this work, the shunt compensator is supposed to mitigate for the source current under non-linear load context by injecting an appropriate current i_{SH} shown in Fig. 16(E) to keep the source current, i_S sinusoidal. However, the capacitor voltage takes long time to attain the determined voltage and most of the capacitor voltage is utilized by the series compensator and for that reason the shunt compensator does not have enough support from the capacitor to inject appropriate compensation current to mitigate for the source current. From Fig. 16(F) it can be

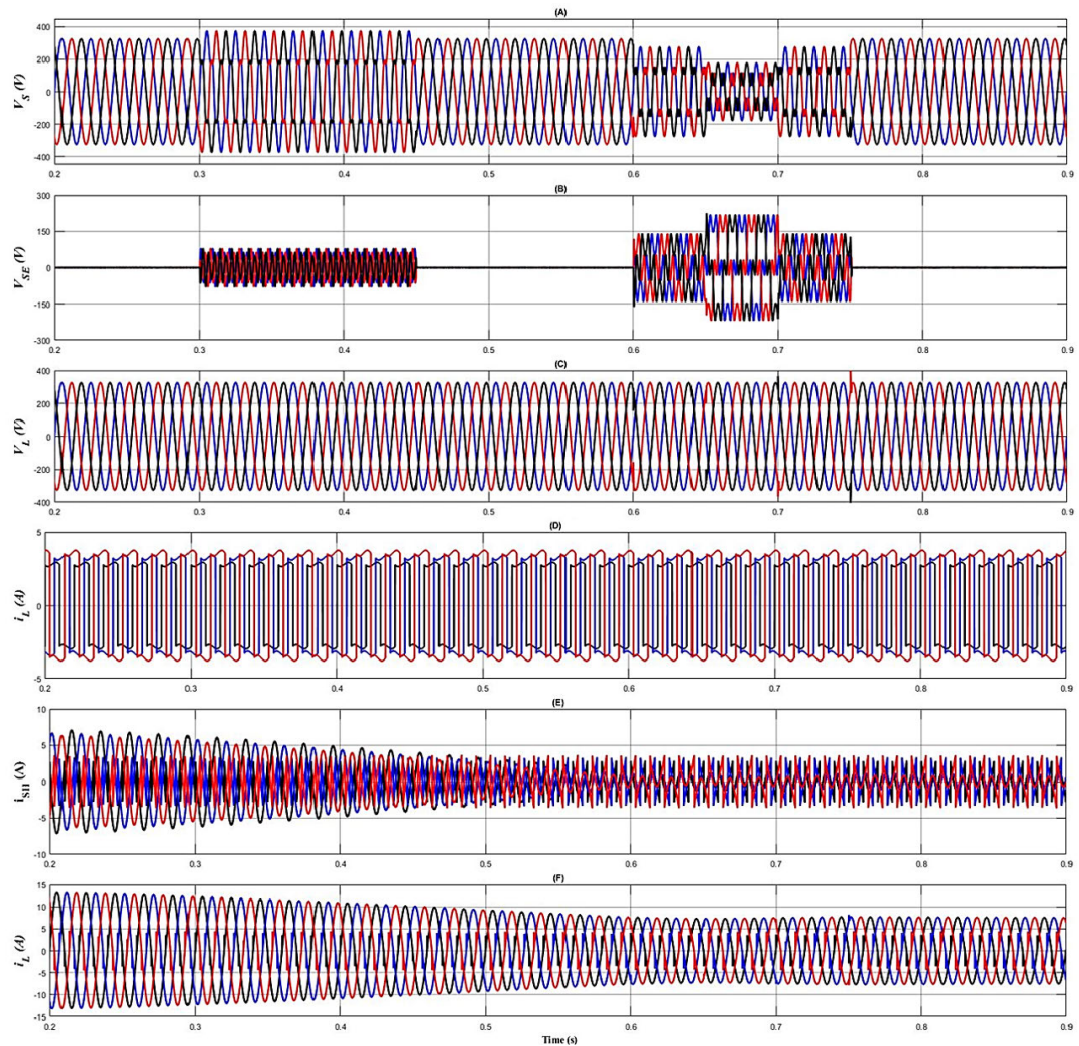


FIGURE 16. Simulation waveform acquired under Case Study 1 for UPQC connecting without PV-BESS, with include (A) three-phase source voltage (B) Injection voltage of Series APF (C) Load Voltage (D) Load Current (E) Injection Current of Shunt APF (F) Source Current.

noticed that the source current is high at the beginning and not pure sinusoidal like the PV-BESS-UPQC case study.

The THD for current under voltage harmonic condition is shown in Fig. 17(A). It can be observed that the THD is 4.66% which is higher than the PV-BESS-UPQC case study. Moreover, Fig. 17(B) shows the THD for current under voltage harmonic with sag condition and can be noticed that the THD is 5.49% which is also higher than the PV-BESS-UPQC case study. Furthermore, Fig. 17(C) shows the THD for voltage and can be seen that the THD is only 0.29% which is slightly higher than the PV-BESS-UPQC case study. From Fig. 18, it can be noticed that the capacitor voltage is rising very slow and the stability is not achieved accurately. Since the capacitor voltage reach to the desired voltage very slow, rapid compensation by the series compensator and the shunt compensator is not possible. Moreover, the capacitor voltage is not stable during 0.35s to 0.45s when the voltage harmonic happened and during 0.6s to 0.75s when the combination of

voltage harmonic and sag happened. These results verified that the shunt compensator is not working properly since the shunt compensator is responsible for capacitor voltage balancing. The capacitor current is also shown in the Fig. 18. However, the UPQC without PV and BESS does not show quality result like the PV-BESS-UPQC.

The summary of the findings of source current and load voltage is tabulated in Table 5 and Table 6. The comparative analysis between the UPQC with PV-BESS and UPQC without PV-BESS can be realized from the Table 5 and Table 6. From Table 5, it can be noticed that before connecting the UPQC during voltage harmonic condition the THD values for the source currents are 53.28%, 52.92% and 53.28% for a, b and c phases. Afterwards, UPQC is integrated in the system with PV and ESS and the THD values are significantly reduced and the values for a, b and c phases are 2.05%, 2.54% and 3.05% respectively. To verify the significance of PV-BESS-UPQC system, the PV and the BESS is removed

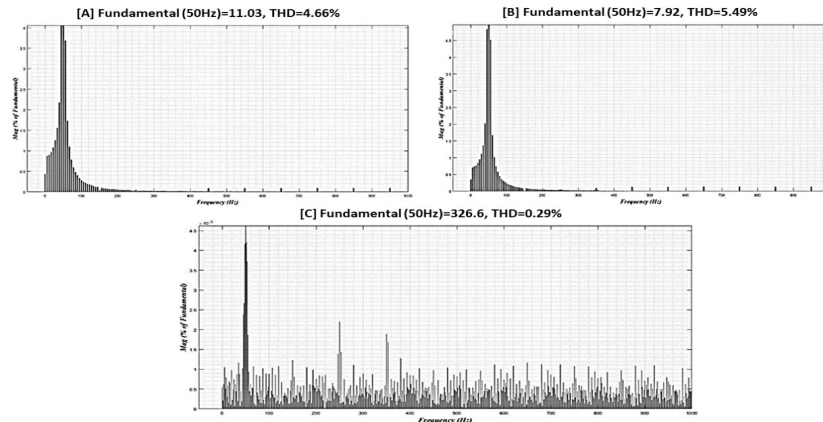


FIGURE 17. Simulation findings acquired under Case Study 1 for UPQC connecting without PV-BESS, (A) THD for current under voltage harmonic condition (B) THD for current under voltage harmonic with sag condition (C) THD for voltage.

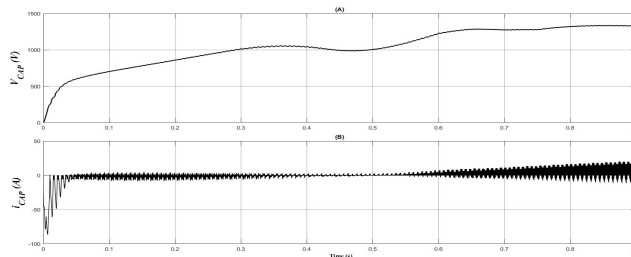


FIGURE 18. Simulation findings obtained under Case Study 1 for UPQC without PV-BESS (A) Total capacitor voltage (B) Total capacitor current.

and observed the performance of the UPQC with DC link capacitor only and it can be observed that the THDs are increased which are 4.66%, 5.63% and 5.69% for a, b and c phases respectively. Besides, during the condition of voltage harmonic with sag without attaching the UPQC the THD values for the source currents are 49.49%, 49.57% and 49.43% for a, b and c phases respectively. After attaching the UPQC in the system with PV and BESS and the THD is observed for phase a, b and c and which are 2.09%, 2.83% and 3.07% respectively. To verify the significance of PV-BESS-UOQC system, the PV and the BESS is removed and observed the performance of the UPQC with DC link capacitor only and it can be observed that the THD is increased which is 5.49%, 6.35% and 6.43% for phase a, b and c respectively.

From Table 6, it can be noticed that before connecting the UPQC during voltage harmonic condition the THD values for the load voltages are 18.81%, 18.82% and 18.82% for phase a, b and c respectively. Next, UPQC is connected in the system with PV-Ess and the THD values are reduced remarkably and the values for phase a, b and c are 0.28%, 0.28% and 0.28% respectively. To validate the significance of PV-BESS-UOQC system, the PV and the BESS is detached and consider the performance of the UPQC with DC link capacitor only and it can be noticed that the THD is increased slightly which is 0.29%, 0.29% and 0.29% for phase a, b

TABLE 5. Comparative source current analysis of the proposed UPQC with PV-BESS and without PV-BESS under Case Study 1.

Analysis Parameter	Voltage Harmonic			Voltage Harmonic with sag (at 0.7 & 0.4 pu)		
	Phase a	Phase b	Phase c	Phase a	Phase b	Phase c
Before attaching UPQC						
THD value (%)	53.28	52.92	53.28	49.49	49.57	49.43
Phase Difference (°)	7.0	6.5	4.2	5.0	4.2	4.0
Power Factor	0.808	0.812	0.905	0.903	0.810	0.910
After attaching UPQC with PV-Ess						
THD value (%)	2.05	2.54	3.05	2.09	2.83	3.07
Phase Difference (°)	0.5	0.3	0.4	0.6	0.4	0.5
Power Factor	0.999	0.999	0.999	0.999	0.999	0.999
After attaching UPQC without PV-Ess						
THD value (%)	4.66	5.63	5.69	5.49	6.35	6.43
Phase Difference (°)	0.5	0.3	0.4	0.6	0.4	0.5
Power Factor	0.999	0.999	0.999	0.999	0.999	0.999

and c respectively. Besides, during the condition of voltage harmonic with sag without attaching the UPQC the THD values for the load voltages are 32.62%, 34.11% and 34.11% for a, b and c phases respectively. Next, attaching the UPQC in the system with PV and ESS and the THD is noticed for a, b and c phases which are 0.28%, 0.28% and 0.28% respectively. To validate the significance of PV-BESS-UOQC system, the PV and the BESS is disconnected and noticed the performance of the UPQC with DC link capacitor only and the THD is increased slightly which is 0.29%, 0.29% and 0.29% for a, b and c phases respectively.

TABLE 6. Comparative load voltage analysis of the proposed UPQC with PV-BESS and without PV-BESS under Case Study 1.

Analysis Parameter	Voltage Harmonic			Voltage Harmonic with sag (0.3 & 0.6 pu)		
	Phase a	Phase b	Phase c	Phase a	Phase b	Phase c
	Before attaching UPQC					
THD value (%)	18.81	18.82	18.82	32.62	34.11	34.11
Phase Angle (%)	0	-120	120	0	-120	120
After attaching UPQC with PV-ESS						
THD value (%)	0.28	0.28	0.28	0.28	0.28	0.28
Compensation Magnitude (%)	100	100.1	99.78	99.939	99.66	99.54
Phase Angle (°)	0	-120	120	0	-120	120
After attaching UPQC without PV-ESS						
THD value (%)	0.29	0.29	0.29	0.29	0.29	0.29
Compensation Magnitude (%)	99.969	99.48	100.2	99.969	99.33	99.3
Phase Angle (°)	0	-120.2	199.9	0	-120.2	120.2

B. CASE STUDY 2: CONSTANT PV IRRADIANCE AT 800 w/m² AT 45°C

1) SCENARIO A: SINUSOIDAL-BALANCE SAG AND SWELL SOURCE VOLTAGE CONDITION WITH HARMONIC NON-LINEAR LOAD AT CONSTANT IRRADIANCE 800 W/M² AT 45°C

In the case study 2, the operation of PV-BESS-UPQC is operated utilizing the constant PV irradiation, which is maintained at 800 W/m² and the temperature is maintained at 45 degree Celsius that follow the Malaysia tropical climate. For the scenario A under case study 2, the PV-BESS-UPQC is considered under context of sinusoidal-balanced source voltage sag and swell condition at PCC. The performance simulation of PV-BESS-UPQC under context of sinusoidal-balanced source voltage sags and swells at PCC are displayed in term of simulation waveform are shown in The different observed waveforms are supply voltages, series compensated voltages, load voltages, load currents, shunt compensated currents, source currents. From Fig. 19(A), it can be noticed that source voltage, V_S at PCC during 0.3s to 0.35s and 0.4s to 0.45s, there is 0.7 pu voltage sag and 0.35s to 0.4s, there is 0.4 pu voltage sag. Moreover, from 0.6s to 0.65s and 0.7s to 0.75s, there is 1.3 pu voltage swell and from 0.65s to 0.7s, there is 1.6 pu voltage swell. An appropriate voltage V_{SE} is injected by the series APF compensator to mitigate for the source voltage at PCC under these contexts. The injected voltage is in phase with the grid voltage during the condition of voltage sag and opposite phase with source voltage during the condition of voltage swell which can be seen in Fig. 19(B) to keep the load voltage, V_L is equivalent to the rated voltage. It can be noticed from Fig. 19(C) that the load voltage is

sinusoidal and equal to the rated voltage. Fig. 19(D) shows the distorted load current, i_L created by the unbalanced non-linear load. Three phase unbalance loads is considered in this work. Since the non-linear load is utilized in this work, the shunt APF compensator mitigates for the source current, i_S under non-linear load context by injecting an appropriate current i_{SH} shown in Fig. 19(E) to keep the source current sinusoidal. Therefore, the source current is maintained sinusoidal and can be seen from Fig. 19(F).

From Fig. 20, it can be seen that the compensation magnitude of load voltage, V_L is achieved appropriately which is equal to the rated voltage. It shows the compensation by the series APF compensator during the condition of voltage sag and voltage swell. It can be observed that 0.3s to 0.35s and 0.35s to 0.4s, there is voltage sag of 0.7 pu and 0.4 pu respectively. The series APF compensator injected appropriate to compensate for the source voltage on both conditions. Therefore, the load voltage achieves the rated voltage during the voltage sag. Moreover, there is 1.3 pu voltage swell and 1.6 pu during the period of 0.6s to 0.65s and 0.65s to 0.7s respectively. An appropriate voltage in opposite phase with the source voltage is injected by the series compensator to compensate the grid voltage.

The THD for current under balanced voltage sag condition is displayed in Fig. 21(A). It can be observed that the THD is 2.09%. Moreover, Fig. 21(B) shows the THD for current under balanced voltage swell condition and can be noticed

that the THD is 2.02%. Furthermore, Fig. 21 (C) shows the THD for voltage and can be seen that the THD is only 0.28%.

From Fig. 22(A), it can be noticed that the measured DC link voltage is stable at 700 V during the condition of voltage sag and voltage swell. The PV current is around 46.2 A observed in Fig. 22 (B) and the power of the PV can be seen in Fig. 22(C) which is 32 KW. The DC link power can be observed in Fig. 22(D) and it is increased during 0.3s to 0.45s so that the load can be supported during insufficient voltage supply. On the other hand, the DC link power is reduced during 0.6s to 0.75s because of over voltage supply from the grid. The power of the BESS is seen in Fig. 22(E) and it is increased during the voltage sag from 0.3s to 0.45s since the current of the BESS is increased whereas the power of the BESS is reduced during voltage swell from 0.6s to 0.75s since the current of the BESS is decreased. The state of charge (SOC) shows in Fig. 22(F) and can be noticed the charging operation of the BESS throughout the process.

In Fig. 23, it can be noticed clearly that the suggested STF-UVG in Fig. 23(A) and standard conventional SRF-PLL technique in Fig. 23(B) are capable of detecting the synchronization phase value accurately in $\sin(\omega t)$ and $\cos(\omega t)$ from the grid voltage which sinusoidal-balanced under sag and swell condition at PCC. Besides, Table 7 summarizes the comparative analysis for source current when simulating the PV-BESS-UPQC with proposed STF-UVG extraction method and the conventional SRF-PLL extraction method. Besides. the comparative analysis for load voltage is tabulated in Table 8 considering the PV-BESS-UPQC with proposed

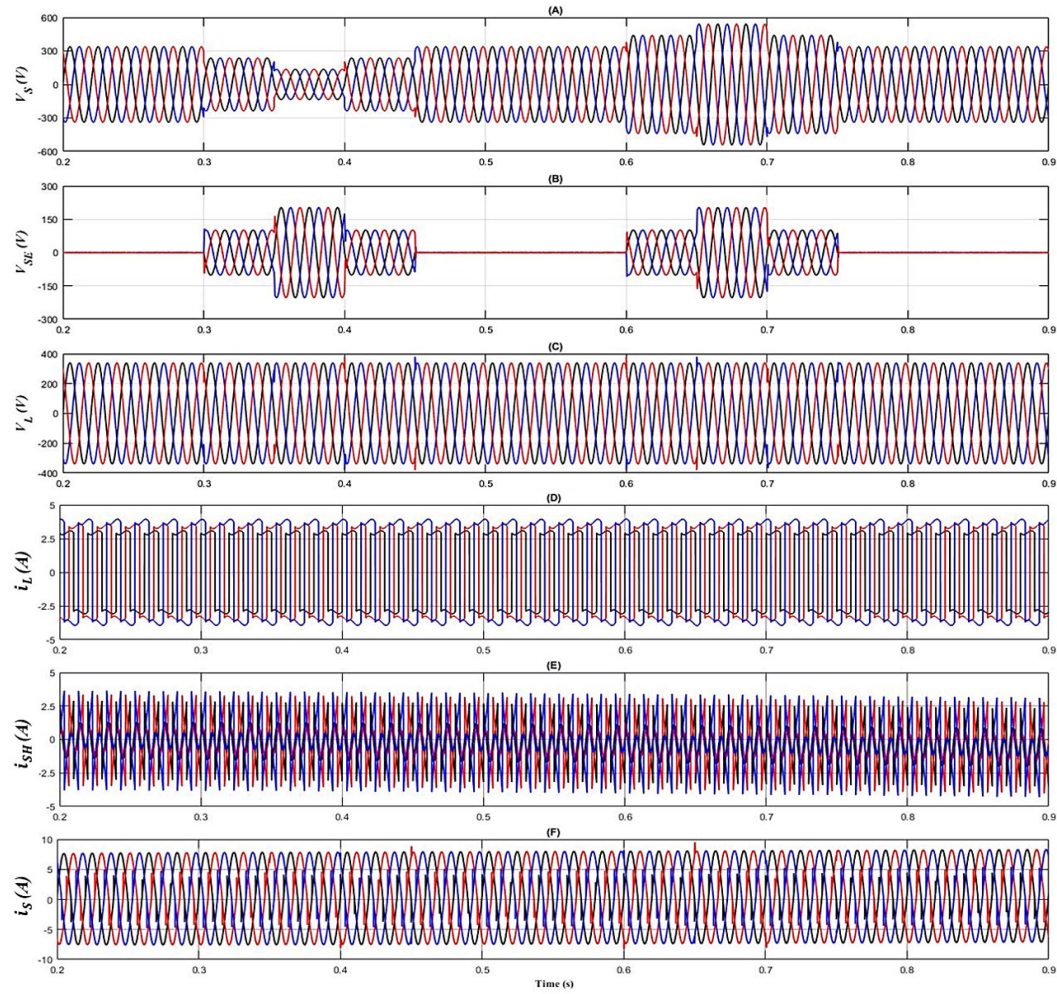


FIGURE 19. Simulation waveform acquired under Case Study 2: Scenario A for balance voltage swell and sag condition, with include (A) three-phase source voltage (B) Injection voltage of Series APF (C) Load Voltage (D) Load Current (E) Injection Current of Shunt APF (F) Source Current.

STF-UVG extraction method and the conventional SRF-PLL extraction method. The comparative analysis is done under the sinusoidal-balanced source voltage sags and swells condition at PCC. The both techniques are mitigating harmonic currents produced by non-linear load and the grid currents are maintained as sinusoidal shape with THD values suggested by IEEE standard 519 which is beneath the 5% harmonic limit. The results show that the THD is slightly lower in the proposed STF-UVG and STF- $dq0$ filter technique than using the SRF-PLL and MAF filter technique. Furthermore, the resulted phase differences between the source voltage and current is large and reduced by the STF-UVG and STF- $dq0$ filter techniques of UPQC. In other words, it proves that the STF-UVG and STF- $dq0$ filter both techniques can synchronize UPQC with the grid effectively. This is because the phase values are detected accurately in $\sin(\omega t)$ and $\cos(\omega t)$ by both techniques. Therefore, the grid current operates in phase with the grid voltage and so unity power factor is nearly achieved which is 0.999. Overall, the STF-UVG extraction method and the conventional SRF-PLL extraction method

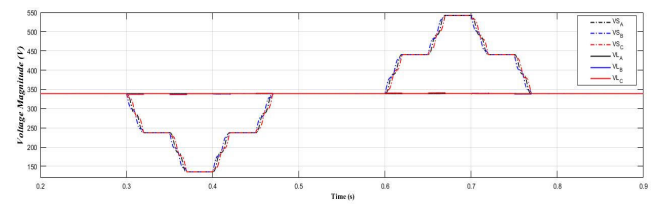


FIGURE 20. Simulation finding showing the detected voltage magnitude under Case study 2: Scenario A for balance voltage sag and swell condition.

both methods perform identically during the source voltage operating condition of sinusoidal-balanced sag and swell for case study 2: scenario A.

2) SCENARIO B: SINUSOIDAL-UNBALANCE SAG AND SWELL SOURCE VOLTAGE CONDITION WITH HARMONIC NON-LINEAR LOAD AT CONSTANT IRRADIANCE 800 W/M² AT 45°

In Scenario B for case study 2, an unbalanced source voltage of swell and sag condition at PCC is considered to test the

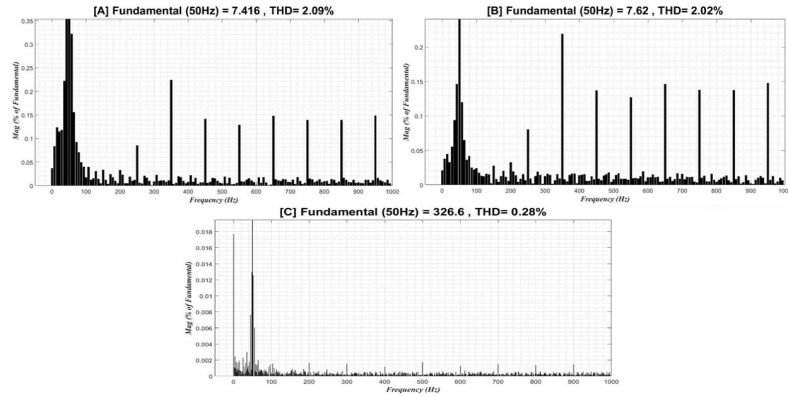


FIGURE 21. Simulation findings acquired under Case Study 2: Scenario A for balance voltage sag and swell condition, (A) THD for current under balance voltage sag condition (B) THD for current under balance voltage swell condition (C) THD for voltage under both conditions.

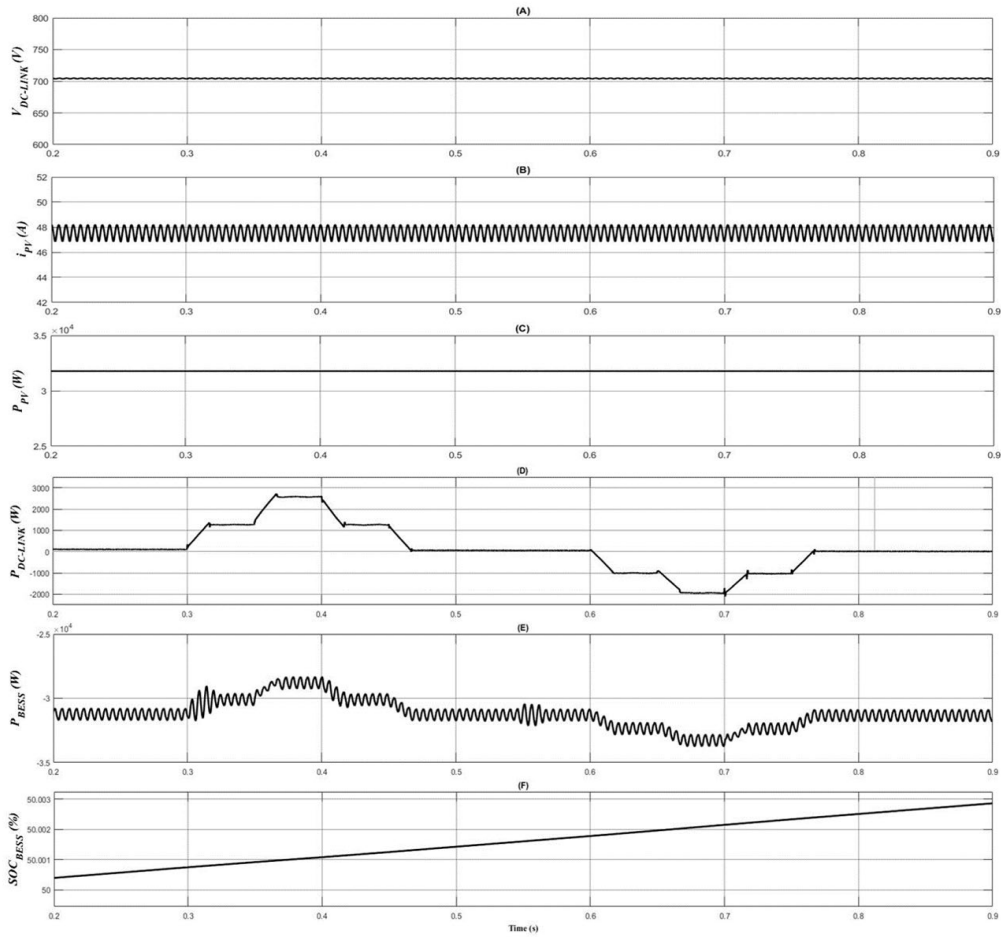


FIGURE 22. Simulation result acquired under Case Study 2: Scenario A for balance voltage sag and swell condition, with include (A) DC-Link Voltage (B) Current of PV (C) Power of PV (D) Output power of DC-Link (E) Power of BESS (F) SOC of BESS.

performance of PV-BESS-UPQC. The performance of UPQC under context of PCC unbalance voltage sags and swells are displayed in figure. The irradiation is maintained constant at

800 W/m². From Fig. 24(A), it can be noticed that during 0.25s to 0.5s, there is voltage swell of 1.2 pu in phase a, 1.4 pu in phase b and 1.6 pu in phase c and from 0.65s to 0.85s, there

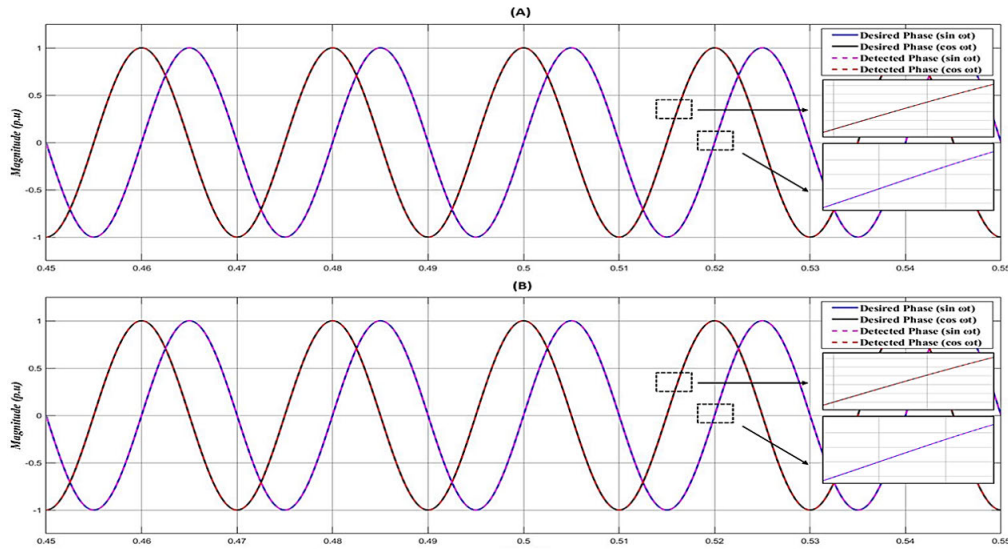


FIGURE 23. Simulation findings showing the detected synchronization reference phase value in $\sin(\omega t)$ and $\cos(\omega t)$ under Case study 2: Scenario A for balance voltage swell and sag condition, with include (A) Detection of synchronization phase by the STF-UVG (B) Detection of synchronization phase by the conventional SRF-PLL.

TABLE 7. Comparative source current analysis of the suggested UPQC using STF technique and standard SRF-MAF technique under Case Study 2: Scenario A.

Analysis Parameter	Balance Voltage Sag (at 0.7 & 0.4 pu)			Balance Voltage Swell (at 1.3 & 1.6 pu)		
	Phase <i>a</i>	Phase <i>b</i>	Phase <i>c</i>	Phase <i>a</i>	Phase <i>b</i>	Phase <i>c</i>
Before Connecting PV-ESS-UPQC						
THD value (%)	53.28	52.92	53.28	49.49	49.57	49.43
Phase Difference (°)	7.0	6.5	4.2	5.0	4.2	4.0
Power Factor	0.808	0.812	0.905	0.903	0.810	0.910
After Connecting PV-BESS-UPQC with the suggested STF						
THD value (%)	2.09	2.67	3.15	2.02	2.79	2.92
Phase Difference (°)	0.4	0.3	0.5	0.4	0.2	0.6
Power Factor	0.999	0.999	0.999	0.999	0.999	0.999
After Connecting PV-BESS-UPQC with the standard SRF-MAF						
THD value (%)	2.12	2.75	3.14	1.99	2.80	3.11
Phase Difference (°)	0.5	0.4	0.7	0.6	0.4	0.8
Power Factor	0.999	0.999	0.999	0.999	0.999	0.999

is voltage sag of 0.8 pu in phase *a*, 0.6 pu in phase *b* and 0.4 pu in phase *c*. An appropriate voltage V_{SE} is injected by the series compensator to mitigate for the source voltage under the context of unbalance sag and swell source voltage which can be seen in Fig. 24(B) to keep the load voltage equivalent

TABLE 8. Comparative load voltage analysis of the proposed UPQC using STF technique and standard SRF-MAF technique under Case Study 2: Scenario A.

Analysis Parameter	Balance Voltage Sag (at 0.3 & 0.6 pu)			Balance Voltage Swell (at 1.3 & 1.6 pu)		
	Phase <i>a</i>	Phase <i>b</i>	Phase <i>c</i>	Phase <i>a</i>	Phase <i>b</i>	Phase <i>c</i>
Before Connecting PV-BESS-UPQC						
THD value (%)	19.73	22.54	22.54	12.14	12.14	12.14
Phase Angle (°)	0	-120	120	0	-120	120
After Connecting PV-BESS-UPQC with the suggested STF technique						
THD value (%)	0.28	0.28	0.28	0.28	0.28	0.28
Compensation Magnitude (%)	100	99.41	99.53	100	100.6	100.5
Phase Angle (°)	0	-120	120	0	-120	120
After Connecting PV-BESS-UPQC with the standard SRF-MAF technique						
THD value (%)	0.28	2.14	2.45	0.28	2.45	2.22
Compensation Magnitude (%)	100	98.9	99.27	100	100.7	100.6
Phase Angle (°)	0	-120.3	119.8	0	-120.2	119.9

to the rated voltage. The sinusoidal load voltage can be noticed from Fig. 24(C) and it is equal to the rated voltage. Fig. 24(D) shows non-linear load distorted current. To keep the source current sinusoidal the shunt compensator, inject the compensation current which is displayed in Fig. 24(E).

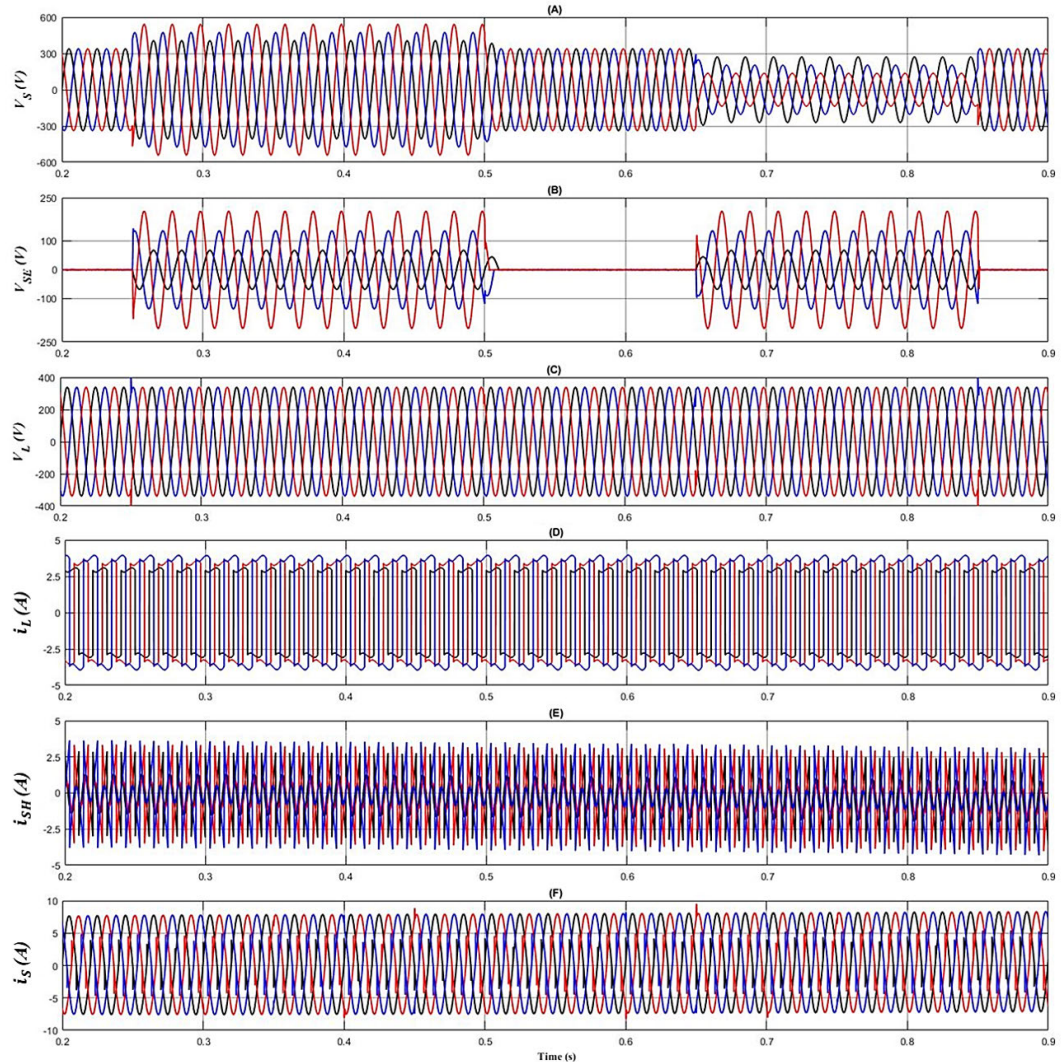


FIGURE 24. Simulation waveform acquired under Case Study 2: Scenario B for unbalance voltage swell and sag condition, with include (A) three-phase source voltage (B) Injection voltage of Series APF (C) Load Voltage (D) Load Current (E) Injection Current of Shunt APF (F) Source Current.

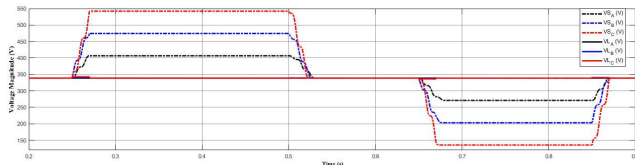


FIGURE 25. Simulation findings acquired the detected voltage magnitude under Case study 2: Scenario B for unbalance voltage sag and swell condition.

Since the non-linear load is utilized in this work, the shunt compensator mitigates for the source current under non-linear load context by injecting an appropriate current i_{SH} to keep the source current sinusoidal. Therefore, the source current is maintained sinusoidal and can be seen from Fig. 24(F). From Fig. 25, it can be seen that the compensation is achieved appropriately during the unbalanced voltage sag and swell. The figure shows the compensation by the series compensator

during the voltage swell from 0.25s to 0.5s and voltage sag from 0.65s to 0.85s. The series compensator injects different voltage magnitude according to the demand. The result proves that the compensation is successfully achieved. Therefore, the load voltage achieved the rated voltage during the condition of unbalanced voltage sag and swell. The DC link voltage can be seen from Fig. 26(A) and it is stable at 700 V during the voltage distortion in the supply, and Fig. 26(B) shows that the PV current is around 46.2 A and the power of the PV is shown in Fig. 26(C) and the DC link power is 32 KW. The DC link power is reduced during voltage swell from 0.25s to 0.5s so that the load can be protected in the overvoltage condition. On the other hand, the DC link power is increased during voltage swell from 0.65s to 0.85s to support the load in the insufficient voltage condition and shown in Fig. 26(D). The power of the BESS is observed in Fig. 26(E) and it is increased during the voltage sag from 0.65s to 0.85s since the current of the BESS is increased

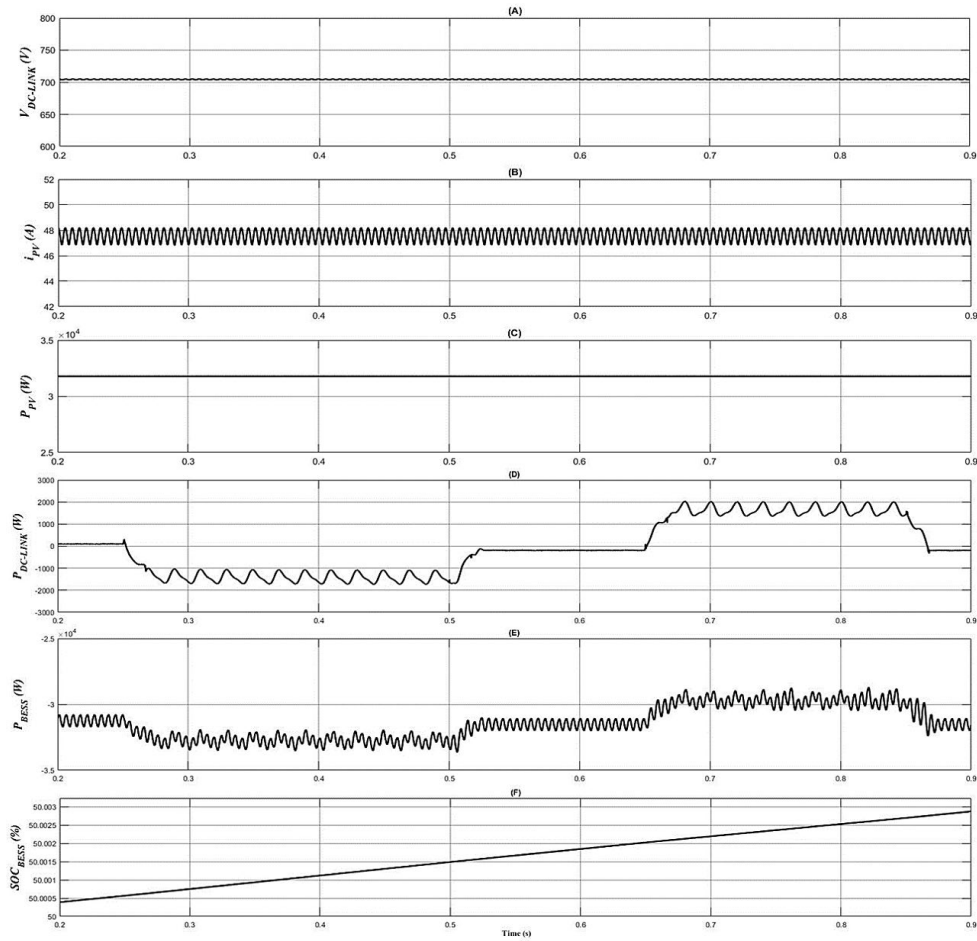


FIGURE 26. Simulation result acquired under Case Study 2: Scenario B for unbalance voltage sag and swell condition, with include (A) DC-Link Voltage (B) Current of PV (C) Power of PV (D) Output power of DC-Link (E) Power of BESS (F) SOC of BESS.

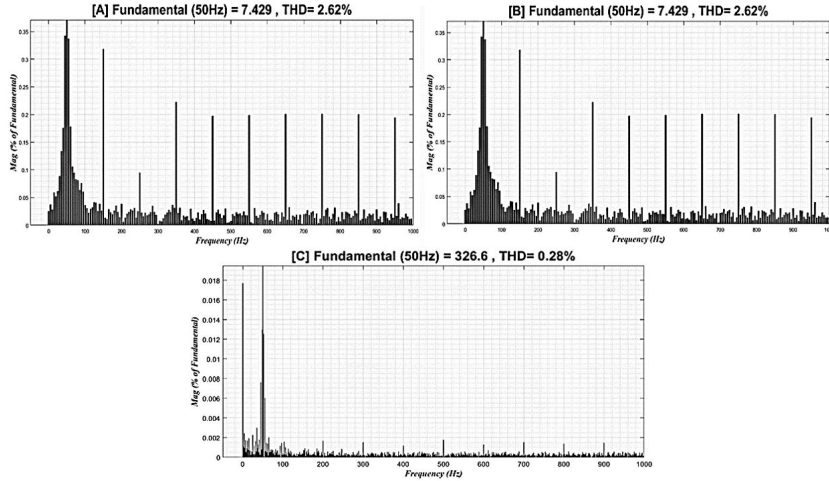


FIGURE 27. Simulation findings acquired under Case Study 2: Scenario B for unbalance voltage swell and sag condition, (A) THD for current under unbalance voltage swell condition (B) THD for current under unbalance voltage sag condition (C) THD for voltage under both condition.

whereas the power of the BESS is reduced during voltage swell from 0.25s to 0.5s since the current of the BESS is decreased. The state of charge (SOC) shows in Fig. 26(F) that the BESS is charged throughout the process.

Fig. 27 shows the THD values under unbalance voltage swell and sag for source current and load voltage. In Table 9, the comparative analysis for source current of the proposed UPQC-STF and UPQC-SRF techniques are tabulated. From

TABLE 9. Comparative source current analysis of the proposed UPQC using STF technique and standard SRF-MAF technique under Case Study 2: Scenario B.

Analysis Parameter	Voltage Unbalance Swell (at 1.2, 1.4 & 1.6 pu)			Voltage Unbalance Sag (at 0.8, 0.6 & 0.4 pu)		
	Phase a	Phase b	Phase c	Phase a	Phase b	Phase c
Before attaching PV-Ess-UPQC						
THD value (%)	53.28	52.92	53.28	49.49	49.57	49.43
Phase Difference (°)	7.0	6.5	4.2	5.0	4.2	4.0
Power Factor	0.808	0.812	0.905	0.903	0.810	0.910
After attaching PV-Ess-UPQC with the suggested STF technique						
THD value (%)	2.62	2.89	3.00	2.62	2.93	3.25
Phase Difference (°)	0.30	0.40	0.60	0.30	0.70	0.50
Power Factor	0.999	0.999	0.999	0.999	0.998	0.999
After attaching PV-Ess-UPQC with the standard SRF-MAF technique						
THD value (%)	4.51	4.92	5.13	4.55	4.69	5.09
Phase Difference (°)	0.40	0.40	0.70	0.30	0.70	0.60
Power Factor	0.998	0.998	0.998	0.998	0.998	0.998

the Table 9, it can be noticed that both UPQC-STF and UPQC-SRF reduced the THD value significantly. Before connecting the UPQC system in the PCC, the THD values were 53.28%, 52.92% and 53.28% for a, b and c phases respectively for unbalance voltage swell and 49.49%, 49.57% and 49.43% for phase a, b and c respectively for unbalance voltage sag. On the other hand, both PV-Ess-UPQC with STF technique and SRF technique reduced the THD. For STF technique, the THD values are 2.62%, 2.89% and 3.00% for a, b and c respectively for unbalance voltage swell and 2.62%, 2.93% and 3.25% for a, b and c respectively for unbalance voltage sag and the almost unity power factor is achieved. For SRF technique, the THD values are 4.51%, 4.92% and 5.13% for a, b and c respectively for unbalance voltage swell and 4.55%, 4.69% and 5.09% for a, b and c respectively for unbalance voltage sag and the almost unity power factor is achieved.

In the Table 10, the comparative analysis for load voltage is summarized considering the PV-BESS-UPQC with proposed STF-UVG extraction method and the conventional SRF-PLL extraction method. The comparative analysis result is obtained considering the unbalanced voltage sags and swells condition at PCC. The results show that before connecting the UPQC system the THDs for load voltages are 12.67%, 13.79% and 14.92% for unbalanced voltage swell condition

TABLE 10. Comparative load voltage analysis of the proposed UPQC using STF technique and standard SRF-MAF technique under Case Study 2: Scenario B.

Analysis Parameter	Unbalance Voltage Swell (at 1.2, 1.4 & 1.6 pu)			Unbalance Voltage Sag (at 0.8, 0.6 & 0.4 pu)		
	Phase a	Phase b	Phase c	Phase a	Phase b	Phase c
Before Connecting PV-BESS-UPQC						
THD value (%)	12.67	13.79	14.92	18.20	22.79	34.28
Phase Angle (°)	0	-120	120	0	-120	120
After Connecting PV-BESS-UPQC with the suggested STF technique						
THD value (%)	0.28	0.37	0.38	0.28	0.33	0.35
Compensation Magnitude (%)	100	100.7	101.2	100	99.65	99.29
Phase Angle (°)	0	-120	120	0	-120	120
After Connecting PV-BESS-UPQC with the standard SRF-MAF technique						
THD value (%)	0.28	1.37	2.31	0.28	1.94	2.72
Compensation Magnitude (%)	100	100.5	101.6	100	99.45	99.54
Phase Angle (°)	0	-119.9	119.4	0	-120.2	120.1

for a, b and c respectively. Besides, for unbalanced voltage sag condition the THDs for load voltages are 18.20%, 22.79% and 34.28% for a, b and c respectively. Next, the PV-BESS-UPQC system is connected using the STF technique and can be noticed that the THDs for load voltages are 0.28%, 0.37% and 0.38% for unbalanced voltage swell condition for phase a, b and c respectively and for unbalanced voltage sag condition the THDs for load voltages are 0.28%, 0.33% and 0.35% for a, b and c respectively. On the other hand, utilizing PV-BESS-UPQC with SRF-MAF technique the THDs for load voltages are 0.28%, 1.37% and 2.31% for unbalanced voltage swell condition for a, b and c respectively and for unbalanced voltage sag condition the THDs for load voltages are 0.28%, 1.94% and 2.72% for a, b and c respectively. It can be observed that the THDs are slightly lower in the proposed STF-UVG technique than the SRF-PLL technique.

Based on Fig. 28(A), it can be observed that the synchronization phase value in $\sin(\omega t)$ and $\cos(\omega t)$ are detected accurately by the suggested STF-UVG method which is equivalent to the expected phase value. On the other hand, minor displacement can be noticed between desired phase value and the detected phase value in the Fig. 28(B) where the standard conventional SRF-PLL technique is implemented. Therefore, it indicates that the standard conventional SRF-PLL technique is not able to extract the phase value accurately

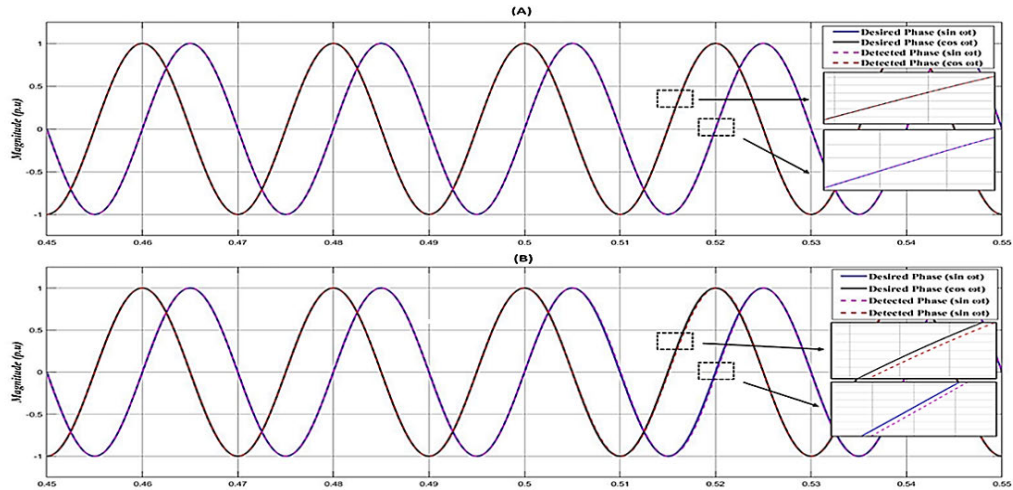


FIGURE 28. Simulation findings of the detected phase value of synchronization reference in $\sin(\omega t)$ and $\cos(\omega t)$ under Case study 2: Scenario A for unbalance voltage swell and sag condition, with include (A) Synchronization phase detected by the STF-UVG (B) Synchronization phase detected by the conventional SRF-PLL.

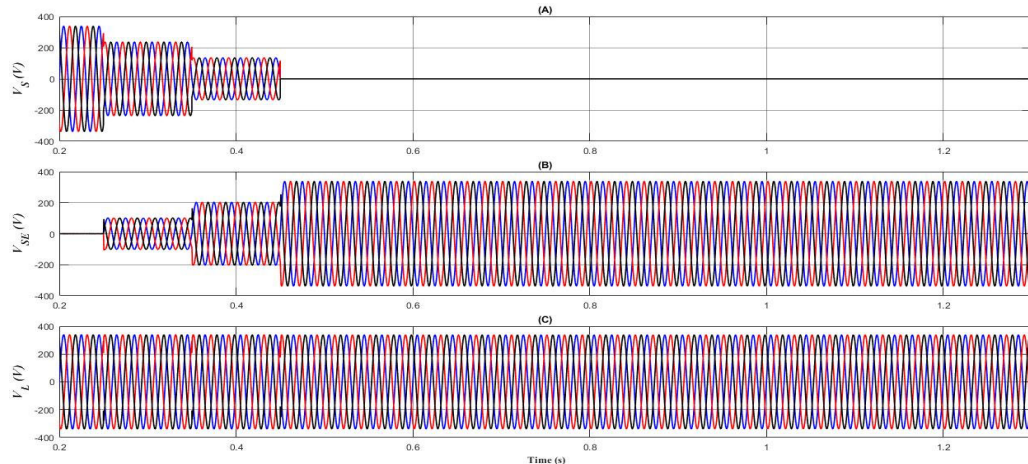


FIGURE 29. Simulation waveform acquired under Case Study 3: Scenario A for voltage interruption condition, with include (A) three-phase source voltage (B) Injection voltage of Series APF (C) Load Voltage.

as desired during an unbalance three-phase source voltage swell and sag condition across the PCC.

C. CASE STUDY 3: VARYING PV IRRADIANCE AND TEMPERATURE PV PANEL

1) SCENARIO A: NON-SINUSOIDAL-UNBALANCE PERMANENT INTERRUPTION SOURCE VOLTAGE WITH HARMONIC NON-LINEAR LOAD AT LOW UNBALANCE PV IRRADIANCE

The operation of UPQC under context of PCC voltage sags and interruption are displayed in Fig. 28. The irradiation is reduced to 0 W/m² from 800 W/m² during 0.35s to 0.9s. The different observed waveforms are supply voltages, series compensated voltages, load voltages, load currents, shunt compensated currents, source currents. From Fig. 29(A) it can be observed that during 0.25s to 0.35s, there is 0.6 pu

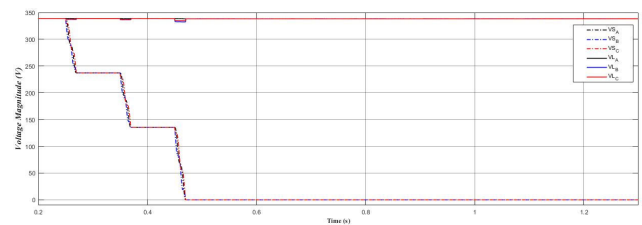


FIGURE 30. Simulation findings acquired the detected voltage magnitude under Case study 3: Scenario A for voltage interruption condition.

voltage sag and 0.35s to 0.45s, there is 0.3 pu voltage sag. Moreover, from 0.45s to the end of the simulation the voltage supply is interrupted. An appropriate voltage V_{SE} is injected by the series compensator to mitigate for the source voltage under these contexts and support the load completely during

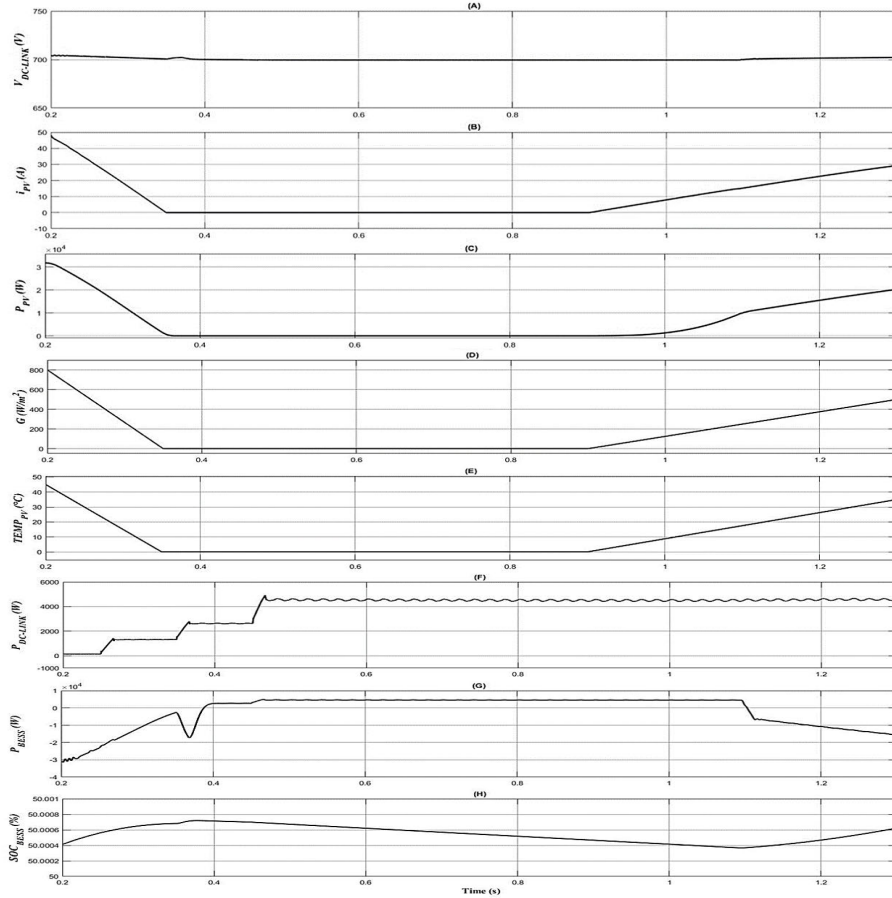


FIGURE 31. Simulation result acquired under Case Study 2: Scenario A for voltage interruption condition, with include (A) DC-Link Voltage (B) Current of PV (C) Power of PV (D) PV Irradiance (E) PV temperature panel (F) Output power of DC-Link (G) Power of BESS (H) SOC of BESS.

voltage interruption occurred in the grid voltage. The voltage injection is displayed in Fig. 29(B). The load voltage is shown in Fig. 29(C) and it can be noticed that the load voltage is equivalent to the rated voltage. Fig. 30 shows the source voltage magnitude and the load voltage magnitude. The dotted lines indicate the source voltages and the straight lines show the load voltages. It can be seen from the Fig. 30 that the compensation is achieved appropriately. The Fig. 30 shows the compensation by the series compensator during the voltage sag from 0.25s to 0.45s and from 0.45s the source voltage is zero and the total load voltage is supplied by the series compensator using the PV and BESS.

An appropriate voltage is injected by the series compensator in phase with the grid voltage to mitigate for the source voltage on both conditions. Therefore, the load voltage achieved the rated voltage during the voltage sag and also during the voltage interruption. From Fig. 31(A), it can be noticed that the DC link voltage is stable at 700 V during the voltage sag and voltage interruption. From Fig. 31(B) it can be noticed that the PV current is around 46.2A until 0.35s and after that it becomes zero because the irradiation is reduced to 0 W/m^2 and the temperature also reduced

to 0 $^{\circ}\text{C}$ which can be seen in Fig. 31(D) and Fig. 31(E) respectively.

From 0.9s the PV current start increasing again since the PV is connected and the irradiation is back to 800 W/m^2 . The power of the PV can be seen in Fig. 31(C) which is 32 KW at the beginning and from 0.35s to 0.9s it becomes zero because the irradiation is reduced to 0 W/m^2 and then it rises again since the irradiation is now returned to 800 W/m^2 . From the Fig. 31(F), the increase of DC link power is noticed during 0.3s to 0.45s and become maximum at 0.45s so that the load can be supported during insufficient voltage supply and also when there is no voltage supplied from the grid. The power of the BESS can be seen in Fig. 31(G) and it can be noticed that the power is decreased in the beginning and then become stable. When the PV is disconnected then the BESS supplied the power to the load through the DC link. At the beginning the BESS is started charging since the PV is still connected but when the PV is disconnected then the BESS started supplying power and start discharging. Afterwards, the PV is connected again at 0.9s and started sending power to the load. At this moment the BESS stopped supplying power and move to charging mode. The state of

charge (SOC) in Fig. 31(H) shows that the BESS is charged at the beginning and then start discharging from 0.35s to 1.1s.

V. CONCLUSION

The construction of three-phase UPQC has been investigated considering the condition of complex power quality problems which are an amalgamation of harmonics, voltage swell, and sags, and voltage interruption under unbalanced and distorted voltage grid condition. Integrating the BESS and PV with the UPQC provides active power capability to the network. The main benefit of BESS integrated with UPQC is that it makes the system capable of supplying and absorbing active power from the PV. Since renewable energy is not completely reliable because of its environment-dependent feature, integrating a BESS will solve the lack of renewable energy resources. Finally, it can be figured that the BESS and PV attached with UPQC can be a good alternative in the distributed generation to upgrade the power quality of the contemporary distribution system. The DC-link voltage is stable because of the continuous supply from the PV-BESS system. Therefore, it can reduce the complexity of the DC-link voltage regulation algorithm. The STF-UVG technique for synchronization phases is applied successfully in the shunt and series APF compensator to generate reference current and voltage. Thus, the UPQC is designed without relying on the PLL components, and mitigation of current and voltage are achieved successfully following the grid condition to ensure the system stability and to achieve almost unity power factor. The implementation of the proposed technique has confirmed that the grid current harmonics follow the IEEE-519 standard. Finally, it is worth mentioning that the proposed system can enhance the overall efficiency of the grid power system.

REFERENCES

- [1] *IEEE Recommended Practice for Monitoring Electric Power Quality*, IEEE Standards 1159-1995, IEEE Standards Coordinating Committee 22 on Power Quality, Jun. 1995, vol. 2009.
- [2] D. De Yong, S. Bhowmik, and F. Magnago, "Optimized complex power quality classifier using one vs. rest support vector machines," *Energy Power Eng.*, vol. 9, no. 10, pp. 568–587, 2017.
- [3] A. Javadi, A. Hamadi, L. Woodward, and K. Al-Haddad, "Experimental investigation on a hybrid series active power compensator to improve power quality of typical households," *IEEE Trans. Ind. Electron.*, vol. 63, no. 8, pp. 4849–4859, Aug. 2016.
- [4] A. Javadi, L. Woodward, and K. Al-Haddad, "Real-time implementation of a three-phase THSeAF based on a VSC and a P+R controller to improve the power quality of weak distribution systems," *IEEE Trans. Power Electron.*, vol. 33, no. 3, pp. 2073–2082, Mar. 2018.
- [5] M. A. Mansor, M. M. Othman, I. Musirin, and S. Z. M. Noor, "Dynamic voltage restorer (DVR) in a complex voltage disturbance compensation," *Int. J. Power Electron. Drive Syst.*, vol. 10, no. 4, pp. 2222–2230, 2019.
- [6] A. Ghosh and G. Ledwich, "Compensation of distribution system voltage using DVR," *IEEE Trans. Power Del.*, vol. 17, no. 4, pp. 1030–1036, Oct. 2002.
- [7] S. Jothibas and M. K. Mishra, "A control scheme for storageless DVR based on characterization of voltage sags," *IEEE Trans. Power Del.*, vol. 29, no. 5, pp. 2261–2269, Oct. 2014.
- [8] A. Farooqi, M. M. Othman, A. F. Abidin, S. I. Sulaiman, and M. A. M. Radzi, "Mitigation of power quality problems using series active filter in a microgrid system," *Int. J. Power Electron. Drive Syst.*, vol. 10, no. 4, pp. 2245–2253, 2019.
- [9] C. Kumar and M. K. Mishra, "Operation and control of an improved performance interactive DSTATCOM," *IEEE Trans. Ind. Electron.*, vol. 62, no. 10, pp. 6024–6034, Oct. 2015.
- [10] Y. Hoon, M. M. Radzi, M. Hassan, and N. Mailah, "Control algorithms of shunt active power filter for harmonics mitigation: A review," *Energies*, vol. 10, no. 12, p. 2038, Dec. 2017.
- [11] L. B. G. Campanhol, S. A. O. da Silva, and A. Goedtel, "Application of shunt active power filter for harmonic reduction and reactive power compensation in three-phase four-wire systems," *IET Power Electron.*, vol. 7, no. 11, pp. 2825–2836, Nov. 2014.
- [12] Y. Hoon, M. A. M. Radzi, M. K. Hassan, and N. F. Mailah, "Operation of three-level inverter-based shunt active power filter under nonideal grid voltage conditions with dual fundamental component extraction," *IEEE Trans. Power Electron.*, vol. 33, no. 9, pp. 7558–7570, Sep. 2018.
- [13] E. Hossain, M. R. Tur, S. Padmanaban, S. Ay, and I. Khan, "Analysis and mitigation of power quality issues in distributed generation systems using custom power devices," *IEEE Access*, vol. 6, pp. 16816–16833, 2018.
- [14] H. Fujita and H. Akagi, "The unified power quality conditioner: The integration of series- and shunt-active filters," *IEEE Trans. Power Electron.*, vol. 13, no. 2, pp. 315–322, Mar. 1998.
- [15] S. K. Khadem, M. Basu, and M. F. Conlon, "Intelligent islanding and seamless reconnection technique for microgrid with UPQC," *IEEE J. Emerg. Sel. Topics Power Electron.*, vol. 3, no. 2, pp. 483–492, Jun. 2015.
- [16] J. M. Guerrero, P. C. Loh, T.-L. Lee, and M. Chandorkar, "Advanced control architectures for intelligent microgrids—Part II: Power quality, energy storage, and AC/DC microgrids," *IEEE Trans. Ind. Electron.*, vol. 60, no. 4, pp. 1263–1270, Apr. 2013.
- [17] B. Han, B. Bae, H. Kim, and S. Baek, "Combined operation of unified power-quality conditioner with distributed generation," *IEEE Trans. Power Del.*, vol. 21, no. 1, pp. 330–338, Jan. 2006.
- [18] K. Hasan, M. M. Othman, N. F. A. Rahman, M. A. Hannan, and I. Musirin, "Significant implication of unified power quality conditioner in power quality problems mitigation," *Int. J. Power Electron. Drive Syst.*, vol. 10, no. 4, p. 2231, Dec. 2019.
- [19] C. K. Sundarabalan, Y. Puttagunta, and V. Vignesh, "Fuel cell integrated unified power quality conditioner for voltage and current reparation in four-wire distribution grid," *IET Smart Grid*, vol. 2, no. 1, pp. 60–68, Mar. 2019.
- [20] S. Devassy and B. Singh, "Design and performance analysis of three-phase solar PV integrated UPQC," *IEEE Trans. Ind. Appl.*, vol. 54, no. 1, pp. 73–81, Jan. 2018.
- [21] L. B. G. Campanhol, S. A. O. da Silva, A. A. de Oliveira, and V. D. Bacon, "Power flow and stability analyses of a multifunctional distributed generation system integrating a photovoltaic system with unified power quality conditioner," *IEEE Trans. Power Electron.*, vol. 34, no. 7, pp. 6241–6256, Jul. 2019.
- [22] A. M. Gee, F. Robinson, and W. Yuan, "A superconducting magnetic energy storage-emulator/battery supported dynamic voltage restorer," *IEEE Trans. Energy Convers.*, vol. 32, no. 1, pp. 55–64, Mar. 2017.
- [23] W. U. Tareen and S. Mekhilef, "Transformer-less 3P3W SAPF (three-phase three-wire shunt active power filter) with line-interactive UPS (uninterruptible power supply) and battery energy storage stage," *Energy*, vol. 109, pp. 525–536, Aug. 2016.
- [24] S. K. Kollimala, M. K. Mishra, and N. L. Narasamma, "Design and analysis of novel control strategy for battery and supercapacitor storage system," *IEEE Trans. Sustain. Energy*, vol. 5, no. 4, pp. 1137–1144, Oct. 2014.
- [25] S. B. Karanki, N. Geddada, M. K. Mishra, and B. K. Kumar, "A modified three-phase four-wire UPQC topology with reduced DC-link voltage rating," *IEEE Trans. Ind. Electron.*, vol. 60, no. 9, pp. 3555–3566, Sep. 2013.
- [26] A. Teke, L. Saribulut, and M. Tumay, "A novel reference signal generation method for power-quality improvement of unified power-quality conditioner," *IEEE Trans. Power Del.*, vol. 26, no. 4, pp. 2205–2214, Oct. 2011.
- [27] V. G. Kinhal, P. Agarwal, and H. O. Gupta, "Performance investigation of neural-network-based unified power-quality conditioner," *IEEE Trans. Power Del.*, vol. 26, no. 1, pp. 431–437, Jan. 2011.
- [28] M. Kesler and E. Ozdemir, "Synchronous-reference-frame-based control method for UPQC under unbalanced and distorted load conditions," *IEEE Trans. Ind. Electron.*, vol. 58, no. 9, pp. 3967–3975, Sep. 2011.
- [29] S. Goleshtan, J. M. Guerrero, and J. C. Vasquez, "Three-phase PLLs: A review of recent advances," *IEEE Trans. Power Electron.*, vol. 32, no. 3, pp. 1897–1907, Mar. 2017.



MUHAMMAD ALIF MANSOR received the Diploma degree in electrical engineering (power) and the bachelor's degree (Hons.) in electrical engineering from Universiti Teknologi MARA (UiTM), Malaysia, in 2015 and 2018, respectively. He is currently pursuing the M.Sc. degree in electrical engineering with the Faculty of Electrical Engineering, UiTM, on the research project of "Classification and Mitigation of Complex Power Quality Problems in Energy Storage System (ESS)". He has been working in power and energy with the Artificial Intelligence Research Laboratory (PEAiRL) Group, UiTM, since February 2019. His research interests include power electronics, power quality, renewable energy, and energy storage.



KAMRUL HASAN received the B.Sc. degree in electrical and electronics engineering from the Ahsanullah University of Science & Technology, Dhaka, Bangladesh, in 2015, and the M.Sc. degree in electrical engineering from Curtin University, Miri, Malaysia, in 2018. He is currently pursuing the Ph.D. degree with the Faculty of Electrical Engineering, UiTM, Shah Alam, Malaysia. He has been working in the Power and Energy with Artificial Intelligence Research Laboratory (PEAiRL) Group, UiTM, since March 2019. His research interests include power electronics, power quality, custom power devices, and renewable energy resources.



MUHAMMAD MURTADHA OTHMAN (Member, IEEE) received the B.Eng. degree (Hons.) from Staffordshire University, U.K., in 1998, the M.Sc. degree from Universiti Putra Malaysia, in 2000, and the Ph.D. degree from Universiti Kebangsaan Malaysia, in 2006. He served as the Head of the Department of the Centre for Electrical Power Engineering Studies (CEPES), from February 2009 to December 2010. Since 2012, he has been serving two times as the Deputy Director for the collaborative research project under the auspices of Ministry of Energy, Green Technology and Water (KeTTHA), Malaysia, and also the Public Works Department (JKR), Malaysia. He also served as the Deputy Director for service commercialization on energy efficiency technology under the collaboration with Centre of Excellence for Engineering and Technology JKR (CREaTE), Malaysia. He was previously appointed as the Chairman of the Energy Efficiency Committee in FEE, UiTM and also the Committee Member in the Master of Electrical Power Engineering Programme, Faculty of Engineering, Universiti Putra Malaysia (UPM). He has served as the Panel Assessor for research grant proposals at the Ministry of Higher Education (MOHE), Malaysia and Latvian Science Council, Europe. He is currently the Director of the UiTM-Solar Energy Research (U-SER) Centre, under the project of 50MW LSSPV, Gambang, Pahang. He is also an Associate Professor with the Faculty of Electrical Engineering (FEE), Universiti Teknologi MARA (UiTM), Malaysia. His area of research interests are artificial intelligence, energy efficiency, transfer capability assessment, integrated resource planning, demand side management, hybrid renewable energy, power system stability, reliability studies in a deregulated power systems, power quality, and active power filters.



SITI ZALIHA BINTI MOHAMMAD NOOR (Member, IEEE) received the bachelor's degree (Hons.) in electrical engineering, the M.Sc. degree in power electronics, and the Ph.D. degree in electrical engineering from Universiti Teknologi MARA (UiTM), Malaysia, in 2005, 2008, and 2018, respectively. She is currently a Senior Lecturer with the Faculty of Electrical Engineering, UiTM. She has authored or coauthored more than 35 technical articles in indexed international journal and conferences. Currently, she has more than 500 students joined the course worldwide. Her research interests are renewable energy, power electronics, modeling and simulation, signal processing, and embedded controller applications. She is a Certified Energy Manager, Certified Professional in Measurement and Verification CPMV), and Qualified Person (QP) SEDA Malaysia Grid-Connected Solar Photovoltaic Systems Design. She is also attached to industry collaborations as the Subject Matter Expert (SME) for the Photovoltaic (PV) system and energy audit. She also received a gold award on the e-Content Development Competition (e-ConDev2018) for Course Renewable Energy-Friendly of The World as an educator and developer of the course.



ISMAIL MUSIRIN received the bachelor's degree (Hons.) in electrical engineering from Universiti Teknologi Malaysia, in 1990, the M.Sc. degree in pulsed power technology from the University of Strathclyde, U.K., in 1992, the Ph.D. degree in electrical engineering from Universiti Teknologi MARA (UiTM), Malaysia, in 2005, and the Diploma degree in electrical power engineering from Universiti Teknologi Malaysia (UTM), in 1987. He started his higher education at UTM. He has been the Head of Programme for the Diploma of Electrical Engineering, UiTM for 3 years from 2004 to 2007, the Head of the Department Electrical Power Engineering in 2007, the Deputy Dean Research and Industrial Networking for 2 years from 2008 to 2010, and the Director for Community of Research UiTM for 4 years from 2014 to 2017. He is currently a Professor of power system with the Faculty of Electrical Engineering. He has authored and coauthored two books, more than 300 articles in international journal and indexed conferences. His research interests include artificial intelligence, optimization techniques, power system analysis, renewable energy, distributed generation, and power system stability. He is a Senior Member of the International Association of Computer Science and Information Technology (IACSIT), and a member of the Artificial Immune System Society (ARTIST) and of the International Association of Engineers (IAENG). He is also an International Journal Reviewer of the IEEE TRANSACTIONS, *Science* (Elsevier), WSEAS, John Wiley, IET, and some other publishers.